HHS Public Access

Author manuscript

Coord Chem Rev. Author manuscript; available in PMC 2017 January 01.

Published in final edited form as:

Coord Chem Rev. 2016 January 1; 306(Pt 2): 678–700. doi:10.1016/j.ccr.2015.03.026.

Recent Advances in Multinuclear Metal Nitrosyl Complexes

Lijuan Li[*] and **Linlin Li**

Department of Chemistry and Biochemistry, California State University, Long Beach, 1250 Bellflower Blvd., Long Beach, CA 90840

Abstract

The coordination chemistry of metal nitrosyls has expanded rapidly in the past decades due to major advances of nitric oxide and its metal compounds in biology. This review article highlights advances made in the area of multinuclear metal nitrosyl complexes, including Roussin's salts and their ester derivatives from 2003 to present. The review article focuses on isolated multinuclear metal nitrosyl complexes and is organized into different sections by the number of metal centers and bridging ligands.

Keywords

Nitric oxide; metal nitrosyl; multinuclear metal nitrosyl; nitrosyl; dinuclear metal nitrosyl; trinuclear metal nitrosyl; tetranuclear metal nitrosyl; pentanuclear metal nitrosyl; hexanuclear metal nitrosyl; octanuclear metal nitrosyl; Roussin's red salt; Roussin's red salt ester; Roussin's black salt; dinitrosyl iron complex; iron sulfur cluster; metal nitrosyl cluster

1. Introduction

Nitric oxide (NO) is a gaseous lipophilic radical molecule that plays important roles in several physiological and pathophysiological processes in mammals, including activating the immune response, serving as a neurotransmitter, regulating the cardiovascular system, and acting as an endothelium-derived relaxing factor [1–3]. NO functions in eukaryotes both as a signal molecule at nanomolar concentrations and as a cytotoxic agent at micromolar concentrations [4]. The latter arises from the ability of NO to react readily with a variety of cellular targets leading to thiol S-nitrosation [5], amino acid N-nitrosation [6], and nitrosative DNA damage [7–8].

Nitric oxide can readily bind to metals to give metal-nitrosyl (M-NO) complexes [9]. Some of these species are known to play roles in biological NO storage and transport [10–28]. The coordination chemistry of metal nitrosyls has expanded rapidly in the past decades. These complexes have different biological, photochemical, or spectroscopic properties due to

[*]To whom correspondence should be addressed. Lijuan.li@csulb.edu.

This manuscript is dedicated to Prof. Peter C. Ford for the wisdom he displayed throughout our fruitful collaboration.

distinctive structural features, and are often studied by using electron paramagnetic resonance (EPR), infrared (IR) vibrational frequencies (ν_{NO}), X-ray crystallography, Mössbauer, theoretical calculations, etc [29–34].

The aim of this review is to highlight advances made in the area of multinuclear metal nitrosyl complexes, including Roussin's salts and their ester derivatives. It summarizes the literature from 2003 to present. There have been several excellent reviews covering different aspects of metal nitrosyl chemistry in recent years [35–42], and we have tried to avoid direct overlap with the subject matter of those articles. This review is focused on recent advances on the synthesis and characterizations of isolated multinuclear metal nitrosyl complexes with structural certainty rather than *in situ* identifications. It is organized by the number of metal centers and further arranged into different sections based on the type of bridging ligands.

2. Dinuclear Metal Nitrosyl Complexes

2.1. Homodinuclear Cluster Linked by Sulfur – RRS and RRE Types

Roussin's Red Salt $[Fe_2(\mu\text{-}S)_2(NO)_4]^{2-}$, (RRS), and Roussin's Red Salt Ester, $[Fe_2(\mu\text{-}SR)_2(NO)_4]$, (RRE), have been known since the mid-nineteenth century [43–44]. They can be considered as the dinuclear form of a dinitrosyl iron complex, (DNIC) [35–46]. The structures of RRS, RRE and DNIC are shown below. RRS and RRE can be generated *in situ* by directly reacting nitric oxide with proteins containing [Fe–S] clusters, such as rubredoxin and ferredoxin [47]. They were discovered as being bound to the cysteine residues of proteins within body tissues [48]. In addition, the reactions of NO with [4Fe-4S] clusters of Wbl proteins and a Rieske-type protein form RRE [49]. Using synthetic model compounds of [2Fe-2S] and [4Fe-4S], the RRE species were also identified from these reactions [50–51].

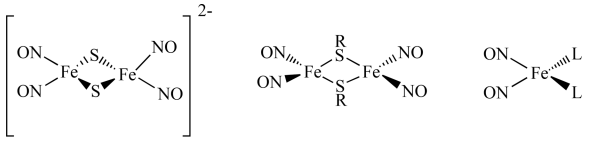

RRS RRE DNIC

RRE and RRS molecules have been tested for their effects on tumor cell growth and are efficient NO donors that lead to eventual cell death [52–53]. The bactericidal effect on the food-spoilage bacterium *Clostridium sporogenes* is effective in the millimolar range [54]. Some water-soluble RREs act as much slower yet higher stoichiometric NO-release agents with low cytotoxicity towards immortalized vascular endothelial cells [55–56]. Because of many recent discoveries of the biological activities of RRS and RRE, there is a renewed interest in preparing new types of RRS and RRE and investigating their properties.

2.1.1. Preparation and Spectroscopic Properties of RRS and RRE—RREs may be synthesized through the alkylation of Roussin's Red Salt (RRS) with an alkyl halide or treatment of $Fe_2(\mu\text{-}I)_2(NO)_4$ with an organic thiol compound in the presence of a proton acceptor as shown in Scheme 1[57].

Lippard *et al*. reported another way to synthesize RRE. An RRE with *t*-Bu, [Fe(S*t*Bu)$(NO)_2]_2$, **1**, was obtained from the reaction of excess NO with (Et_4N)[Fe(S*t*Bu)$_3$(NO)]. The latter was generated *in situ* by treating $(Et_4N)_2$[Fe(S*t*Bu)$_4$] with 1 mol-equiv of NO (g) at low temperature (Scheme 2) [58].

Recently we reported two different ways of preparing a series of Roussin's Red Salt Esters $[Fe_2(\mu\text{-SR})_2(NO)_4]$, **2**, (R = n-Pr, **2a**, t-Bu, **2b or 1**, 6-methyl-2-pyridyl, **2c**, and 4,6-dimethyl-2-pyrimidyl, **2d**). One method is to mix freshly prepared $Fe(NO)_2(CO)_2$ with equal molar amounts of the corresponding thiol ligands in the presence of potassium carbonate at room temperature for 72 h; and another way is to treat $Fe(NO)_2(CO)_2$ with equal molar of thiolate ligands at room temperature for 48 h (Scheme 3) [59].

The infrared spectra of these compounds were studied in detail in both KBr pellets and in THF solution. The typical IR absorptions of nitroysl groups (ν_{NO}) shifted from 1807, 1760 cm^{-1} to 1805–1823, 1770–1793 and 1743–1759 cm^{-1}, due to these sulfur-containing ligands only acting as weak electron donors. These RREs displayed one weak and two strong NO stretching frequencies in solution, but only two strong NO stretching frequencies in solid, attributed to the *trans*-isomer in solid state and the co-existence of *cis*- and *trans*- isomers in solution (Figure 1). The vibrational modes of the *cis*- and *trans*-isomers were further confirmed by the frequency calculations using Density Functional Theory (DFT). The calculated results for the *cis*- isomer showed four different vibrational modes, whereas the *trans*- isomer resulted in only two vibrational modes. The IR spectra of the *cis*- isomer simulated with Amsterdam Density Functional (ADF) software and plotted using different peak widths (Figure 2) indicated that the peak width and intensity overlap of the *cis*- and *trans*- isomers make the vibrational band at 1704 cm^{-1} unresolved. Hence, these complexes actually showed only three vibrational bands for the NO moieties in the experimental solution IR spectra.

The molecular structures of complexes were determined by X-ray diffraction analysis, which showed that all four complexes crystallized as the *trans*- isomer (Figure 3). Further theoretical calculations on geometry optimizations using DFT were also performed on the *cis*-and *trans*- isomers and the results showed that the transformation of the *cis*- and *trans*-isomers can be easily achieved because of the very small energy difference of ∼3 Kcal/mol (Figure 4).

The redox behavior of these complexes was studied by cyclic voltammetry (CV) in CH_2Cl_2. These complexes exhibited irreversible oxidations. Complexes **2a** and **2b** had two quasi-reversible one-electron reductions at −1.16, −1.84 V and −1.20, −1.81 V, respectively, but complexes **2c-2d** only showed one quasi-reversible one-electron reduction at −0.99 and −0.91 V, respectively (Figure 5). All of these reductions were attributed to iron-sulfur-based redox processes. The $E_{1/2}$ value for the first reduction peak became more positive (easier to reduce) in the order of **2b, 2a, 2c**, and **2d**. This is consistent with the reduced electron donor effect of the R group in this order. These results indicate that the electronic property of the R group of RREs significantly influences the electrochemical properties of the relevant complexes.

Using a similar method, Liaw's group also prepared monodentate-cysteine-containing peptides KCAAK-/KCAAHK-bound RREs by the addition of 1 equiv of $Fe(CO)_2(NO)_2$ to the aqueous solution of monodentate- cysteine-containing peptide KCAAK [60]. The water-soluble dinuclear species $[Fe(NO)_2S(CH_2)_2NH_3Cl]_2$, $[Fe(NO)_2S(CH_2)_2NH_3I]_2$, $[Fe(NO)_2LCEE]_2$ (LCEE = L-cysteine ethyl ester hydrochloride), and $[Fe(NO)_2pyrim]_2$ pyrim = pyrimidine-2-thiol) were obtained by Berke *et al*., and the possibility of using these compounds for NO donor prodrugs was studied. Electrochemical methodology was used in addition to the UV-vis method, which allowed the rate of NO release to be determined as ranging from 0.63×10^{-5}/mM to 1.62×10^{-5}/mM [61].

Vanin recently reported that binuclear forms of DNICs with thiol-containing ligands, i.e. cysteine or glutathione, could be easily prepared in vitro by the treatment of aqueous solutions of thiols with gaseous NO in the presence of Fe^{2+} ions at neutral pH [62–63]. Vincent *el al*. also showed that the [2Fe-2S] containing spinach ferredoxin I reacted with NO at pH 6.0, and generated more protein-bound RREs in addition to DNICs because of trace amount of O_2. RRE is also favored by nitrosylation in the presence of the thiolate scavenging reagent, iodoacetamide, suggesting that the role of O_2 is in oxidative sequestration of cysteine thiolates [64].

2.1.2. Photolytic Properties—The photochemistry of various RREs was investigated by Ford's group. The release of NO with moderate quantum yields (λ = 366 nm, Φ_{RES} = 0.02–0.13) was observed for the series of RREs of the form $Fe_2(SR)_2(NO)_4$ (where R = CH_3, CH_2CH_3, $CH_2C_6H_5$, CH_2CH_2OH, and $CH_2CH_2SO_3^-$) [65]. The RREs released ∼ 4 mol of NO per mole of cluster upon UV-vis photolysis. Nanosecond flash photolysis studies indicated that the initial photoreaction is the reversible dissociation of NO. In order to modify biological specificity and light-gathering properties, Ford's group also designed RRE derivatives that have pendant porphyrin chromophores. By varying the R group, Ford synthesized the supermolecular complex $Fe_2(NO)_4\{(\mu\text{-}S,\mu\text{-}S')P\}$, PPIX-RRE, **3**, (where (S,S')P is the bis(2-thiolatoethyl) diester of protoporphyrin IX, PPIX = 7,12-diethenyl-3,8,13,17-tetramethyl-2,18-porphine-dipropionic acid) [66]. The photochemical properties were investigated by both single-photon excitation (SPE) and two-photon excitation (TPE). The photoexcitation of PPIX-RRE in an aerated chloroform solution led to the photodecomposition of the cluster and release of NO with quantum yields of $(5.2 \pm 0.7) \times 10^{-4}$ and $(2.5 \pm 0.5) \times 10^{-4}$ for 436 and 546 nm, respectively. PPIX-RRE is a significantly more effective NO generator at longer wavelength excitation than other RREs for which R is a simple alkyl group [67].

Ford also prepared and investigated the photochemical properties of several water soluble dye derivatized $Fe_2(\mu\text{-}RS)_2(NO)_4$ compounds, such as Fluor-RRE, **4** [68], and AFX-RRE, **5**. Under continuous photolysis, the Fluor-RRE and AFX-RRE decomposed by releasing NO with moderate quantum yields [Φ (**4**) = 0.0036 and φ (**5**) = $(4.9 \pm 0.9) \times 10^{-3}$, at λ_{irr} = 436 nm]. TPE was also used to sensitize NO release from Fluor-RRE [69]. The attachment of a pendant dye chromophore as an antenna significantly improves the effective rate for photochemical NO generation, which draws the possibility of therapeutic applications of such compounds closer [70–71]. Chiou et al. also reported NO releasing and its cleavage of DNA, as well as anticancer activity of a water soluble RRE, $[Fe(NO)_2(\mu\text{-}SCH_2CH_2P(O)$

$(CH_2OH)_2)]_2$, prepared by the reaction of $Fe(NO)_2(CO)_2$ with $HSCH_2CH_2P(O)(CH_2OH)_2$ [72].

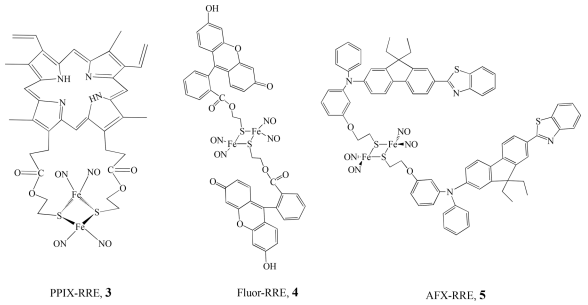

PPIX-RRE, **3** Fluor-RRE, **4** AFX-RRE, **5**

2.1.3. Reactions of RRE and RRS—The RRE can be reduced by adding one or two electrons forming the anionic form of RRE, $[Fe_2(\mu\text{-}RS)_2(NO)_4]^-$ or $[Fe_2(\mu\text{-}RS)_2(NO)_4]^{2-}$ (RRE^- or RRE^{2-}). The reduced species were prepared by the reaction of neutral $[Fe_2(\mu\text{-}RS)_2(NO)_4]$ with a slight excess of cobaltocene or $Li(BHEt_3)$ in THF as shown in Scheme 4. The IR spectra of the monoanionic complexes $[Fe_2(\mu\text{-}RS)_2(NO)_4]^-$ showed that the corresponding ν_{NO} bands are shifted by 100 cm^{-1} to a lower frequency in comparison with neutral species due to the negative charge (Figure 1).

Roussin's Red Salt Esters are diamagnetic and EPR-silent. The EPR spectra of the reduced species, $[Fe_2(\mu\text{-}RS)_2(NO)_4]^-$, exhibited an isotropic signal at g = 1.998 ~ 2.004 without hyperfine splitting in the temperature range from 180K to 298K (Figure 6). At even lower temperatures, such as 110K, complex **2a**$^-$ displayed an axial EPR signal at $g_\perp$ = 2.007 and $g_\parallel$ = 1.916. This is quite different from the typical DNICs. The main EPR characteristics of DNICs are the g values close to 2.03 and the hyperfine structures, which arise from the coupling between the unpaired electron and the nitrogen of the NO (^{14}N, I = 1, 99.6% natural abundance).

The spin density distributions of the singly occupied molecular orbit (SOMO) for the RRE^- and DNIC are shown in Figure 7. For the RRE^-, 60–63% of the electrons are delocalized on two irons, 25.0–25.8% of the electrons are delocalized on two sulfurs, and only 2–6% of the electrons are delocalized on four NOs. Because most of the unpaired electron density is delocalized over the Fe and S atoms and the most natural abundance of isotopes of these are ^{56}Fe and ^{32}S, whose nuclear spins (I) are zero, the lack of hyperfine splitting in the EPR spectra can be understood. The differences between the g values for RRE^- (~2.000) and the typical DNICs (2.03) can also be explained by the amount of electron density delocalized on Fe, which dictates the g value. The distribution of electron density on the SOMO of complex $[Fe(NO)_2(CO)_2]^+$ show that Fe and NO moiety possess 54.4% and 41.8% of the electron density, respectively. The calculated distribution of electrons on the iron in DNICs (54%) is lower than the values obtained by ^{57}Fe enriched EPR experiments on other g = 2.03 species [73] due to an over-delocalized distribution of the charge by DFT.

Recently, Liaw also reported the isolation of two reduced forms of RREs: $[(NO)_2Fe(\mu\text{-}SR)_2Fe(NO)_2]^-$ {R = t-Bu or Et; Cation = K(Na)-18crown-6-ether, PPN, or Me4N) [74–75].This anionic RRE^- can interchange with RRE in a protic solvent (MeOH). The same

group also isolated a double negatively charged RRE, $[PPN]_2[Fe_2(\mu\text{-}StBu)_2(NO)_2]$ [76]. The IR ν_{NO} stretching frequencies of $[PPN]_2[Fe_2(\mu\text{-}StBu)_2(NO)_2]$ shifted by $-30\ cm^{-1}$ from the reduced RRE $[(NO)_2Fe(\mu\text{-}StBu)]_2^-$. The UV-vis spectrum of the product displayed absorptions at 270 and 396 nm for $[PPN]_2[Fe_2(\mu\text{-}StBu)_2(NO)_2]$, while the reduced RRE $[(NO)_2Fe(\mu\text{-}StBu)]_2^-$ displayed an intense transition absorption around 982 nm.

The interconversion between RREs and DNICs was investigated by Liaw's group. They reported that the RRE $[Fe(\mu\text{-}SR)(NO)_2]_2$,**6**, (R = C_6H_4-o-NHCOPh, **6a**, and C_6H_4-o-COOH, **6b**) can transform into neutral DNICs by the addition of the Lewis base $[OPh]^-$ to the THF solution [77–78]. Using a combination of EPR spectroscopy and IR $\nu_{(NO)}$ stretching frequencies, the interconversion among the neutral $\{Fe(NO)_2\}^9$ complex $[(SC_6H_4\text{-}o\text{-}NHCOPh)(Im)Fe(NO)_2]$ (Im = imidazole), the anionic $\{Fe(NO)_2\}^9$ complex $[(SC_6H_4\text{-}o\text{-}NHCOPh)_2Fe(NO)_2]^-$, and the RRE was also studied (Scheme 4) [79].

Similarly, the formation of an RRS $[Fe_2(\mu\text{-}S)_2(NO)_4]^{2-}$ from a DNIC in aqueous solution was observed and the transformation of RRS back to $[HS]^-$ bound DNIC was followed by releasing H_2S. A similar transformation of another compound, $[Fe(NO)(SH)(\mu\text{-}S)]_2^{2-}$, **7**, was also reported (Scheme 5) [80]. The reaction pathway between RRE, $[(\mu\text{-}S(CH_2)_2NH_2)Fe(NO)_2]_2$, **8**, and mixed-thiolate-containing reduced RRE $[(\mu\text{-}SC_6H_5)(\mu\text{-}S(CH_2)_2NH3)Fe_2(NO)_4]^-$, **9**, via a DNIC was also studied and revealed that it was triggered by cysteamine (Scheme 6) [81].

2.1.4. Theoretical Calculations on RRE and RRS—Jawarska calculated the electronic structures, geometries and electronic spectra of an RRS dianion and RRE using the RB3LYP and UB3LYP methods. The electronic structure emerging from these calculations may be described as a composition of two $\{Fe(NO)_2\}^9$ units, in which ferric ion (S = 5/2) is antiferromagnetically coupled to two NO^- ligands (each with S = 1), giving S = 1/2; the units are antiferromagnetically coupled to each other yielding a total S = 0. The S^{2-} bridges (in RRS) or SR^- bridges (RRE) mediate the antiferromagnetic coupling. The calculated spectra of RRS and RRE showed excellent agreement with the experimental spectra [82].

A detailed theoretical study of spin couplings in RRS, based on broken-symmetry density functional theory (DFT, chiefly OLYP/STO-TZP) was presented by Ghosh *et al* [83]. Three nitrosylated binuclear clusters were studied: $[Fe_2(NO)_2(Et\text{-}HPTB)(O_2CPh)]^{2+}$ (Et-HPTB = N,N,N',N'-tetrakis-(N-ethyl-2-benzimidazolylmethyl)-2-hydroxy-1,3-diaminopropane), $[Fe(NO)_2\{Fe(NO)(NS))\}$-S,S'], and Roussin's red salt dianion $[Fe_2(NO)_4(\mu\text{-}S))]^{2-}$. These nitrosylated iron-sulfur clusters possess some exceptionally high Fe-Fe Heisenberg coupling constants (J) (J is defined by Heisenberg spin Hamiltonian: $\mathscr{H}$=JS(A)·S(B); J ≈ 10^2, 10^3, and $10^3\ cm^{-1}$, respectively).

2.2. Homodinuclear Cluster Linked by Sulfur (Not RRE or RRS)

2.2.1. {M(NO)$_2$} and {M(NO)} Centers Linked by Sulfur—In an effort to model the active site of the [Fe-Fe] hydrogenases, homodiiron nitrosyl complexes linked by sulfur mimicking Cys-X-Cys binding of $Fe(NO)_2$ to proteins or thio-biomolecules have been studied. Darensbourg's group has continued using bidentate dithiolate ligands, such as N_2S_2

{N_2S_2 = N ,N′ -bis(2-mercaptoethyl)-1,4-diazacycloheptane (bme-dach) or N ,N′ -bis(2-mercaptoethyl)-1,4-diazacyclooctane (bme-daco)}, and prepared a series of diiron nitrosyl complexes. Complex [(NO)Fe(bme-dach)Fe$(NO)_2$][BF_4], **10**, was obtained by direct mixing of [(bme-dach)Fe]$_2$ with the N-heterocyclic carbene containing trinitrosyliron complex [(IMes)Fe$(NO)_3$][BF_4], [IMes =1,3-bis(2,4,6-trimethylphenyl)imidazol-2-ylidene] as shown in Scheme 7 [84].

A reaction of [NO][BF_4] and complex [(NO)Fe$(SC_9H_6N)_2$] in a 1:1 stoichiometry led to the formation of complex (ON)Fe(μ-$SC_9H_6N)_2$Fe$(NO)_2$][BF_4]. The characterization by IR, UV-vis, ^{1}H-NMR and single-crystal X-ray diffraction indicated that the antiferromagnetic coupling between the two S= ½ {Fe(NO)}^{7} [S_2Fe$(NO)_2$] and [(NO)FeS_2N_2] cores may account for the EPR silence of the complex [85]. A few examples of asymmetric homodinuclear metal nitrosyls linked by S and SR were also reported. For instance, the diiron thiolate/sulfinate nitrosyl complexes [(ON)Fe(S,S-$C_6H_3R)_2$Fe$(NO)_2]^-$, **11**, (R = H, **11a**, 2-Me, **11b**) and [(ON)Fe(S,SO_2-C_6H_4)(S,S-C_6H_4)Fe$(NO)_2]^-$, **12**, were prepared by the reaction of Fe$(CO)_2(NO)_2$ and [(ON)Fe(S,S-$C_6H_3R)_2]^-$ or [(ON)Fe(SO_2,S-C_6H_4)(S,S-C_6H_4)]$^-$ in THF. Complexes **11** and **12** are best described as {Fe(NO)}^{7}-{ Fe(NO)2}^{9} with electronic coupling (antiferromagnetic interaction with a J value of - 182 cm^{-1} for complex **11a**) to account for the absence of paramagnetism (SQUID) and an EPR signal [86]. In metal nitrosyl complexes, the Enemark-Feltham notation {MNO}^{x}, where × represents the total number of electrons associated with the metal *d* and the π* (NO) orbitals, are commonly used due to the difficulty in determining the metal oxidation state [87]. Theoretical calculations by DFT method were carried out on diiron trinitrosyl complexes **10** and **11a**. The ground state energetics (singlet/triplet), geometric parameters, and nitrosyl vibrational frequencies were calculated and the results showed that complex **11a** is a singlet and complex **10** is a triplet, consistent with the experimental results [88].

2.2.2. {Fe(NO)$_2$} and {Fe(NO)$_2$} Linked by Mixed S and SR—The addition of Me_2S_3 (or $HSCPh_3$) to [$(NO)_2$Fe$(SEt)_2]^-$ resulted in the formation of anionic mixed thiolate-sulfide-bridged compound [$(NO)_2$Fe(μ-SEt)(μ-S)Fe$(NO)_2]^-$, **13** [89]. The electronic structures of **13** and the RRS were also investigated by S K-Edge X-ray absorption spectroscopy. These compounds are best described as [{$Fe^{III}(NO^-)_2$}^{9}-{ $Fe^{III}(NO^-)_2$}^{9}] according to the Enemark - Feltham notation [90].

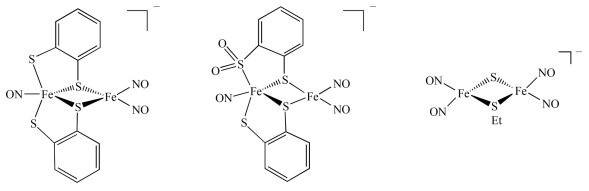

11 12 13

2.2.3. {M(NO)} and {M(NO)} Linked by Sulfur—Using ligands such as $PhPepSH_4$ and $Cl_2PhPepSH_4$, Mascharak's group prepared two diiron mononitrosyl compounds, $(Et_4N)_2$[{Fe(PhPepS)(NO)}$_2$], **14a**, and $(Et_4N)_2$[{Fe(Cl_2PhPepS)(NO)}$_2$], **14b**. They were obtained by reaction of excess NO with $(Et_4N)_2$[Fe(PhPepS)(Cl)] in aprotic solvents such as

MeCN and DMF as shown in Scheme 8 [91]. The photochemical properties were also investigated and relate to the photoregulation of Fe-NHase by NO [92].

Other types of diiron mononitrosyl complexes linked by sulfur $[(NO)Fe(S,S\text{-}C_6H_2\text{-}3,6\text{-}Cl_2)_2]_2$, **15**, and $[(NO)Fe(S,SO_2\text{-}C_6H_2\text{-}3,6\text{-}Cl_2)(S,S\text{-}C_6H_2\text{-}3,6\text{-}Cl_2)]_2^{2-}$ were obtained from sulfur oxygenation of the five-coordinated iron-thiolate nitrosyl complex containing the $\{Fe(NO)\}^6$ core [93]. The interconversions between the dinuclear complexes with the mononuclear complexes under sulfur oxygenation, redox processes, and photolysis were reported.

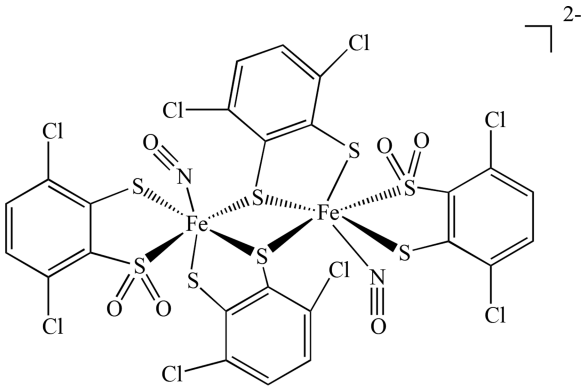

15

Lippard also reported a complex with two nickel mononitrosyl centers linked by a thiol ligand, $(Et_4N)_2[Ni_2(NO)_2(\mu\text{-}SPh)_2(SPh)_2]$, **16**. It was prepared by treating a solution of $(Et_4N)_2[Ni(SPh)_4]$ with 1 equiv of $NOBF_4$ in CH_3CN. The reaction stoichiometry was determined as 1 equiv of Ph_2S_2, 1 equiv of Et_4NBF_4, and 0.5 equiv of $(Et_4N)_2[Ni_2(NO)_2(\mu\text{-}SPh)_2(SPh)_2]$ (Scheme 9) [94]. The cobalt analogs of the RRE $Co_2(NO)_4(\mu\text{-}ER)_2$, (ER = S-t-Bu, Se-t-Bu, S-Bu, S-Et, S-Ph) was reported by Bitterwolf's group. They were synthesized by the reaction of organic thiol or selenol compounds with the readily prepared $[Co(NO)_2Cl]_2$. The compounds were only characterized by IR and Mass spectrometry as they are unstable in light and decompose even at a low temperature [95].

2.2.4. {M(NO)} and M Linked by Sulfur—In an effort to model the active site of the diiron hydrogenases, Rauchfuss's group reported nitrosyl derivatives of diiron dithiolato carbonyls. They were prepared starting from the precursor $Fe_2(S_2C_nH_{2n})(dppv)(CO)_4$ (dppv = cis-1,2-bis(diphenylphosphinoethylene) as shown in Scheme 10 [96]. Utilizing a $S_2C_nH_{2n}$ (n = 2, 3) ligand, the same group also synthesized a single NO bridged compound $[Fe_2(S_2C_3H_6)(\mu\text{-}NO)(CO)_4(PMe_3)_2]BF_4$, **17** (Scheme 11). The nitrosyl complexes undergo reversible reductions at −1.5 V versus Ag/AgCl, which is ∼1 V smaller (less negative value) than those of the related CO adducts [97]. Its structural and spectroscopic features were also investigated by DFT calculations and the results show that the primary spin density is delocalized over the {Fe(NO)} unit [98].

2.3. Homodinuclear Nitrosyl Complexes Linked by Bisphosphines

Examples of dimetallic metal nitrosyl complexes linked by bisphospines are limited compared with monometallic phosphine compounds [99–102]. One example was reported by us, in which several linear diiron species, $(NO)_2FeP\text{-}X\text{-}PFe(NO)_2$, **18**, [X = CH_2, **18a**, C≡C, **18b**, $(CH_2)_6$, **18c**, and *p*-C_6H_4, **18d**] were prepared from $Fe(NO)_2(CO)_2$ via addition of the desired ligand (Scheme 12). Depending on the reaction conditions employed, either linear diiron constructs connected by one bis(phosphine) linker, $(NO)_2FePPh_2\text{-}X\text{-}PPh_2Fe(NO)_2$, or macrocyclic species spanned by two bridging ligands, $[(NO)_2Fe]_2(PPh_2\text{-}X'\text{-}PPh_2)_2$, **19** (X' = CH_2, **19a**, C≡C, **19b**), can be obtained [103]. The iron-iron distances in both the linear and macrocyclic compounds are all significantly longer than the related distances found in other structurally characterized species that are described as possessing a metal-metal bond.

Based on the observed IR frequencies, the nitrosyl groups are best described as linear donating NO^+ fragments. In both the solid and liquid states, the macrocyclic DPPM-supported complex exhibited four distinct IR absorptions (1733, 1721, 1687, and 1668 cm^{-1}), while the related ten-membered ring compound containing DPPA displayed only two nitrosyl stretching signals (1723 and 1679 cm^{-1}). This is attributed to the ring sizes which affect the interaction of the two $Fe(NO)_2$ centers. Table 1 lists common spectroscopic data for selected compounds.

2.4. Homodinuclear Nitrosyl Complexes Linked by N/O/C

2.4.1. {M(NO)$_2$} and {M(NO)$_2$} Centers—The two metal nitrosyl centers can also be connected through nitrogen or oxygen atoms in addition to sulfur. Several N/O linked diiron dinitrosyl complexes $[Fe_2(SC_6H_4\text{-}o\text{-}NHC(O)Ph)_2(NO)_4]$ were obtained by varying the ligand structure slightly [104]. They were all synthesized by the reaction of $Fe(CO)_2(NO)_2$ with bis(o-benzamidophenyl) disulfide in good yield and the product was characterized by ^1H NMR, IR, and UV-vis spectra.

A dinuclear iron nitrosyl complex with N,S linkage $[Fe_2(C_{14}H_{12}N_3S)_2(NO)_4]$, **20**, was prepared by Li's group [105]. The complex, shown in Figure 8, was characterized by IR, UV-vis, electrochemistry and single crystal X-ray diffraction. It possesses a "chair-shape" structure from the connections between two iron centers with the S-C-N frames of benzimidazole. The redox behavior of complex **20** was studied by CV in CH_2Cl_2 with $[NBu_4][PF_6]$ as the supporting electrolyte. The complex showed irreversible oxidations, consistent with the fact that the complex is very unstable and ready to lose NO in air. Complex **20** exhibited two reversible one-electron reductions at −1.44, −2.06V, two quasi-reversible one-electron reductions at −1.02, −1.16V and one irreversible reduction at −0.72V. All of these reductions can be attributed to iron-sulfur-nitrogen-based and ligand-based redox processes. Comparing with other RREs, such as **2**, complex **20** possesses more reduction processes and less negative value for the first reduction peak, showing that complex **20** is easier to be reduced as its ligand has a smaller electron donor effect. Another binuclear nitrosyl iron complex bridged by N,S ligand benzimidazole-2-thiolyl $[Fe_2(SC_7H_5N_2)_2(NO)_4]\cdot 2C_3H_6O$ was reported by Sanina's group. The structure and

properties were studied by using X-ray, Mössbauer, IR, mass spectrometry, and SQUID-magnetometry [106].

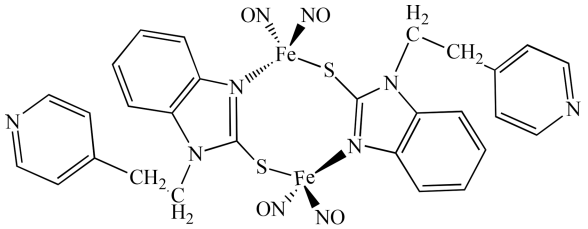

20

Recently Liaw reported the X-ray crystal structure of $[Fe(NO)_2(\mu\text{-}OPh)]_2^{2-}$, **21**, the first diiron nitrosyl linked by oxygen atom. It was prepared from $[(NO)_2Fe(OPh)_2]^-$ through one electron reduction (Scheme 13). Compound **21** is best described as $\{Fe(NO)_2\}^{10}$-$\{Fe(NO)_2\}^{10}$ according to the Enemark - Feltham notation. This μ-oxo diiron compound can be converted to RRE^{2-} by addition of $[St\text{-}Bu]^-$[107].

A dinuclear complex $[Fe(NO)_2(\mu\text{-}SC_6H_4\text{-}o\text{-}N(CH_3)_2)(\mu\text{-}CO)Fe(NO)_2]^-$, **22**, with mixed thiolate-CO-bridged ligands was isolated (Scheme 14) and characterized by IR, UV- vis, EPR, and X-ray crystallography [108]. This complex possesses the butterfly-like [Fe(μ-S)(μ-CO)Fe] core with a shorter Fe-Fe distance of 2.5907 Å due to the shorter Fe-S and Fe-C bond distances and is best described as $[\{Fe(NO)_2\}^{10}$-$\{Fe(NO)_2\}^{10}]$.

Lippard's group also investigated reactions between cobalt(II) complexes containing tetraazamacrocyclic tropocoronand (TC) ligands and nitric oxide and reported that a bis(cobalt dinitrosyl) complex $[Co_2(NO)_4(TC\text{-}6,6)]$, **23**, was formed when [Co(TC-6,6)] was exposed to gaseous NO [109]. The end product depended on the ring size: in the same reaction with [Co(TC-5,5)], only the mononitrosyl complex [Co(NO)(TC-5,5)] was isolated.

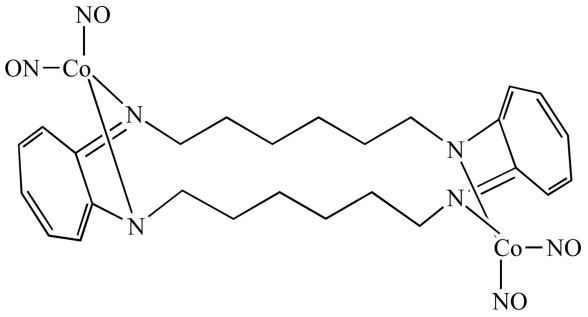

23

2.4.2. {M(NO)} and {M(NO)} Centers—The importance of flavodiiron nitric oxide reductases (FNORs) for bacterial pathogenesis and their ability to detoxify NO has prompt scientists to investigate the mechanism of NO reduction by these enzymes [110–114]. Recently, Lehnert and co-workers reported the isolation of a diiron dinitrosyl model complex $[Fe_2(BPMP)(OPr)(NO)_2](BPh_4)_2$, which was prepared from treating the diferrous precursor complex $[Fe_2(BPMP)(OPr)](BPh_4)_2$ with NO(g) in an anaerobic solution [115]. The crystal structure of this complex showed two end-on-coordinated $\{FeNO\}^7$ units, and

each iron center is coordinated by two pyridine units and shared phenolate and propionate bridges to generate a pseudo-octahedral geometry. Both $\{FeNO\}^7$ units (each S = 3/2) are weakly antiferromagnetically coupled. This complex represents the first example of a functional model system for FNORs as two electrons reduction leads to the clean formation of N_2O in quantitative yield. Another structurally characterized non-heme diiron dinitrosyl complex is $[Fe_2(Et\text{-}HPTB)(O_2CPh)(NO)_2](BF_4)_2$, where Et-HPTB = N,N,N',N'-tetrakis-(N-ethyl-2-benzimidazolylmethyl)-2-hydroxy-1,3-diaminopropane, reported by Lippard *et al*. [116]. Recently, on the basis of Resonance Raman and low-temperature photolysis FT-IR data, the diferrous site of an FMN-free FDP (flavodiiron protein) from *Thermotoga maritima* (Tm deflavo-FDP) triggering the turnover of 2NO to N_2O via a NO-semibridging $Fe^{II}(\mu\text{-}NO)Fe^{III}$ intermediate was proposed [117].

2.4.3. Organometallic Examples—NO can coordinate with metals in either bridging or terminal fashion. The latter can also have a variety of configurations, as manifest by M-N-O angles ranging between 120 and 180°. Typically, M-N-O angles between 160–180° are considered as linear (NO^+) and 120–140° are considered as bent (NO^-). For example, a nitrosyl-bridged dinuclear complex [Cp*Ru(μ-NO)$_2$RuCp*], **24**, was characterized by X-ray crystallography, which revealed that the bridging nitrosyl ligands in the complex form an almost planar Ru_2N_2 four-membered ring with the Ru–Ru distance of 2.5366(5) Å [118]. The addition of *i*PrNi^{I}NO (*i*Pr = N,N'-bis(2,6-diisopropylphenyl)imidazole) to 1% Na/Hg in ether (1:1 ratio) resulted in a dinuclear complex{*i*PrNi}$_2$(μ-NO)(μ-I), **25** [119]. Single-crystal X-ray structure shows a relatively short Ni-Ni bond at 2.314(1) Å.

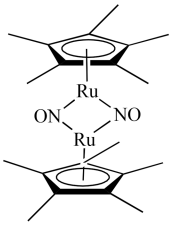

24

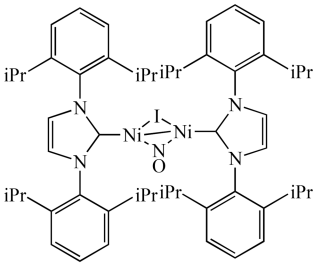

25

Han and Kadish reported the synthesis and X-ray crystal structures of two neutral diruthenium complexes $[Ru_2(dpf)_4(NO)]$, **26**, and $[Ru_2(dpf)_4(NO)_2]$ (dpf = diphenylformamidinate anion). Their electrochemical and spectroscopic properties were also investigated together with a reduced anionic diruthenium complex **26**$^-$ through *in-situ* FTIR spectroelectrochemistry [120]. Recently the same group also reported the effect of axial ligands on the spectroscopic and electrochemical properties of several diruthenium compounds $[Ru_2(dpb)_4(X)]$, (X = Cl, CO, NO) [121]. $[Ru_2(dpb)_4(NO)]$ undergoes two successive one-electron reductions and a single one-electron oxidation, all of which involve the diruthenium unit. These two complexes were further characterized by FT-IR spectroelectrochemistry.

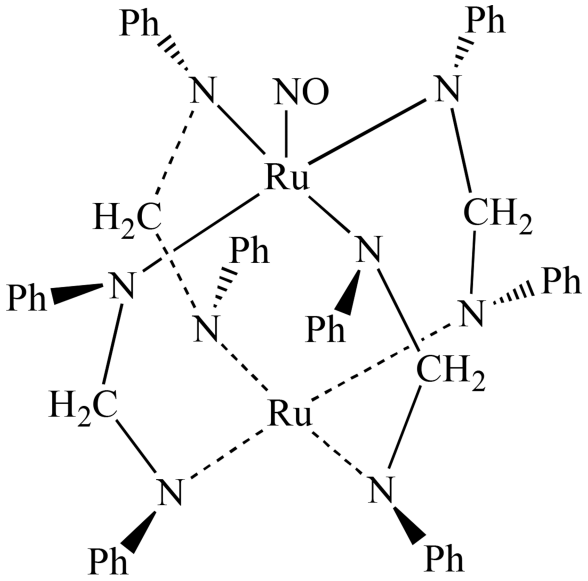

26

A bimetallic nitrosyl compound, $[cat]_3[Pt_2(\mu\text{-}pop)_4(NO)]$ was obtained from chemical oxidation of $[cat]_4[Pt_2(\mu\text{-}pop)_4]$ ($cat^+ = Bu_4N^+$ or $PPN^+ = [Ph_3P{=}N{=}PPh_3]^+$; pop = pyrophosphite, $[P_2O_5H_2]^{2-}$ with $[NO][BF_4]$. The X-ray structure showed that the anion possesses the usual lantern-shaped $Pt_2(\mu\text{-}pop)_4$ framework with a large Pt-Pt distance [2.8375(6) Å]; and that one of the platinum atoms has a bent nitrosyl group occupying an axial position. The X-ray photoelectron (XP) spectrum confirmed the presence of two inequivalent platinum atoms [122]. However, the nitrosyl group exhibited fluxionality on the NMR time-scale and migrated between the metal atoms at room temperature.

2.5. Heterobimetalic Nitrosyl Complexes

2.5.1. Linked by Sulfur—The heterobimetallic nitrosyl compounds ligated by sulfur atoms is of potential importance in understanding the mode of action of enzymes containing such structures at their active site, e.g. nitrogenase with its $MoFe_7S_9$ cofactor [123], hydrogenase with two iron or nickel and iron atoms bridged by two sulfurs [124–126], and nitrile hydratase with an iron or cobalt centre ligated by three cysteinyl sulfurs [127–128]. For instance, The NiFe hydrogenase from *D. gigas* catalyses the reversible oxidation of molecular hydrogen. This enzyme utilizes a binuclear complex as the active site, in which one Ni and one Fe atom are covalently linked by the S atoms of two cysteine residues and by one unidentified ligand [129–130]. These observations prompted many researchers to search for synthetic pathways to binuclear, μ-S thiolate bridged NiFe complexes in which NO binds to an Fe atom.

Continuing from some earlier work on heterobimetallics of nickel-iron dinitrosyl complexes [131–132], Bouwman reported that when the nickel complex [Ni(xbsms)] [H_2xbsms = α,α‘-bis(4-mercapto-3,3-dimethyl-2-thiabutyl)-o-xylene] reacted with $[Fe(CO)_2(NO)_2]$, the heterodinuclear nitrosyl complex $[Ni(xbsms)Fe(NO)_2]$, **27**, was isolated [133].

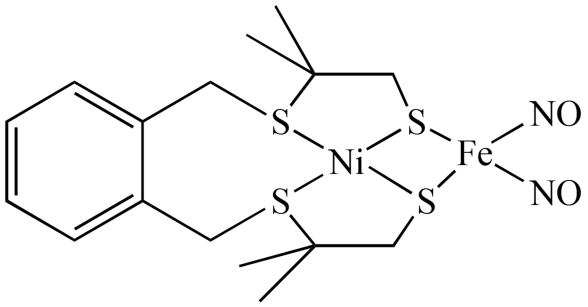

27

Utilizing metallodithiolates Ni(N_2S_2) as ligands that bear similarity in their first coordination sphere to the NHase biological site, Darensbourg's group reported several new heterobimetallic nitrosyl compounds [134]. The reaction of $Fe(CO)_2(NO)_2$ and Ni(N_2S_2) (N_2S_2 = bem-dach) by a single CO replacement yielded [Ni(N_2S_2)]$Fe(NO)_2(CO)$, **28**, (Scheme 15) while an excess of $Fe(CO)_2(NO)_2$ led to triply bridging thiolate sulfurs in a cluster of core composition $Ni_2S_4Fe_3$ [135].

Recently, the same group also synthesized two additional compounds, {Ni(bme-daco)[$Fe(NO)_2I]_2$]}, **29**, and [V≡O(bme-daco)·$Fe(NO)_2I$], **30**. They were prepared by mixing metalloligand, Ni(bme-daco) or V≡O(bme-daco) with ∼1:3 ratio of $(\mu\text{-}I)_2[Fe(NO)_2]_2$ in THF (Scheme 16) [136]. The EPR studies showed that both **29** and **30** are EPR silent due to strong coupling between paramagnetic centers, despite the relatively long distance of V⋯Fe (3.75 Å). These complexes can dissociate to form the solvated (solv)$Fe(NO)_2I$ centers, which exhibit hyperfine couplings between ^{127}I with the unpaired electron on the iron center.

By a similar approach, the Co–Fe bimetallic complex [(NO)Co(bme-dach)(IMes)$Fe(NO)_2$][BF_4], **31**, was also reported (Scheme 17) [137]. Comparing with the homobimetallic complex **10** discussed earlier, the Co-Fe distance is 3.697 Å, which is much longer than the Fe–Fe bond distance of 2.7857(8) Å in the homobimetallic complex. The addition of $W(CO)_4$ to [(N_2S_2)M(NO)] (M =Ni, Fe and Co; N_2S_2 = bme-dach) generated [(N_2S_2)M(NO)]$W(CO)_4$, **32**. These complexes have two IR vibrational probes ($\nu_{(NO)}$ and $\nu_{(CO)}$) for (N_2S_2)M(NO) complexes [138–140].

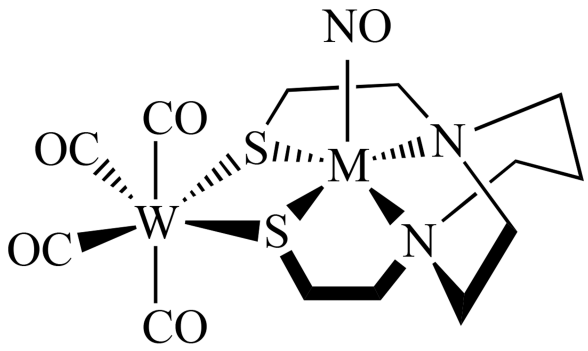

M = Ni, Fe, Co

32

There are also some organometallic examples of bimetallic nitrosyl complexes. For instance, Ishii and co-workers synthesized a series of the bis(sulfido)-bridged heterobimetallic complexes [Cp*M(PMe_3)(μ-S)$_2$M'(NO)Cp*], **33**, (M = Rh, Ir; M' = Mo, W) from the reaction of the group 9 bis(hydrosulfido) complexes [Cp*M($SH)_2$(PMe_3)] (M = Rh, Ir) with the group 6 nitrosyl complexes [Cp*M'Cl_2(NO)] (M' = Mo, W) in the presence of NEt_3. Further methylation of the Rh-Mo complex resulted in S-methylation, giving the methanethiolato complex [Cp*Rh(PMe_3)(μ-SMe)(μ-S)Mo(NO)Cp*]$^+$, **34** (Scheme 18) [141]. Similar reactions of the group 10 bis(hydrosulfido) complexes [M($SH)_2$(dppe)] (M = Pd, Pt; dppe = Ph_2 P($CH_2)_2PPh_2$), and [M($SH)_2$(dpmb)] (dpmb = o -C_6H_4 ($CH_2PPh_2)_2$) give rise to the group 10-group 6 complexes [(dppe)M(μ-S)$_2$M'(NO)Cp*], (M = Pd, Pt; M' = Mo, W) and [(dpmb)M(μ-S)$_2$M'(NO)Cp*] [142]. The Pt-W complex undergoes either S- or O-methylation to form a mixture of [(dppp)Pt(μ-SMe)(μ-S)W(NO)Cp*][OTf], and [(dppp)Pt(μ-S)$_2$W(NOMe)Cp*][OTf], (OTf = OSO_2CF_3).

2.5.2. Linked by N/O—Kostin et al. isolated heteronuclear complexes of [RuNO($NO_2)_4$OHM($Ph_3PO)_3$], **35**, from the reaction of nitrosotetranitrohydroxy-ruthenate ions and M^{2+} (M = Ni, Co, and Zn) in the presence of Ph_3PO [143]. In these complexes, the distorted octahedral coordination sphere of the nonferrous metal is composed of three oxygen atoms from phosphine oxide ligands and three oxygen atoms bridging OH and NO_2 groups from [RuNO($NO_2)_4$OH]$^{2-}$. Some theoretical investigations of the activation and cleavage of the N-O bond in dinuclear mixed-metal nitrosyl systems, such as [($NH_2)_3$M–NO–M'($NH_2)_3$], (M = Cr, or M; M' = V or Nb) were also reported by Stranger [144].

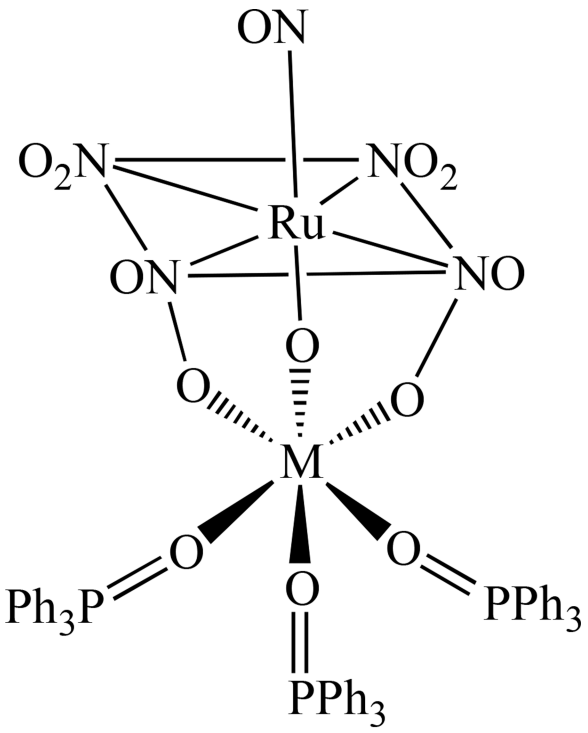

35

3. Trinuclear Metal Nitrosyl Complexes

3.1. Bridged by Sulfur

There are only a few reported metal nitrosyl compounds with three metal centers. For example, Liaw *et al*. prepared a trinuclear iron-thiolate-nitrosyl complex containing a core of Fe_3S_6. The neutral trinuclear iron-thiolate-nitrosyl, $[(ON)Fe(\mu\text{-}S,S\text{-}C_6H_4)]_3$, **36**, was synthesized by the protonation of the mononuclear iron-thiolate-nitrosyl [PPN][$(NO)Fe(S,S\text{-}C_6H_4)_2$] by HBF_4 in THF (Scheme 19) [145]. The cationic species $[(ON)Fe(\mu\text{-}S,S\text{-}C_6H_4)]_3[PF_6]$ obtained from the oxidation of this complex is diamagnetic. Various spectroscopic (IR, UV-vis, EPR, NMR), magnetic, and Fe/S/N K-edge X-ray absorption spectroscopy (XAS) measurements indicated that the unpaired electron is mainly allocated in one of the iron atoms and is best described as $\{Fe(NO)\}^7$.

Recently, Lippard and co-workers reported the isolation of a trimetallic cobalt nitrosyl complex $[Co(NO)_2(SPh)]_3$, **37**. It was prepared by the addition of stoichiometric Me_3OBF_4 to $(Et_4N)[Co(NO)_2(SPh)_2]$ in CH_3CN (Scheme 20) [146]. This compound is diamagnetic, with structural parameters and spectroscopic features similar to that of Roussin's black salt, RBS.

3.2. Bridged by N/O/C

A series of linear trinuclear palladium nitrosyl complexes with η^2-coordinated arene molecules having formula of $Pd_3(NO)_2(\mu\text{-}RCO_2)_4(\eta^2\text{-arene})_2$, **38**, (R = CF_3, arene = toluene, R = CCl_3, arene = benzene) was reported by Sromnova [147–148]. The substitution of arene by η^2 - coordinated alkenes generated $Pd_3(NO)_2(\mu\text{-}CF_3CO_2)_4(\eta^2\text{-L})_2$, (L = $Me_3CCH{=}CH_2$, $CH_2{=}CHPh$) and $Pd_4(\mu\text{-}NO)_2(\mu\text{-}CF_3CO_2)_4(\eta^2\text{-}CH_2{=}CHPh)_4$. X-ray diffraction analysis showed that the metal atoms form a linear chain in which each terminal atom is linked to the central atom via two bridging trifluoroacetate groups. The nitrosyl ligands are coordinated to the terminal palladium atoms in a bent end-on fashion [149].

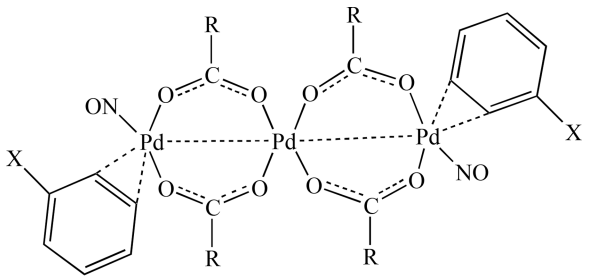

R = CF_3, CCl_3 ; X = Me, H

38

Earlier work by Slep showed that the $\{RuNO\}^6$ fragment could be incorporated into a dinuclear species that behaved as a donor acceptor (D–A) system, similar to the mixed-valent systems [150]. Continuing this work, the same group reported a linear homotrinuclear compound trans-$[ClRu(py)_4(NC)Ru(py)_4(CN)Ru(py)_4(NO)](PF_6)_4$, **39**, which was prepared by reaction between the nitro complex trans-$[(NC)Ru(py)_4(CN)Ru(py)_4(NO_2)]^+$ and the solvento complex obtained by reaction between $[ClRu(py)_4(NO)]^{3+}$ and N^{3-} in acetone (Scheme 21). The new complex was investigated through spectroscopic methods, spectroelectrochemistry, and supplemented by DFT calculation. The one-electron reversible reduction at 0.49 (acetonitrile) or 0.20 V (water) *vs* AgCl/Ag is centered on the nitrosyl moiety, while oxidation at 0.71 or 0.57 V *vs* AgCl/Ag occurs on the chlororuthenium side of the molecule [151].

4. Tetranuclear Metal Nitrosyl Complexes

4.1 Linked by Sulfur

The most commonly studied tetranuclear metal nitrosyl compounds are the Roussin's black salt (RBS) type clusters. It was first produced by the reaction of nitrous acid, potassium hydroxide, potassium sulfide, and iron(II) sulfate in aqueous solution [152]. RBS is well known as a broad-spectrum antimicrobial agent that has been used for more than 100 years to combat pathogenic anaerobes. It consists of four irons, three sulfurs, and seven nitrosyls, as shown below. It is one of the few iron-sulfur clusters that possess the sulfur-voided $[Fe_4S_3]$ cuboidal subunit found in the FeMo cofactor of nitrogenase [153].

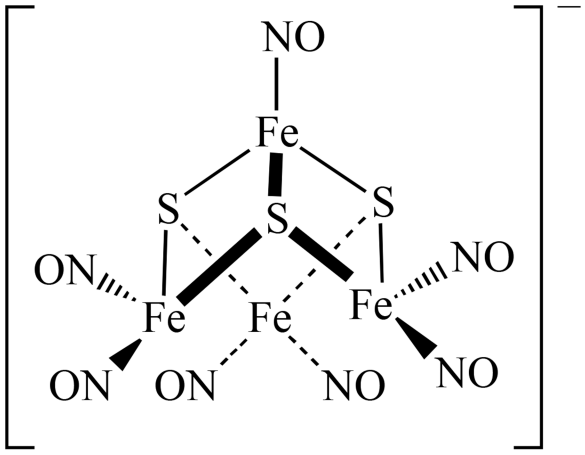

RBS

4.1.1. Biological Activities of RBS—Roussin's black salt is a nitric oxide donor. The NO donated by RBS has proven to be toxic to some melanoma cancer cells [154]. Since the discovery that RBS causes rapid relaxation of smooth muscle cells in the *taenia coli* upon photon release of NO [155], there have been many studies related to the biological activities of RBS [156]. For instance, RBS releases approximately 3.7 moles of NO per one mole of RBS after irradiated with UVA (300–420 nm, max 354 nm, 2.0mW/cm^2) for 5–30 min. Both short- and long-term effects of photogenerated NO were investigated on the two neoplastic cell lines: human (SK-MEL188) and mouse (S91). Exogenous NO from the RBS is toxic to cells in a dose-dependent manner. NO and its short-lived metabolites are responsible for cellular death. The RBS in dark is toxic to those cancer cells at concentrations above 1 μM. The antimicrobial activity of the RBS on the hyperthermophilic archaeon *Pyococcus furiosus was* also reported [157].

In addition, it is known that iron–sulfur clusters react with NO to regulate intracellular iron levels, and the oxidative stress response involves degradation of the clusters to generate protein-bound or low-molecular-weight dinitrosyliron complexes, which can trigger protein conformational changes by binding these proteins to DNA and other cellular targets [158]. Several of the regulatory proteins known to respond to NO contain iron-sulfur clusters that function as the sensory module [159].

4.1.2. Synthesis and Spectroscopic Properties of RBS—It is known that RBS can be synthesized by the conversion of RRS in mildly acidic conditions. This reaction is reversible and RRS can be reformed upon alkalization of the reaction solution. Liaw recently showed that dinitrosyl iron complexes $[E_5Fe(NO)_2]^-$ (E = S, Se) could also serve as a precursor of Roussin's black salt $[Fe_4E_3(NO)_7]^-$ and the conversion can be achieved by adding acid HBF_4 or oxidant $[Cp_2Fe][BF_4]$ in THF [160].

Recently, we reported a new solvent-thermal method to prepare RBS. A tetranuclear cluster $(Me_4N)[Fe_4S3(NO)_7]$, was isolated from heating a mixture of $FeCl_2$ $4H_2O$, thiourea, $(CH_3)_4NCl$, and $NaNO_2$ in methanol at 85°C for 48 hours, as shown in Scheme 22 [161].

The IR spectrum of this complex showed three stretching frequencies at 1799, 1744 and 1710 cm^{-1}. The CV of the compound had three quasi-reversible reductions with half-wave potentials of −1.09, −1.71, and −2.21 V *vs* ferrocene/ferrocenium ion in 0.1 M $(NBu_4)(PF_6)$ in CH_3CN. X-ray crystal structure of the complex showed the average Fe-Fe distance is 2.705 Å, which is clearly shorter than the relevant value of 2.764 Å for dianion $[Fe_4S_3(NO)_7]^{2-}$. This difference was explained by the antibonding character of the HOMO of $[Fe_4S_3(NO)_7]^{2-}$. However, the counter ion showed no effect on the structure parameters.

Sheppard *et al*. summarized the characteristics of vibrational spectra for various modes of NO bonding to metal clusters with relation to the X-ray structures. Some of the factors examined were: modes of bonding, charge, electron withdrawing co-axial groups, solvents, *etc* [162]. In addition to the values of $\nu(^{14}NO)$ themselves, the isotopic band shift—{defined as $[\nu(^{14}NO)\text{-}\nu(^{15}NO)]$}, and the isotopic band ratio $[\nu(^{15}NO/\nu^{14}NO)]$, could also be used as criteria to distinguish between linear and bent NO groups.

Using semi-empirical quantum chemical methods, Stasicka's group calculated possible products for reactions of the RBS anion and a series of pseudo-cubane complexes with S-donor or N-donor ligands [163]. The results justify the hypothesis that a pseudo-cubane adduct, $[Fe_4(\mu_3\text{-}S)_3(\mu_3\text{-}SR)(NO)_7]^{2-}$ will form. The same group also reported the calculations of the electronic structure, geometry, and electronic spectra of the RBS anion using the RB3LYP and UB3LYP methods [164]. A detailed theoretical study of spin couplings in RBS, based on broken-symmetry density functional theory (DFT, chiefly OLYP/STO-TZP) calculations, was presented by Ghosh *et al*. [83] The electronic structure of the RBS may be described as composed of the one $\{Fe(NO)\}^7$ unit, in which ferric ion (S = 5/2) is antiferromagnetically coupled to a NO^- ligand (S = 1) giving S = 3/2; such a unit is antiferromagnetically coupled to three $\{Fe(NO)_2\}^9$ units, each of which is formed by a ferric ion (S = 5/2) antiferromagnetically coupled to two NO^- ligands with S = 1. The resulting total spin of RBS is S = 0. The S^{2-} bridges mediate the antiferromagnetic coupling. The calculated UV-vis transitions were mainly of charge transfer character, that is consistent with the experimental observations.

4.1.3. The RBS Identified from the Reaction of NO with [Fe-S] Clusters—It is known that [4Fe-4S] clusters serve as targets of reactive nitrogen oxide species in biology; thus researchers have used natural [4Fe-4S] proteins to investigate these reactions. For instance, in one study using recombinant *Pyrococcus furiosus* ferredoxin (D14C mutant), the EPR-silent $[Fe_4S_3(NO)_7]^-$ was detected as the major product by nuclear resonance vibrational spectroscopy (NRVS) [165]. Using combination of NRVS and EPR-spectroscopic techniques, Lippard and others showed that the major products in nitrosylating specific [Fe-S] proteins are the diamagnetic species, e.g. RRE, RRS, or RBS, in addition to the DNIC with a characteristic EPR signal g = 2.03 [166].

Using synthetic model [4Fe-4S] clusters, possible pathways for the reactions of iron-sulfur clusters with nitric oxide in biological systems have been studied. Lippard reported that $[Fe_4S4(SR)_4]^{2-}$ (R = Ph, CH_2Ph, t-Bu, or 1/2 (CH_2)-m-C_6H_4) reacts with NO(g) and proceeds in the absence of added thiolate to yield a RBS [167]. In contrast, $(Et_4N)_2[Fe_4S_4(SPh)_4]$ reacts with NO(g) in the presence of 4 equiv of $(Et_4N)(SPh)$ yielding the expected DNIC. Recently, Lippard also prepared site-differentiated synthetic models for the biological [4Fe-4S] clusters $[Fe_4S_4(LS_3)L']^{2-}$ (LS_3 = 1,3,5-tris(4,6-dimethyl-3-mercaptophenylthio)-2,4,6-tris(p -tolylthio)benzene; L′ = Cl, SEt, SPh, N_3, 2-SPyr, Tp, S_2CNEt_2) and studied their reactivity toward NO(g) and Ph_3CSNO [168]. In all cases, the reactions proceed via formation $[Fe_4S_4(NO)_4]^-$, **40**, (S = 1/2) species, which ultimately converts to RBS.

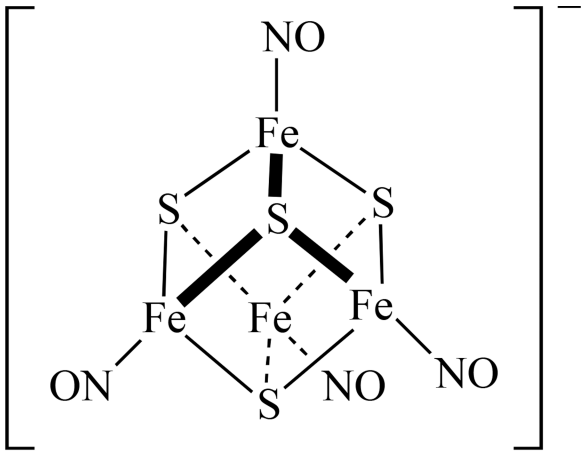

40

The transformations between DNICs with iron sulfur nitrosyl clusters were investigated [169]. A reaction of $[(NO)_2Fe(SR)_2]^-$ (R = Et, Ph) with S_8 and HBF_4 yielded RBS, which was reduced by [Na][biphenyl] to generated reduced RBS^-, $[Fe_4S_3(NO)_7]^{2-}$, which further converted into complex **40**, along with byproduct $[(NO)_2Fe(SR)_2]^-$ upon treating with $[Fe(SPh)_4]^{2-}$ and S_8 (Scheme 23). This tetranuclear cluster, **40**, was characterized by IR, UV-vis, and single-crystal X-ray diffraction.

4.1.4. Other Tetranuclear Complexes Linked by Sulfur (Not RBS)—Two methods of making $(PPN)_2[Fe_4S_4(NO)_4]$ were reported by Coucouvanis [170]. One is by using a 1:2 ratio of $(PPN)[Fe_4S_3(NO)_7]$ and $(PPN)_2[Fe_4(CO)_{13}]$ in MeCN, followed by the addition of Bu_4NSH, and heating the mixture under reflux for 24 h. Another method is to add excess of Bu_4NSH in $(PPN)_2[Fe_8S_6(NO)_8]$ in DMF and heated at 80 °C for 24 h. The same group also isolated a tetrasulfidotetrairon-hexanitrosyl cluster $(PPN)_2[Fe_4S_4(NO)_6]$, **41**. It was synthesized by mixing $(NH_4)[Fe_4S_3(NO)_7]$ and $(PPN)_2[Fe_4(CO)_{13}]$ in ∼1:2 ratio in MeCN and followed by the addition of Bu_4NSH. The mixture was allowed to react for 8 h at −20 °C to isolate the product.

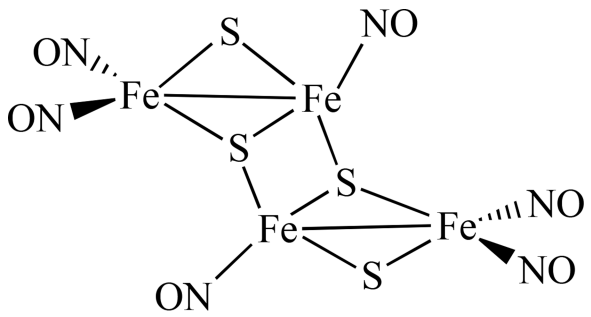

41

Liaw *et al* reported synthesis of $[Fe_4(\mu_3\text{-}S)_2(\mu_2\text{-}NO)_2(NO)_6]^{2-}$, **42**, through the reaction of $[Fe_2(\mu_2\text{-}S)_2(NO)_4]^{2-}$ with two equiv. of [(TMEDA)Fe(NO)$_2$] (TMEDA = tetramethylethylenediamine) in CH_3CN (Scheme 24). The $Fe_4S_2NO_8$ complex posesses both bridging and terminal NO ligands [171]. The complex **42** with semi-bridging nitroxyls acts as a key intermediate in the transformation of the RRS into RBS. The IR ν_{NO} and ^{15}N NMR spectra recorded at various temperatures indicated that this complex is fluxional, scrambling terminal and bridging NO ligands at an elevated temperature. Such a fluxional behavior was also noticed earlier in a triiron hexanitrosyl cluster [73].

Utilizing a chelating ligand, Darensbourg reported that the reaction of PPN[$FeI_2(NO)_2$] with Na_2S_3' (S_3' = $S(CH_2)_2S(CH_2)_2S$) in a 1:1 mixture of MeOH/THF resulted in a tetranuclear $Fe_4(S_3')_2(NO)_8$ and its structure was established by X-ray crystallography [172]. Le Brun and co-workers proposed the formation of a tetranuclear octanitrosyl complex $[Fe_4(NO)_8(Cys)_4]$ (Cys = systeine) from the nitrosylation reaction of the [4Fe-4S] cluster of WhiB-like proteins. Further DFT calculations based on model complexes indicated that such a species may be stable [173].

4.2. Linked by N/O/C

The first tetranuclear nitrosyl complex linked by nitrogen atoms, $Fe_4(NO)_8(Im\text{-}H)_4$, **43**, was reported by Li and Ford. It was synthesized by mixing one equivalent of $Fe(NO)_2(CO)_2$ with two equivalents of imidazole (Im) in methylene chloride at room temperature under a nitrogen atmosphere [174]. Two similar complexes [(2-isopropylimidazole)$Fe(NO)_2]_4$ and [(benzimidazole)$Fe(NO)_2]_4$ were prepared by Darensbourg [175]. The X-ray crystal structure shows four iron centers that are linked together through four deprotonated imidazole bridging ligands forming a neutral 16-membered rhombic macrocycle with alternating imidazolates and irons as shown in Figure 9. Each iron center possesses a pseudo-tetrahedral geometry and is coordinated to four nitrogen atoms–two from the nitrosyl ligands and two from the imidazolate ligands (Im-H). The molecule has dimensions of 8.18 × 8.70 Å (Fe1⋯Fe1 × Fe2⋯Fe2). A solvent molecule, acetone, is crystallized inside the cavity.

The nitrosyl stretching frequencies ν_{NO} occur at 1796 cm^{-1} and 1726 cm^{-1}, that is even higher than single substituted analog $Fe(NO)_2(CO)(IM)$, suggesting that the oxidation of the

$Fe(NO)_2$ units took place to balance deprotonation of the bridging ligands. The observed ν_{NO} makes complex **43** $\{Fe(NO)_2\}^9$, which is consistent with the data obtained from the Mössbauer measurement. The EPR and solution IR studies in polar solvents show that the tetrameric molecule is fragmented and solvated to give $Fe(NO)_2$(Im-H)(THF) or its protonated analog seventeen electron species $[Fe(NO)_2(Im\text{-}H)(THF)]^+$ as shown in Scheme 25. The characteristic g value close to 2.03 and the small hyperfine coupling constants (2 – 3 G) indicate that the unpaired electrons are localized on the Fe center. Nitric oxide release from this tetrameric complex was studied by thermo methods which showed stepwise loss of NO between 100–140°C, 180–220°C, 340–420°C, and 480- 520°C.

Stromnova reported a series of tetranuclear palladium nitrosyl carboxylate complexes, $Pd_4(\mu\text{-}NO)_2(OCOR)_6$, (R =/$CMe_3$, Me, Ph, $CHMe_2$, CH_2Cl), which were synthesized by the reaction of Pd(NO)Cl with silver carboxylates Ag(OCOR). X-ray crystal structure of $Pd_4(\mu\text{-}NO)_2(\mu\text{-}OCOCMe_3)_6$ was determined [176]. The four Pd atoms form an almost rectangular Pd_4 skeleton with the pair of bridging ligands on each side of the rectangle. The same group also reported a tetranuclear complex $Pd_4(NO)4(CF_3COO)4$ which was generated from the reaction of tetranuclear carbonyl complex $Pd_4(CO)_4(CF3COO)_4$ with NO. Another tetranuclear $Pd_4(\mu\text{-}NO)_2(\mu\text{-}CF_3CO_2)_4(\eta^2\text{-}CH_2{=}CHPh)_4$ complex was also isolated, that has a tetrahedral core, with η^2-coordinated styrene molecules and half-bridging nitrosyl and carboxylate groups [177]. The direct reaction of $Pd_3(\mu\text{-}RCO_2)_6$ (R = CH_3, CMe_3) with NO gives corresponding nitrosyl complexes $Pd_4(\mu\text{-}NO)_2(\mu\text{-}RCO_2)_6$.

5. Pentanuclear Metal Nitrosyl Complexes

5.1. Linked by Sulfur

Only a few pentametallic nitrosyl compounds have been synthesized. Darensbourg and co-workers synthesized a trigonal paddlewheel with iron-dithiolato ligand paddles, $\{[(bme\text{-}dach)Fe(NO)]_3Ag_2\}[BF_4]_2$, which was prepared by the reaction of $AgBF_4$ with (bme-dach)Fe(NO) [178]. The EPR and magnetic studies showed the complex is paramagnetic (g = 2.024) with three $\{Fe(NO)\}^7$ units. The same group also reported a heteropentametallic complex $Ni_2(N_2S_2)_2[Fe(NO)_2]_3$, ($N_2S_2$ = bme-dach), in which the two nickels and three irons are linked by triply bridging thiolate sulfurs in a cluster of core composition $Ni_2S_4Fe_3$. It was prepared through the reaction of $Ni(N_2S_2)$ with an excess of $Fe(CO)_2(NO)_2$ [135] The reactivity property of the pentametallic complex towards CO was investigated and revealed that the cluster converts back to $Ni(N_2S_2)Fe(NO)_2(CO)$.

Stasicka's group reported that RRS is inert in an alkaline medium, but can readily transform into the various polynuclear clusters such as $[Fe_4(\mu_3\text{-}S)_3(NO)_7]^-$, $[Fe_5(\mu_3\text{-}S)_4(NO)_8]^-$, and $[Fe_7(\mu_3\text{-}S)_6(NO)_{10}]^-$ via the proposed protonated intermediate $[Fe_2(\mu_2\text{-}SH)_2(NO)_4]$ under acidic conditions [179].

5.2. Linked by N/O

Shishilov et al. reported that the reaction of $Pd_4(\mu\text{-}NO)_2(\mu\text{-}RCO_2)_6$ (R = CMe_3, cyclo-C_6H_{11}) complexes with acetonitrile in acetone led to the formation of complexes $Pd_5(\mu\text{-}NO)(\mu\text{-}NO_2)(\mu\text{-}CMe_3CO_2)_6(CH_3C(=N)OC(=N)CH_3)$ and $Pd_5(\mu\text{-}NO)(\mu\text{-}C_6H_{11}CO_2)_7(CH_3C(=N)OC(=N)CH_3)$ [180]. They represent palladium carboxylate clusters

containing a 5-nuclear cyclic metal core, as established by X-ray diffraction analysis. Three Pd atoms coordinate the acetimidic anhydride ligand. The main structural features of the two complexes are similar.

6. Hexanuclear Metal Nitrosyl Complexes

6.1. Bridged by Sulfur

Coucouvanis reported two methods of synthesizing of $(PPN)_2[Fe_6S_6(NO)_6]$. Both of them are complicated multistep procedures through other iron-sulfur-nitrosyl clusters: one by refluxing $(PPN)[Fe_4S_3(NO)_7]$, $(PPN)_2[Fe_4(CO)_{13}]$ and Bz_2S_3 in MeCN for 24 h; and another by mixing $(PPN)_2[Fe_8S_6(NO)_8]$ with Bz_2S_3 in DMF at room temperature for 24 h [170].

Recently we also reported a hexanuclear iron-sulfur nitrosyl cluster, $[(n\text{-}Bu)_4N]_2[Fe_6S_6(NO)_6]$, **44**, which was synthesized using simpler solvent-thermal reactions by mixing $[(n\text{-}Bu)_4N][Fe(CO)_3NO]$, sulfur, and methanol in a vial under a nitrogen atmosphere and heated to 120°C for 48 hours in an autoclave, and was subsequently allowed to cool to room temperature [161]. The IR spectrum displayed one strong characteristic NO stretching frequency at 1698 cm^{-1} (ν_{NO}) in solution with the characteristic of NO^+. The redox behavior was also studied by CV and showed two cathodic current peaks at Epc = −0.30 and −1.29 V and three anodic peaks at Epa = 0.08, −0.23 and −1.19 V, where the first reduction peak is much stronger than the second one. The cyclic voltammograms were also recorded using various scan rates from 0.1 V/S to 1.0 V/S (Figure 10). When faster scan rates were applied, the first reduction peak was separated to two reductions. Meanwhile, the faster the scan rate, the clearer the separation observed between the two reduction peaks. The intensity of the unusually strong peak is a result of mixed redox processes. One is the quasi-reversible reduction and the other is from an irreversible electrochemical process, in which the compound goes through a typical electron transfer and chemical reaction (ECE) mechanism creating a product that is easier to reduce (less negative value) than the original one, which results in an overlap of the reduction potentials.

6.2. Bridged by Se

Despite many known examples of iron-sulfur nitrosyl clusters, iron-selenium nitrosyl clusters are extremely rare. Recently, we were able to isolate a new class of iron-selenium nitrosyl cluster with a formula of $[(n\text{-}Bu)_4N]_2[Fe_6Se_6(NO)_6]$, **45**. Complex **45** was prepared by the solvent-thermal reactions of one equivalent of $[(n\text{-}Bu)_4N][Fe(CO)_3NO]$ and four equivalents of selenium in methanol in a sealed vial under a nitrogen atmosphere and heated to 120°C for 48 hours in an autoclave, during which the formation of the product was monitored by FT-IR spectroscopy [161].

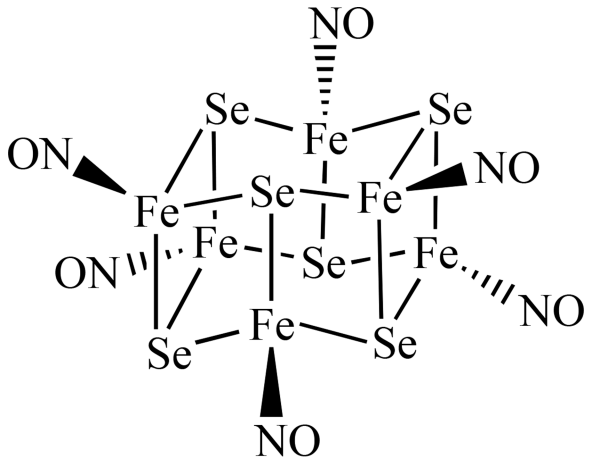

45

The IR spectrum displayed one strong characteristic NO stretching frequency at 1694 cm^{-1} (ν_{NO}) in solution with the characteristic of NO^+. The X-ray crystallographic study showed two parallel “chair-shape” structures, consisting of three iron and three selenium atoms, and are connected by Fe-Se (Figure 11). Each iron center is bonded to three selenium atoms and a nitrogen atom from the nitrosyl ligand with pseudo tetrahedral center geometry. There is a fairly strong interaction between the two iron centers as reflected by the relatively short average Fe-Fe distance of 2.730 Å.

The electrochemistry of complex **45** was studied by cyclic voltammetry (Figure 12). Complex **45** showed two cathodic current peaks at Epc = −0.42 (unusually strong) and −1.36 V and three anodic peaks at Epa = −0.04, −0.38 and −1.30 V. Detailed electrochemical studies such as scanning CV with different potential ranges showed that the oxidation peak at −0.04 V is the product of the reduction at −0.42 V. The intensity of the unusually strong peak at Epc = −0.42 V is a result of at least three processes. One is the quasi-reversible reduction at $E_{1/2}° = -0.41$ V and the other two are from an irreversible electrochemical process that occurred at Epc = −0.42 V, in which the compound went through a typical electron transfer and chemical reaction (ECE) mechanism of which its product reduces easier (less negative value) than the original one, resulting in an overlap of the reduction potentials and subsequently, a very strong peak. The peak at Epa = −0.04 V is the product from such a chemical reaction.

6.3. Linked by N/O/C

Lehnert obtained a metallacrown hexamer complex, $[Fe(BMPA\text{-}Pr)(NO)]_6[ClO_4]$, **46**, (BMPA-Pr = N-propanoate-N, N-bis(2-pyridylmethyl)amine) [181]. The carboxylate group of each unit bridges two adjacent iron centers, giving ring structures wherein all six NO moieties point toward the center of the ring as shown in Figure 13. EPR spectra of the hexameric complexes showed evidence of weak electronic coupling between the {Fe(BMPA-Pr)-(NO)} units indicating that these hexamers remain intact in solution.

7. Octanuclear Metal Nitrosyl Complexes

7.1. Linked by Sulfur

The synthesis of octanuclear iron-sulfur nitrosyl clusters were explored by Coucouvanis' group. $(PPN)_2[Fe_8S_6(NO)_8]$, [PPN = bis(triphenylphospine)iminium] was obtained from the reaction of $(NH_4)[Fe_4S_3(NO)_7]$ with $(PPN)_2[Fe_4(CO)_{13}]$ in high yield (Scheme 26) [182]. It was proposed that the reaction might proceed through the abstraction of nitrosyls from $[Fe_4S_3(NO)_7]^-$ by the $[Fe_4(CO)_{13}]^{2-}$ cluster and the possible formation of an $[Fe_4S_3(NO)_4]^-$ intermediate, which subsequently self-coupled to form the $[Fe_8S_6(NO)_8]^{2-}$ cluster, **47**. The two-electron-reduced cluster $[Fe_8S_6(NO)_8]^{4-}$ was isolated as both PPN^+ and K^+ salts upon reduction of the cluster using an excess of potassium anthracenide. The potassium salt was characterized by X-ray crystallography and identified as a $K_4(DMF)_{13}[Fe_8S_6(NO)_8]$ cluster.

Several octanuclear nitrosyl complexes with mixed metals were prepared by using $(PPN)_2[Fe_6S_6(NO)_6]$ as a precursor molecule. For instance, $(PPN)_2[(CO)_6Mo_2Fe_6(NO)_6]$, was obtained from mixing a $[Fe_6S_6(NO)_6]$ cluster with $Mo(CO)_3(MeCN)_3$ at room temperature, and $(PPr_3)_2Cu_2Fe_6S_6(NO)_6$, was obtained by mixing the $[Fe_6S_6(NO)_6]$ cluster with $[Cu(MeCN)_4]PF_6$, and tripropyl phosphine (PPr_3). A similar reaction using the cluster with $[Ni(MeCN)_6](BF_4)_2$ and PPr_3 resulted in two products: $(PPr_3)_2Ni_2Fe_6S_6(NO)_6$, and $(PPr_3)_3Ni_3Fe_4S_6(NO)_4$ [170].

7.2 Linked by N/O/C

Shishilov and co-workers reported that the reaction of the palladium carbonyl carboxylate $Pd_6(\mu\text{-}CO)_6(\mu\text{-}RCO_2)_6$ (R = Pr, *i*-Bu, *t*-Bu) with gaseous nitrogen monoxide generated two octanuclear complexes: $Pd_8(\mu\text{-}NO_2)_4(\mu\text{-}CO)_2(\mu\text{-}NO)_2(\mu\text{-}RCO_2)_8$ and $Pd_8(\mu\text{-}NO_2)_4(\mu\text{-}NO)_4(\mu\text{-}RCO_2)_8$ [183–184].

8. Conclusions

The extraordinarily significant roles that nitric oxide plays in biological systems have brought a renewed interest in the coordination chemistry of metal nitrosyls, as many of these compounds also exhibit biological activities ranging from releasing, storing, and transporting nitric oxide, to acting as a cytotoxic agent towards cancerous cells. This review illustrates a broad overview of advances in the synthesis, spectroscopic properties, and reactivity of multinuclear metal nitrosyl complexes, including Roussin's salts and ester derivatives, over the last decade. The examples cited in this review show the tremendous effort that is still being applied to the preparation and understanding of new transition metal nitrosyl complexes. A variety of methods in preparing these systems have been surveyed. A majority of the complexes have been investigated by common characterization methods such as IR, UV-vis, EPR, NMR, X-ray crystallography, Mössbauer, SQUID, CV, DFT calculations, etc. Less common techniques such as X-ray absorption spectroscopy, Resonance Raman, and NRVS have also been applied to study these systems recently. A very good understanding on the systems has been achieved. The next step would be to connect the understanding on structures and properties with biological activities and applications so that the full potential of these complexes can be unlocked.

Acknowledgements

We wish to thank the National Institute of Health (NIH) MBRS SCORE Program (2SC3GM092301-05) for financial support.

References

1. Culotta E, Koshland DE. Science. 1992; 258:1862–1865. [PubMed: 1361684]
2. Lancaster JR Jr, Hibbs JB Jr. Proc. Natl. Acd. Sci. U. S. A. 1990; 87:1223–1227.
3. Feldman PL, Griffith OW, Stuehr DJ. Chem. Eng. News. 1993; 71:26–38.
4. Bruckdorfer R. Mol. Aspects Med. 2005; 26:3–31. [PubMed: 15722113]
5. Attia AA, Makarov SV, Vanin AF, Silaghi-Dumitrescu R. Inorg. Chim. Acta. 2014; 418:42–50.
6. Kwon YM, Weiss B. J. Bacteriol. 2009; 191:5369–5376. [PubMed: 19561128]
7. Weiss B. J. Bacteriol. 2006; 188:829–833. [PubMed: 16428385]
8. Tennyson AG, Lippard SJ. Chem. & Biol. 2011; 18:1211–1220. [PubMed: 22035790]
9. Richter-Addo, GB.; Legzdins, P. “Metal Nitrosyls”. New York: Oxford University Press; 1992.
10. Ignarro, LJ. Nitric Oxide: Biology and Pathobiology. 2nd ed.. Burlington: Elsevier Inc; 2010.
11. Bredt DS, Hwang PM, Glatt CE, Lowenstein C, Reed RR, Snyder SH. Nature. 1991; 351:714–718. [PubMed: 1712077]
12. Heo J, Campbell SL. Biochemistry. 2004; 43:2314–2322. [PubMed: 14979728]
13. Moncada S, Palmer RMJ, Higgs EA. Pharmacol. Rev. 1991; 43:109–142. [PubMed: 1852778]
14. Clarke MJ, Gaul JB. Structure and Bonding. 1993; 81:147–181.
15. Ignarro LJ, Buga GM, Wodd KS, Byrns RE, Chaudhuri G. Proc. Natl. Acad. Sci. 1987; 84:9265–9269. [PubMed: 2827174]
16. Denninger JW, Marletta MA. Biochim. Biophys. Acta. 1999; 1411:334–350. [PubMed: 10320667]
17. Welter R, Yu L, Yu CA. Arch. Biochem. Biophys. 1996; 331:9. [PubMed: 8660677]
18. Foster MW, Cowan JA. J. Am. Chem. Soc. 1999; 121:4093–4100.
19. Palmer RMJ, Ferrige AG, Moncada S. Nature. 1987; 327:524–526. [PubMed: 3495737]
20. Hidalgo E, Bollinger JM, Bradley TM, Walsh CT, Demple B. J. Biol. Chem. 1995; 270:20908–20914. [PubMed: 7673113]
21. de Mel A, Murad F, Seifalian AM. Chem Rev. 2011; 111:5742–5767. [PubMed: 21663322]
22. Muller B, Kleschyov AL, Stoclet JC. Brit J Pharmacol. 1996; 119:1281–1285. [PubMed: 8937735]
23. Vanin FA, Serezhenkov VA, Mikoyan VD, Genkin MV. Nitric Oxide. 1998; 2:224–234. [PubMed: 9851363]
24. Ding H, Demple B. Proc. Natl. Acad. Sci. U.S.A. 2000; 97:5146–5150. [PubMed: 10805777]
25. Butler AR, Megson IL. Chem. Rev. 2002; 102:1155–1165. [PubMed: 11942790]
26. Szaciłowski K, Chmura A, Stasicka Z. Coord. Chem. Rev. 2005; 249:2408–2436.
27. Tonzetich ZJ, McQuade LE, Lippard SJ. Inorg. Chem. 2010; 49:6338–6348. [PubMed: 20666391]
28. Vanin AF. Nitric Oxide. 2009; 21:1–13. [PubMed: 19366636]
29. Goodrich LE, Paulat F, Praneeth VKK, Lehnert N. Inorg. Chem. 2010; 49:6293–6316. [PubMed: 20666388]
30. Wasser IM, de Vries S, Moënne-Loccoz P, Schröder I, Karlin KD. Chem. Rev. 2002; 102:1201–1234. [PubMed: 11942794]
31. Wang PG, Xian M, Tang X, Wu X, Wen Z, Cai T, Janczuk AJ. Chem. Rev. 2002; 102:1091–1134. [PubMed: 11942788]
32. Ford PC, Lorkovic IM. Chem. Rev. 2002; 102:993–1018. [PubMed: 11942785]
33. Coppens P, Novozhilova I, Kovalevsky A. Chem. Rev. 2002; 102:861–884. [PubMed: 11942781]
34. Andrews L, Citra A. Chem. Rev. 2002; 102:885–912. [PubMed: 11942782]
35. Mingos DMP. Struct. Bond. 2014; 154:1–52.
36. Wright AM, Hayton TW. Comm. Inorg. Chem. 2012; 33:207–248.

37. Berto TC, Speelman AL, Zheng S, Lehnert N. Coord. Chem. Rev. 2013; 257:244–259.
38. Ford PC, Pereira JCM, Miranda KM. Struct. Bond. 2014; 154:99–136.
39. Cruza CD, Sheppard N. Spectrochim. Acta Part A. 2011; 78:7–28.
40. Lewandowska H. Struct. Bond. 2013; 153:45–114.
41. Lehnert N, Scheidt WR, Wolf MW. Struct Bond. 2014; 154:155–224.
42. Salmon DJ, Tolman WB. Struct. Bond. 2014; 154:137–154.
43. Roussin J. Ann Chim Phys. 1858; 52:285–303.
44. Hoffmann KA, Wiede OFZ. Anorg. Chem. 1895; 9:295–301.
45. Chau CN, Wojcicki A. Polyhedron. 1992; 11:851–852.
46. Crayston JA, Glidewell C, Lambert RJ. Polyhedron. 1990; 9:1741–1746.
47. Reddy D, Lancaster JR Jr, Cornforth DP. Science. 1983; 221:769–770. [PubMed: 6308761]
48. Yukl ET, Elbaz MA, Nakano MM, Moënne-Loccoz P. Biochemistry. 2008; 47:13084–13092. [PubMed: 19006327]
49. Tinberg CE, Tonzetich ZJ, Wang H, Do LH, Yoda Y, Cramer SP, Lippard SJ. J. Am. Chem. Soc. 2010; 132:18168–18176. [PubMed: 21133361]
50. Harrop TC, Tonzetich ZJ, Reisner E, Lippard SJ. J. Am. Chem. Soc. 2008; 130:15602–15610. [PubMed: 18939795]
51. Crack JC, Green J, Thomson AJ, Le Brun NE. Acc. Chem. Res. 2014; 47:3196–3205. [PubMed: 25262769]
52. Ren B, Zhang N, Yang J, Ding H. Mol. Microbiol. 2008; 70:953–964. [PubMed: 18811727]
53. Maraj SR, Khan S, Cui XY, Cammack R, Joannou CL, Hughes MN. Analyst. 1995; 120:699–703.
54. Cui XY, Joannou CL, Hughes MN, Cammack R. FEMS Microbiol. Lett. 1992; 98:67–70. [PubMed: 1459420]
55. Vanin AF. Open Conf. Proc. J. 2013; 4:47–53.
56. Landry AP, Duan X, Huang H, Ding H. Free Radical Biology & Medicine. 2011; 50:1582–1590. [PubMed: 21420489]
57. Rauchfuss TB, Weatherill TD. Inorg. Chem. 1982; 21:827–830.
58. Harrop TC, Song D, Lippard SJ. J. Am. Chem. Soc. 2006; 128:3528–3529. [PubMed: 16536520]
59. Wang R, Camacho-Fernandez MA, Xu W, Zhang J, Li L. Dalton Trans. 2009:777–786. [PubMed: 19156270]
60. Lin ZS, Lo FC, Li CH, Chen CH, Huang WN, Hsu IJ, Lee JF, Horng JC, Liaw WF. Inorg. Chem. 2011; 50:10417–10431. [PubMed: 21939194]
61. Dillinger SA, Schmalle HW, Fox T, Berke H. Dalton Trans. 2007:3562–3571. [PubMed: 17680047]
62. Vanin AF, Poltorakov AP, Mikoyan VD, Kubrina LN, Burbaev DS. Nitic Oxide-Biol. Ch. 2010; 23:136–149.
63. Broillet MC. S-Nitrosylation of proteins. Cell. Mol. Life Sci. 1999; 55:1036–1042. [PubMed: 10442087]
64. Grabarczyk DB, Ash PA, Vincent KA. J. Am. Chem. Soc. 2014; 136:11236–11239. [PubMed: 25079052]
65. Conrado CL, Bourassa JL, Egler C, Wecksler S, Ford PC. Inorg. Chem. 2003; 42:2288–2293. [PubMed: 12665362]
66. Conrado CL, Wecksler S, Egler C, Magde D, Ford PC. Inorg. Chem. 2004; 43:5543–5549. [PubMed: 15332805]
67. Wecksler SR, Mikhailovsky A, Ford PC. J. Am. Chem. Soc. 2004; 126:13566–13567. [PubMed: 15493884]
68. Wecksler SR, Hutchinson J, Ford PC. Inorg. Chem. 2006; 45:1192–1200. [PubMed: 16441130]
69. Wecksler SR, Mikhailovsky A, Korystov D, Ford PC. J. Am. Chem. Soc. 2006; 128:3831–3837. [PubMed: 16536559]
70. Wecksler SR, Mikhailovsky A, Korystov D, Buller F, Kannan R, Tan LS, Ford PC. Inorg. Chem. 2007; 46:395–402. [PubMed: 17279817]

71. Ford PC. Acc. Chem. Res. 2008; 41:190–200. [PubMed: 18181579]
72. Chang HH, Huang HJ, Ho YL, Wen YD, Huang WN, Chiou SJ. Dalton Trans. 2009:6396–6402. [PubMed: 19655074]
73. Li L, Morton JR, Preston KF. Mag. Reson. Chem. 1995; 31:s14–s19.
74. Lu TT, Tsou CC, Huang HW, Hsu IJ, Chen JM, Kuo TS, Wang Y, Liaw WF. Inorg. Chem. 2008; 47:6040–6050. [PubMed: 18517190]
75. Tsou CC, Lu TT, Liaw WF. J. Am. Chem. Soc. 2007; 129:12626–12627. [PubMed: 17900121]
76. Shih WC, Lu TT, Yang LB, Tsai FT, Chiang MH, Lee JF, Chiang YW, Liaw WF. J. Inorg. Biochem. 2012; 113:83–93. [PubMed: 22709927]
77. Lu TT, Chiou SJ, Chen CY, Liaw WF. Inorg. Chem. 2006; 45:8799–8806. [PubMed: 17029392]
78. Tsai ML, Hsieh CH, Liaw WF. Inorg. Chem. 2007; 46:5110–5117. [PubMed: 17444639]
79. Tsai ML, Liaw WF. Inorg. Chem. 2006; 45:6583–6585. [PubMed: 16903707]
80. Tsou CC, Chiu WC, Ke CH, Tsai JC, Wang YM, Chiang MH, Liaw WF. J. Am. Chem. Soc. 2014; 136:9424–9433. [PubMed: 24917476]
81. Lu CY, Liaw WF. Inorg. Chem. 2013; 52:13918–13926. [PubMed: 24266608]
82. Jaworska M, Stasicka Z. New J. Chem. 2005; 29:604–612.
83. Hopmann KH, Noodleman L, Ghosh A. Chemistry. 2010; 16:10397–10408. [PubMed: 20623807]
84. Hsieh CH, Darensbourg MY. J. Am. Chem. Soc. 2010; 132:14118–14125. [PubMed: 20857969]
85. Lu TT, Yang LB, Liaw WF. J. Chin. Chem. Soc. 2010; 57:909–915.
86. Chen HW, Lin CW, Chen CC, Yang LB, Chiang MH, Liaw WF. Inorg. Chem. 2005; 44:3226–3232. [PubMed: 15847431]
87. Enemark JH JH, Feltham RD. RD (1974) Coord. Chem. Rev. 1974; 13:339–406.
88. Brothers SM, Darensbourg MY, Hall MB. Inorg. Chem. 2011; 50:8532–8540. [PubMed: 21819054]
89. Lu TT, Huang HW, Liaw WF. Inorg. Chem. 2009; 48:9027–9035. [PubMed: 19705817]
90. Lu TT, Lai SH, Li YW, Hsu IJ, Jang LY, Lee JF, Chen IC, Liaw WF. Inorg. Chem. 2011; 50:5396–5406. [PubMed: 21618997]
91. Harrop TC, Olmstead MM, Mascharak PK. Inorg. Chem. 2005; 44:6918–6920. [PubMed: 16180848]
92. Rose MJ, Betterley NM, Oliver AG, Mascharak PK. Inorg. Chem. 2010; 49:1854–1864. [PubMed: 20067276]
93. Lee CM, Chen CH, Chen HW, Hsu JL, Lee GH, Liaw WF. Inorg. Chem. 2005; 44:6670–6679. [PubMed: 16156625]
94. Harrop TC, Song D, Lippard SJ. J. Inorg. Biochem. 2007; 101:1730–1738. [PubMed: 17618690]
95. Bitterwolf TE, Pal P. Inorg. Chim. Acta. 2006; 359:1501–1503.
96. Olsen MT, Justice AK, Gloaguen F, Rauchfuss TB, Wilson SR. Inorg. Chem. 2008; 47:11816–11824. [PubMed: 19007207]
97. Olsen MT, Bruschi M, De Gioia L, Rauchfuss TB, Wilson SR. J. Am. Chem. Soc. 2008; 130:12021–12030. [PubMed: 18700771]
98. Hsieh CH, Erdem OF, Harman SD, Singleton ML, Reijerse E, Lubitz W, Popescu CV, Reibenspies JH, Brothers SM, Hall MB, Darensbourg MY. J. Am. Chem. Soc. 2012; 134:13089–13102. [PubMed: 22774845]
99. Li L. Comm. Inorg. Chem. 2002; 23:335–353.
100. Holloway LR, Li L. Struct. Bond. 2014; 154:53–98.
101. Jones MW, Powell DR, Richter-Addo GB. J. Organomet. Chem. 2014; 754:63–74.
102. Holloway LR, Clough AJ, Li JY, Tao EL, Tao FM, Li L. Polyhedron. 2014; 70:29–38. [PubMed: 24860235]
103. Li L, Reginato N, Urschey M, Stradiotto M, Liarakos JD. Can. J. Chem. 2003; 81:468–475.
104. Serres RG, Grapperhaus CA, Bothe E, Bill E, Weyhermuller T, Neese F, Wieghardt K. J. Am. Chem. Soc. 2004; 126:5138–5153. [PubMed: 15099097]
105. Wang R, Xu W, Zhang J, Li L. J. Mol. Struc. 2009; 923:110–113.

106. Sanina N, Roudneva T, Shilov G, Morgunov R, Ovanesyan N, Aldoshin S. Dalton Trans. 2009; 10:1703–1706. [PubMed: 19240901]
107. Yeh SW, Lin CW, Li YW, Hsu IJ, Chen CH, Jang LY, Lee JF, Liaw WF. Inorg. Chem. 2012; 51:4076–4087. [PubMed: 22404753]
108. Chen CH, Chiou SJ, Chen HY. Inorg. Chem. 2010; 49:2023–2025. [PubMed: 20128597]
109. Kozhukh J, Lippard SJ. J. Am. Chem. Soc. 2012; 134:11120–11123. [PubMed: 22742582]
110. Silaghi-Dumitrescu R, Kurtz DM Jr, Ljungdahl LG, Lanzilotta WN. Biochemistry. 2005; 44:6492. [PubMed: 15850383]
111. Kurtz DM Jr. Dalton Trans. 2007:4115–4121.
112. Hayashi T, Caranto JD, Wampler DA, Kurtz DM Jr, Moenne-Loccoz P. Biochemistry. 2010; 49:7040. [PubMed: 20669924]
113. Blomberg LM, Blomberg MRA, Siegbahn PEM. J. Biol. Inorg. Chem. 2007; 12:79. [PubMed: 16957917]
114. Borovik AS, Hendrich MP, Holman TR, Munck E, Papaefthymiou V, Que L Jr. J. Am. Chem. Soc. 1990; 112:6031.
115. Zheng S, Berto TC, Dahl EW, Hoffman MB, Speelman AL, Lehnert N. J. Am. Chem. Soc. 2013; 135:4902–4905. [PubMed: 23472831]
116. Feig AL, Bautista MT, Lippard SJ. Inorg. Chem. 1996; 35:6892–6898. [PubMed: 11666858]
117. Hayashi T, Caranto JD, Matsumura H, Kurtz DM Jr, Moënne-Loccoz P. J. Am. Chem. Soc. 2012; 134:6878–6884. [PubMed: 22449095]
118. Kuwata S, Kura S, Ikariya T. Polyhedron. 2007; 26:4659–4663.
119. Varonka MS, Warren TH. Organomet. 2010; 29:717–720.
120. Han B, Shao J, Ou Z, Phan TD, Shen J, Bear JL, Kadish KM. Inorg Chem. 2004; 43:7741–7751. [PubMed: 15554639]
121. Manowong M, Han B, McAloon TR, Shao J, Guzei IA, Ngubane S, Caemelbecke EV, Bear JL, Kadish KM. Inorg. Chem. 2014; 53:7416–7428. [PubMed: 25004282]
122. Bennett MA, Bhargava SK, Bond AM, Bansal V, Forsyth CM, Guo SX, Privér SH. Inorg. Chem. 2009; 48:2593–2604. [PubMed: 19226168]
123. Rees DC, Chan MK, Kim J. Adv. Inorg. Chem. 1993; 40:89–119.
124. Volbeda A, Charon MH, Piras C, Hatchikian EC, Frey M, Fontecilla-Camps JC. Nature. 1995; 373:580–587. [PubMed: 7854413]
125. Peters JW, Lanzilotta WN, Lemon BJ, Seefeldt LC. Science. 1998; 282:1853–1858. [PubMed: 9836629]
126. Halcrow MA. Angew. Chem., Int. Ed. Engl. 1995; 34:1193–1195.
127. Nagashima S, Nakasako M, Dohmae N, Tsujimura M, Takio K, Odaka M, Yohda M, Kamiya N, Endo I. Nat. Struct. Biol. 1998; 5:347–351. [PubMed: 9586994]
128. Huang W, Jia J, Cummings J, Nelson M, Schneider G, Lundquist Y. Structure. 1997; 5:691–699. [PubMed: 9195885]
129. Volbeda A, Garcin E, Piras C, de Lacey AL, Fernandez VM, Hatchikian EC, Frey M, Fontecilla-Camps JC. J. Am. Chem. Soc. 1996; 118:12989–12996.
130. Volbeda A, Charon MH, Piras C, Hatchikian EC, Frey M, Fontecilla-Camps JC. J. Inorg. Biochem. 1995; 59:637.
131. Osterloh F, Saak W, Haase D, Pohl S. Chem. Commun. 1997:979.
132. Liaw WF, Chiang CY, Lee GH, Peng SM, Lai CH, Darensbourg MY. Inorg. Chem. 2000; 39:480–484. [PubMed: 11229566]
133. Verhagen JA, Lutz M, Spek AL, Bouwman E. Eur. J. Inorg. Chem. 2003:3968–3974.
134. Chiang CY, Miller ML, Reibenspies JH, Darensbourg MY. J. Am. Chem. Soc. 2004; 126:10867–10874. [PubMed: 15339171]
135. Hsieh CH, Chupik RB, Brothers SM, Hall MB, Darensbourg MY. Dalton Trans. 2011; 40:6047–6053. [PubMed: 21552576]
136. Pinder TA, Hsieh SKMH, Lunsford AM, Bethel RD, Pierce BS, Darensbourg MY. Inorg. Chem. 2014; 53:9095–9105. [PubMed: 25144614]

137. Hsieh CH, Chupik RB, Pinder TA, Darensbourg MY. Polyhedron. 2013; 58:151–155.
138. Rampersad MV, Jeffery SP, Reibenspies JH, Ortiz CG, Darensbourg DJ, Darensbourg MY. Angew. Chem., Int. Ed. 2005; 44:1217–1220.
139. Rampersad MV, Jeffery SP, Golden ML, Lee J, Reibenspies JH, Darensbourg, Darensbourg MY. J. Am. Chem. Soc. 2005; 127:17323–17334. [PubMed: 16332082]
140. Hess JL, Conder HL, Green KN, Darensbourg MY. Inorg. Chem. 2008; 47:2056–2063. [PubMed: 18260623]
141. Arashiba K, Matsukawa S, Kuwata S, Tanabe Y, Iwasaki M, Ishii Y. Organomet. 2006; 25:560–562.
142. Arashiba K, Iizuka H, Matsukawa S, Kuwata S, Tanabe Y, Iwasaki M, Ishii Y. Inorg. Chem. 2008; 47:4264–4274. [PubMed: 18426202]
143. Kostin G, Borodin A, Emely anov V, Naumov D, Virovets A, Rohmer MM, Varnek A. J. Mol. Struct. 2007; 837:63–71.
144. Cavigliasso G, Christian G, Stranger R, Yates BF. Dalton Trans. 2009; 14:956–964. [PubMed: 19173078]
145. Hsu IJ, Hsieh CH, Ke SC, Chiang KA, Lee JM, Chen JM, Jang LY, Lee GH, Wang Y, Liaw WF. J. Am. Chem. Soc. 2007; 129:1151–1159. [PubMed: 17263396]
146. Tennyson AG, Dhar S, Lippard SJ. J. Am. Chem. Soc. 2008; 130:15087–15098. [PubMed: 18928257]
147. Sromnova TA, Paschenko DV, Boganova LI, Daineko MV, Katser SB, Churakov AV, Kuz'mina LG, Howard JAK. Inorg. Chim. Acta. 2003; 350:283–288.
148. Stromnova TA, Dayneko MV, Churakov AV, Kuz'mina LG, Campora J, Palma P, Carmona E. Inorg. Chim. Acta. 2006; 359:1613–1618.
149. Dayneko MV, Stromnova TA, Alekseev LS, Shamsiev RS, Belov AP, Kochubei DI, Novgorodov BN. Russ. J. Inorg. Chem. 2005; 50:365–371.
150. Roncaroli F, Baraldo LM, Slep LD, Olabe JA. Inorg. Chem. 2002; 41:1930–1939. [PubMed: 11925190]
151. De Candia AG, Singh P, Kaim W, Slep LD. Inorg Chem. 2009; 48:565–573. [PubMed: 19093847]
152. Marchlewski L. J. Sachs. Z. Anorg. Allg. Chem. 1892; 2:175–181.
153. Einsle O, Tezcan FA, Andrade SLA, Schmid B, Yoshida M, Howard JB, Rees DC. Science. 2002; 297:1696–1700. [PubMed: 12215645]
154. Janczyk A, Wolnicka-Glubisz A, Chmura A, Elas M, Matuszak Z, Stochel G, Urbanska K. Nitric Oxide. Biol. Ch. 2004; 10:42–50.
155. Matthews EK, Seaton ED, Forsyth MJ, Humphrey PP. Br J Pharmacol. 1994; 113:87–94. [PubMed: 7812636]
156. Allen PK, Morris RE. Struct. Bond. 2014; 154:225–256.
157. Hamilton-Brehm SD, Schut GJ, Adams MW. Appl. Environ. Microbiol. 2009; 75:1820–1825. [PubMed: 19201977]
158. Stys A, Galy B, Starzyński RR, Smuda E, Drapier JC, Lipiński P, Bouton C. J. Biol. Chem. 2011; 286:22846–22854. [PubMed: 21566147]
159. Crack JC, Green J, Hutchings MI, Thomson AJ, Le Brun NE. Antioxid. Redox Signal. 2012; 17:1215–1231. [PubMed: 22239203]
160. Chen TN, Lo FC, Tsai ML, Shih KN, Chiang MH, Lee GH, Liaw WF. Inorg. Chim. Acta. 2006; 359:2525–2533.
161. Wang R, Xu W, Zhang J, Li L. Inorg. Chem. 2010; 49:4814–4819. [PubMed: 20459063]
162. De La Cruz C, Sheppard N. Spectrochim. Acta A Mol. Biomol. Spectrosc. 2011; 78:7–28. [PubMed: 21123107]
163. Chmura A, Szaciłowski K, Waksmundzka-Góra A, Stasicka Z. Nitric Oxide. 2006; 14:247–260. [PubMed: 16337819]
164. Jaworska M, Stasicka Z. J. Mol. Struct. 2006; 785:68–75.

165. Tonzetich ZJ, Wang H, Mitra D, Tinberg CE, Do LH, Jenney FE, Adams MWW Jr, Cramer SP, Lippard SJ. J. Am. Chem. Soc. 2010; 132:6914–6916. [PubMed: 20429508]
166. Tinberg CE, Tonzetich ZJ, Wang H, Do LH, Yoda Y, Cramer SP, Lippard SJ. J. Am. Chem. Soc. 2010; 132:18168–18176. [PubMed: 21133361]
167. Harrop TC, Tonzetich ZJ, Reisner E, Lippard SJ. J. Am. Chem. Soc. 2008; 130:15602–15610. [PubMed: 18939795]
168. Victor E, Lippard SJ. Inorg. Chem. 2014; 53:5311–5320. [PubMed: 24773390]
169. Tsou CC, Lin ZS, Lu TT, Liaw WF. J. Am. Chem. Soc. 2008; 130:17154–17160. [PubMed: 19053409]
170. Kalyvas H, Coucouvanis D. Polyhedron. 2007; 26:4765–4778.
171. Yeh SW, Tsou CC, Liaw WF. Dalton Trans. 2014; 43:9022–9025. [PubMed: 24821662]
172. Chiang CY, Miller ML, Reibenspies JH, Darensbourg MY. J. Am. Chem. Soc. 2004; 126:10867–10874. [PubMed: 15339171]
173. Crack JC, Smith LJ, Stapleton MR, Peck J, Watmough NJ, Buttner MJ, Buxton RS, Green J, Oganesyan VS, Thomson AJ, Le Brun NE. J. Am. Chem. Soc. 2011; 133:1112–1121. [PubMed: 21182249]
174. Wang X, Sundberg EB, Li L, Kantardjieff K, Herron S, Lim M, Ford PC. Chem. Comm. 2005:477–479. [PubMed: 15654375]
175. Hess JL, Hsieh CH, Brothers SM, Hall MB, Darensbourg MY. J. Am. Chem. Soc. 2011; 133:20426–20434. [PubMed: 22074010]
176. Stromnova TA, Paschenko DV, Boganova LI, Daineko MV, Katser SB, Churakov AV, Kuz'mina LG, Howard JAK. Inorg. Chim. Acta. 2003; 350:283–288.
177. Podobedov RE, Stromnova TA, Churakov AV, Kuzmina LG, Efimenko IA. J. Organomet. Chem. 2010; 695:2083–2088.
178. Hess JL, Young MD, Murillo CA, Darensbourg MY. J. Mol. Struct. 2008; 890:70–74.
179. Szaciłowski K, Chmura A, Stasicka Z. Coord. Chem. Rev. 2005; 249:2408–2436.
180. Shishilov ON, Akhmadullina NS, Rezinkova YN, Podobedov RE, Churakova AV, Efimenko IA. Dalton Trans. 2013; 42:3712–3720. [PubMed: 23302794]
181. Berto TC, Hoffman MB, Murata Y, Landenberger KB, Alp EE, Zhao J, Lehnert N. J. Am. Chem. Soc. 2011; 133:16714–16717. [PubMed: 21630658]
182. Kalyvas H, Coucouvanis D. Inorg. Chem. 2006; 45:8462–8464. [PubMed: 17029349]
183. Stromnova TA, Shishilov ON, Churakov AV, Kuz'mina LG, Howard JAK. Chem. Commun. 2007:4800–4802.
184. Shishilov ON, Stromnova TA, Efimenko IA, Churakov AV, Howard JAK, Minaeva NA. J. Organomet. Chem. 2011; 696:2023–2029.

Highlights

The extraordinary significant roles that nitric oxide plays in biological systems have brought a renewed interest in the coordination chemistry of metal nitrosyls, as many of these compounds also exhibit biological activities ranging from releasing, storing, and transporting nitric oxide, to acting as a cytotoxic agent towards cancerous cells. This review illustrates a broad overview of advances in the synthesis, spectroscopic properties, and reactivity of multinuclear metal nitrosyl complexes, including Roussin's salts and ester derivatives, over the last decade.

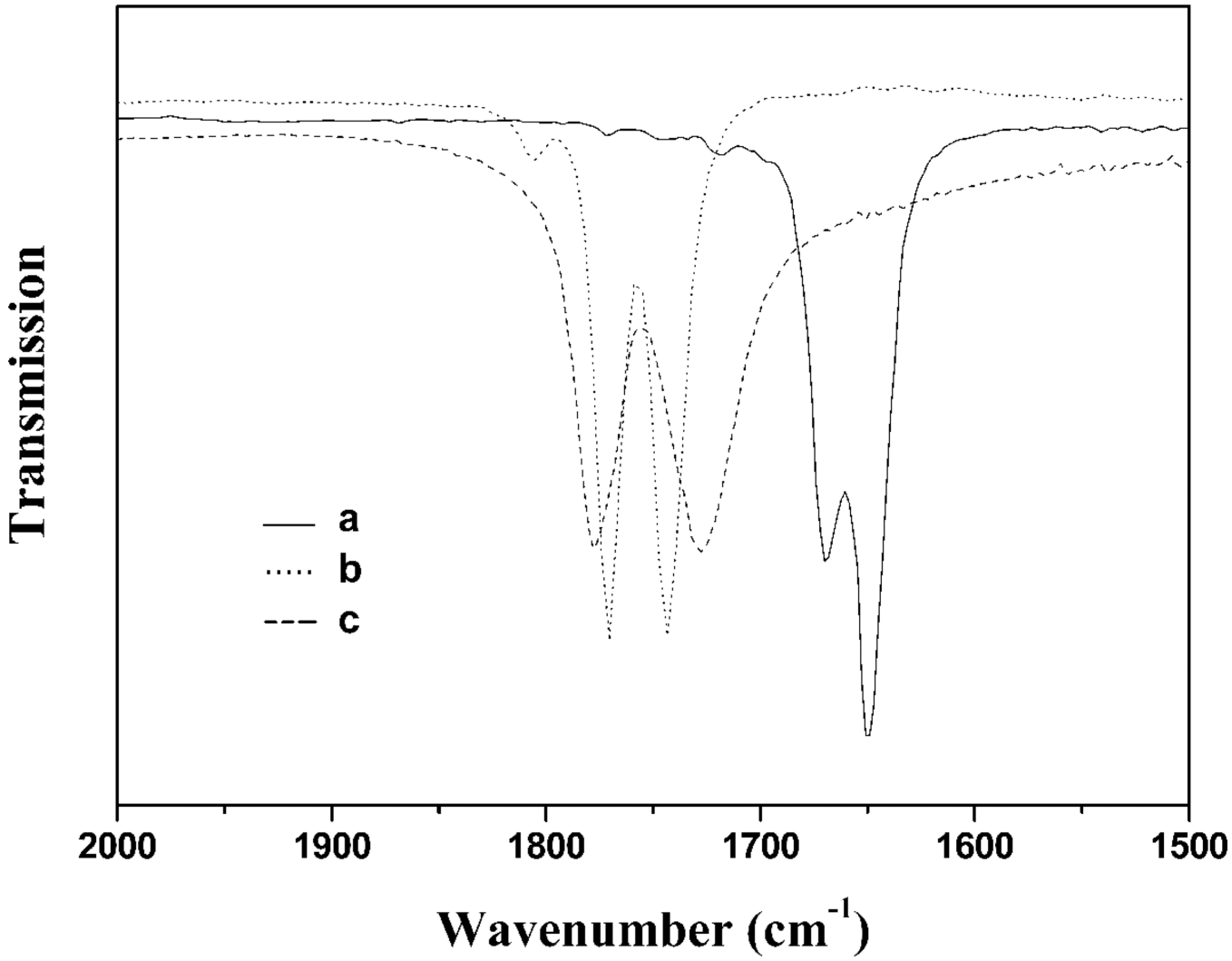

Figure 1.

Experimental infrared spectra of RRE complexes in the nitrosyl stretching region: (a) **2b**$^{-}$ recorded in tetrahydrofuran, (b) **2b** recorded in tetrahydrofuran (mixture of the *cis*- and *trans*- isomers), and (c) **2c** recorded in KBr (only *trans*-isomers) [59].

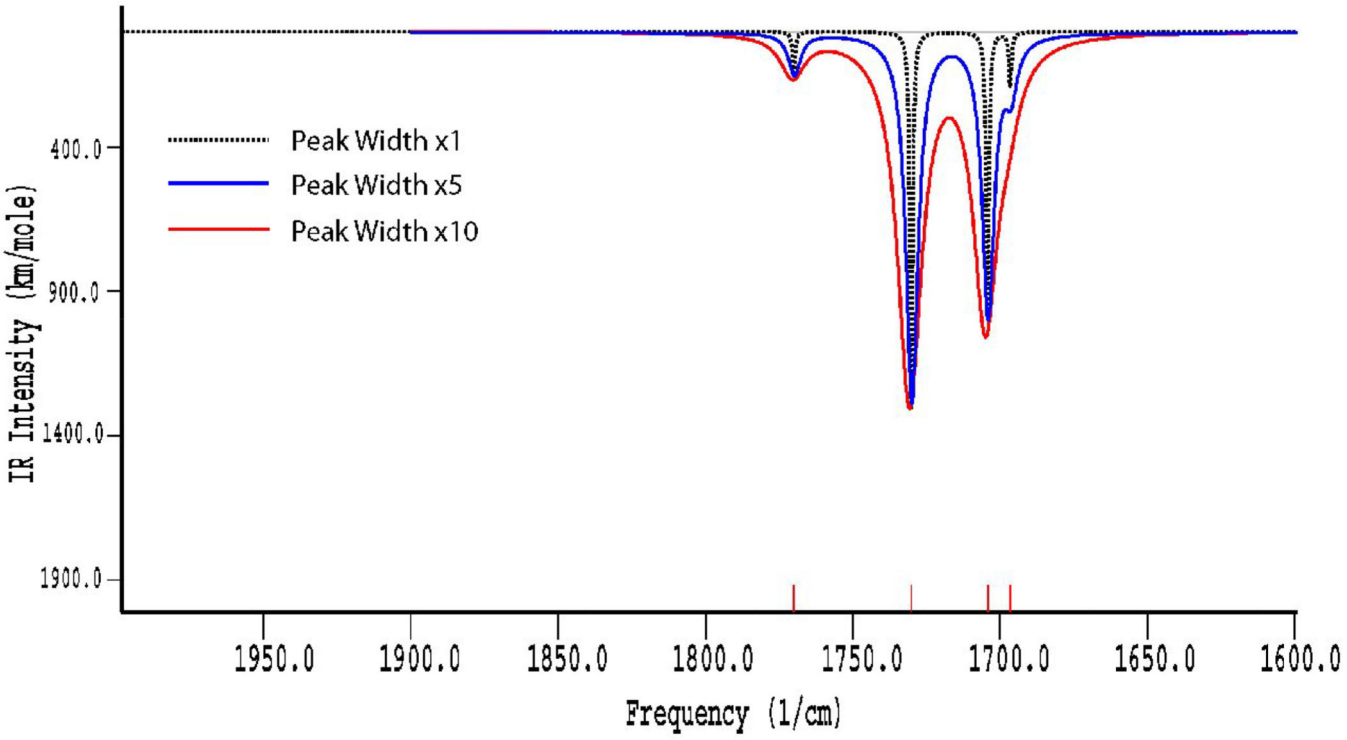

Figure 2.
The calculated vibrational spectra using different peak widths for the *cis*- isomer of the RRE complex **2a** [59].

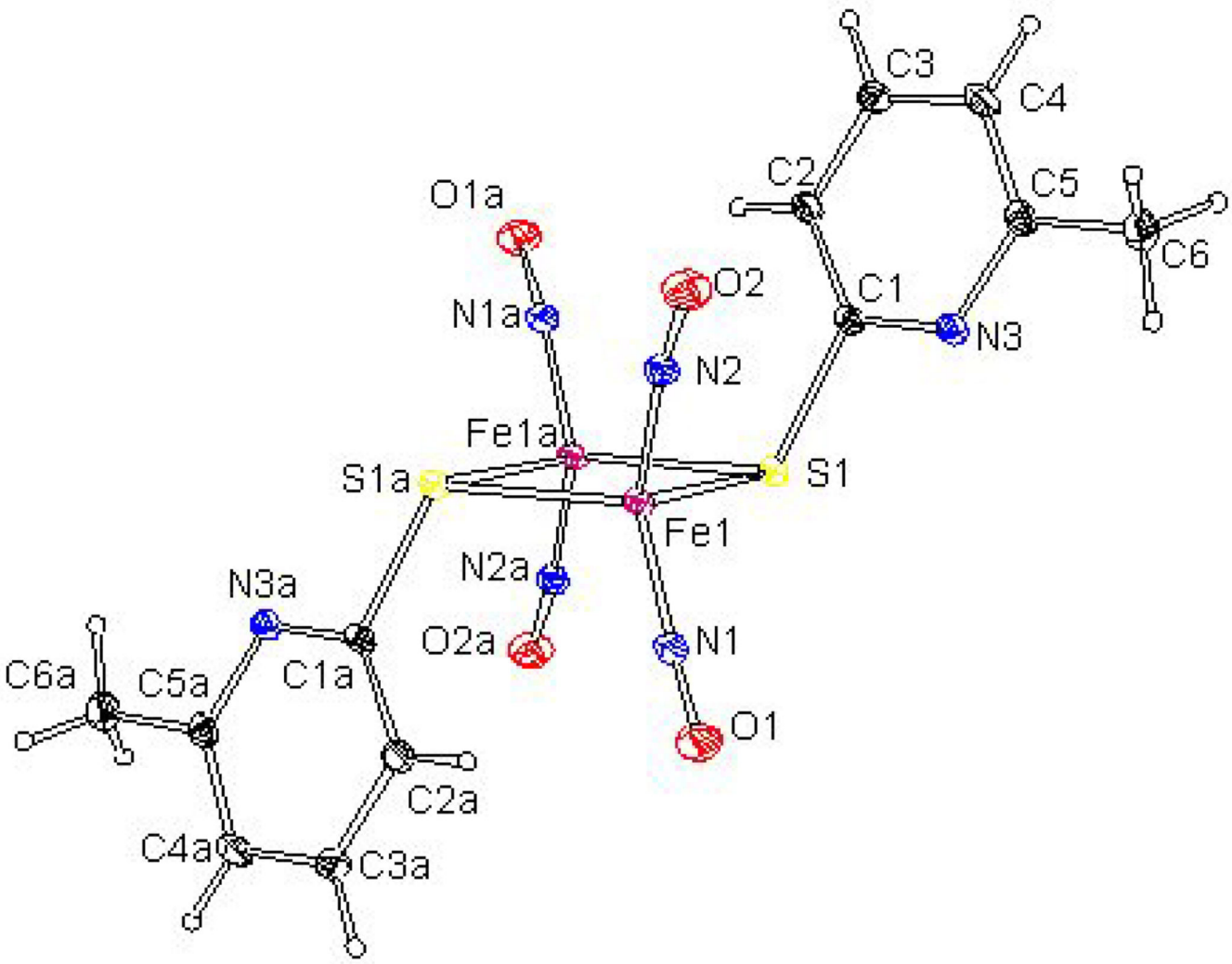

Figure 3.
An X-ray crystallographic representation of RRE. Hydrogen atoms are eliminated for clarity [59].

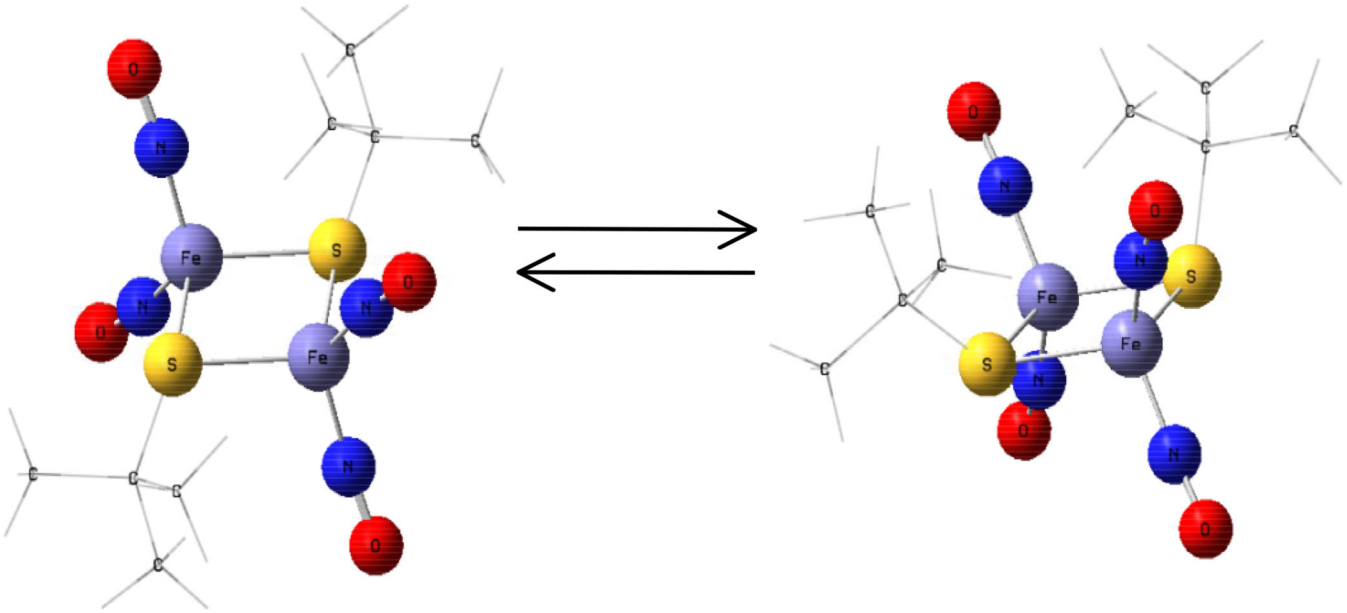

Figure 4.
Geometry optimizations using DFT showing conversion of the *cis*- and *trans*- isomers [59].

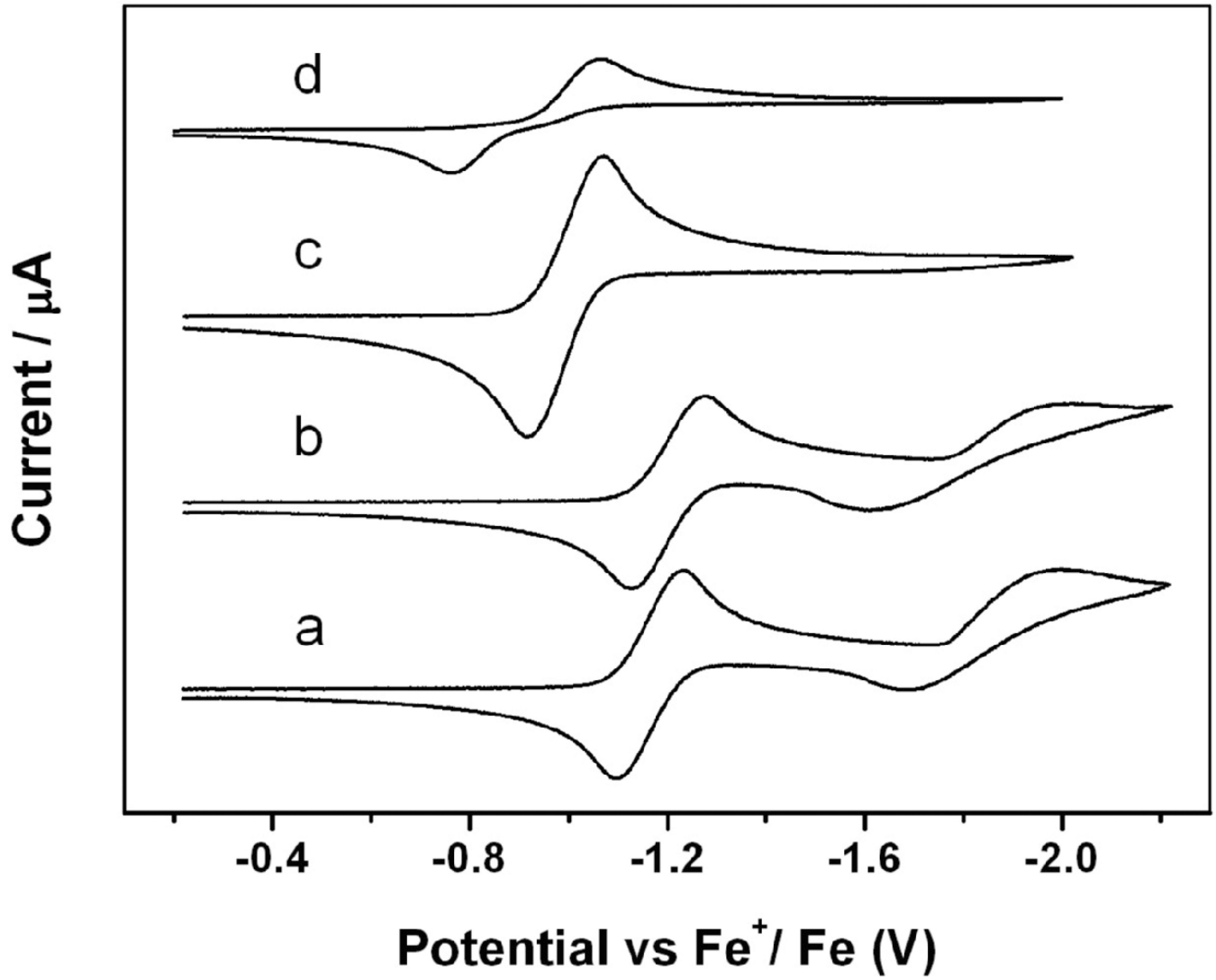

Figure 5.
Cyclic voltammograms of a 2 mM solution of the RRE complex **2a** (a), **2b** (b), **2c** (c), and **2d** (d) in 0.1 M $[NBu_4][PF_6]$–CH_2Cl_2 [59].

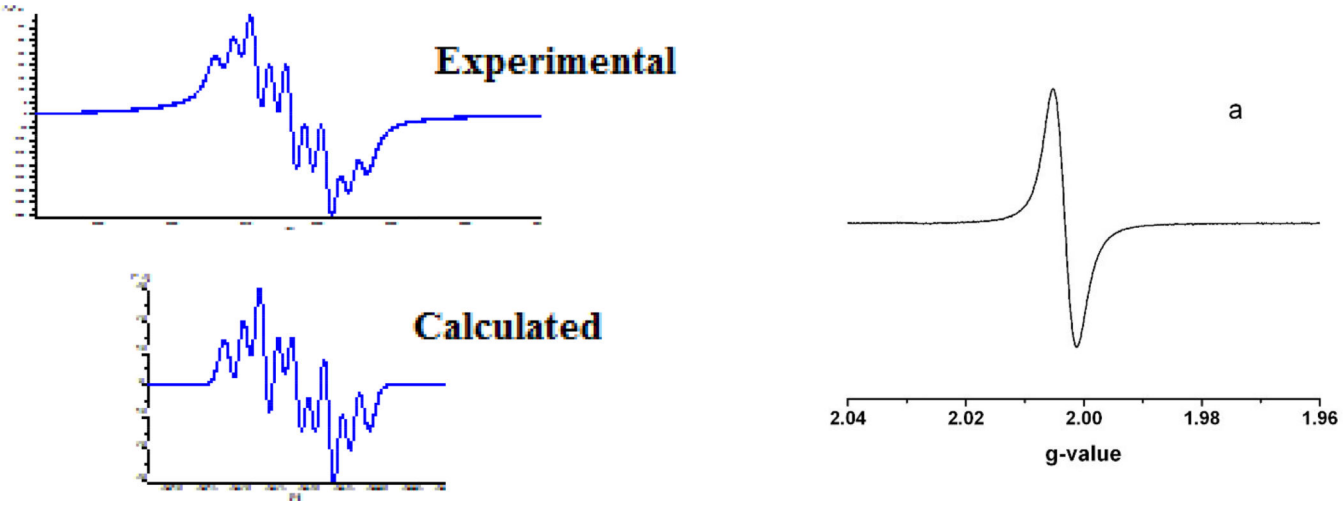

Figure 6.

Comparison of the EPR spectra of a typical DNIC (experimental and simulation) recorded at 170K [174] and RRE^{-} (a) recorded at temperatures ranging from 298–180K [59].

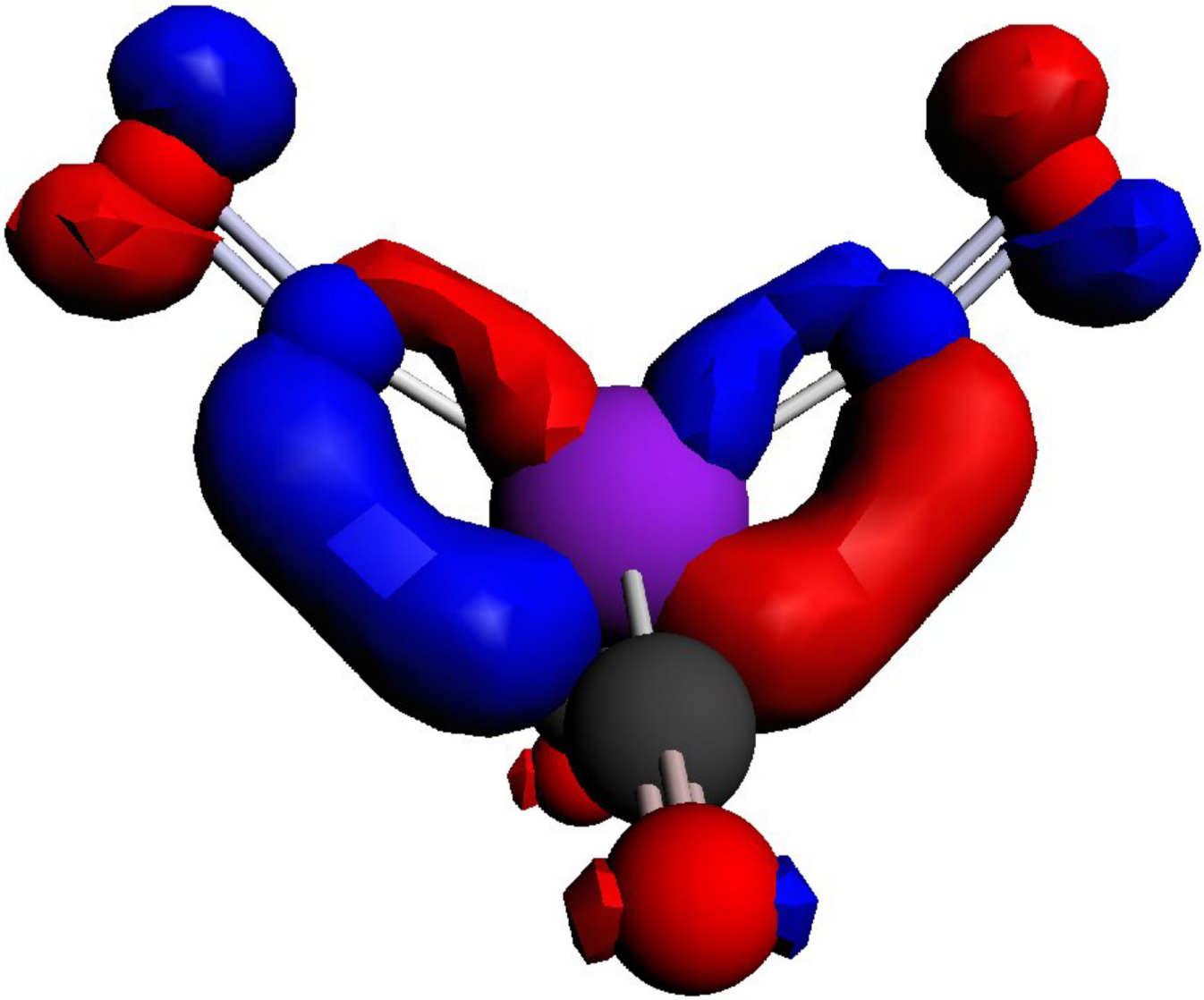

Figure 7.
Comparison of the distribution of electron density on the SOMO of complex RRE^{-} and $[Fe(NO)_2(CO)_2]^{+}$ calculated by DFT [59].

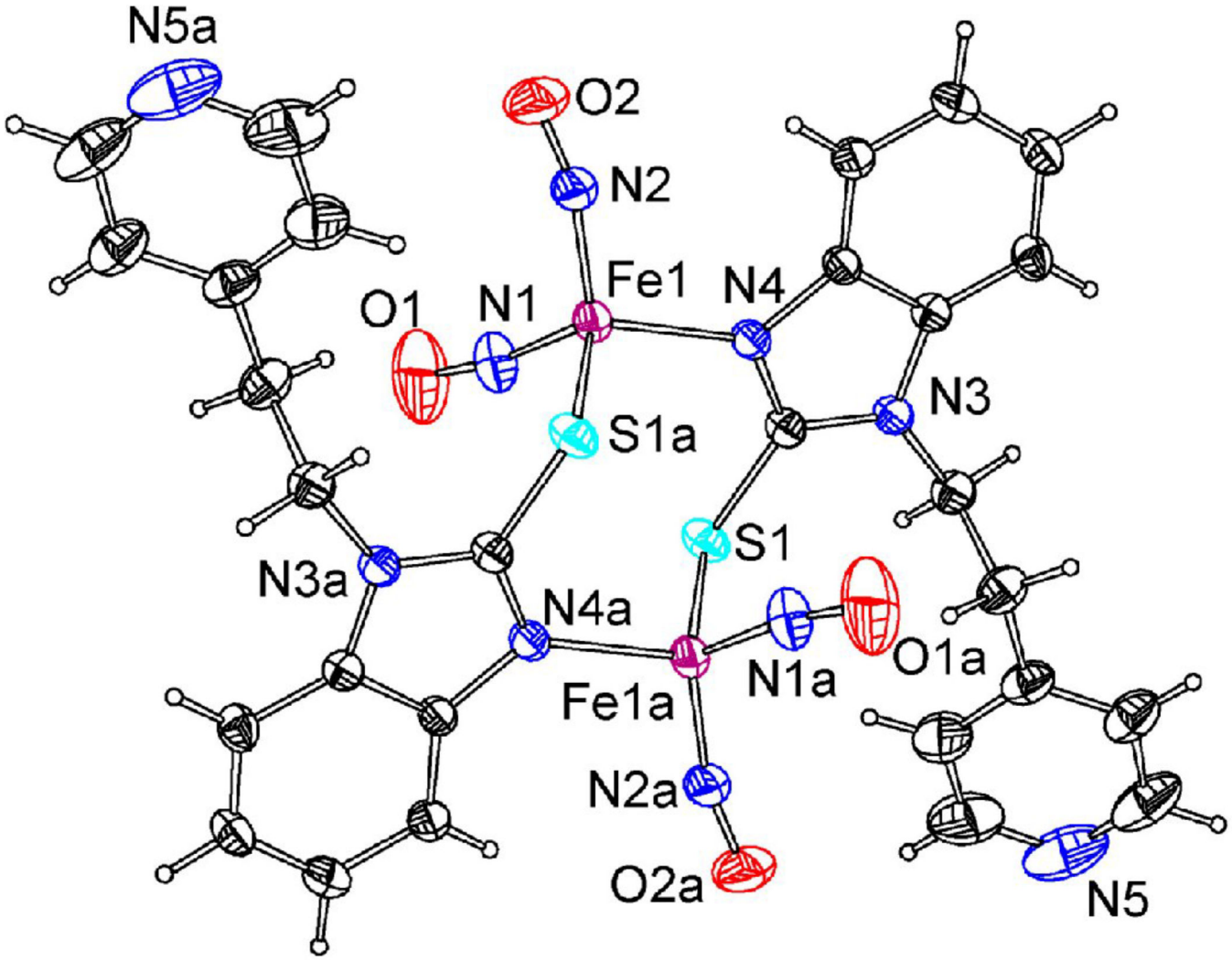

Figure 8.
X-ray crystal structure of **20** [105].

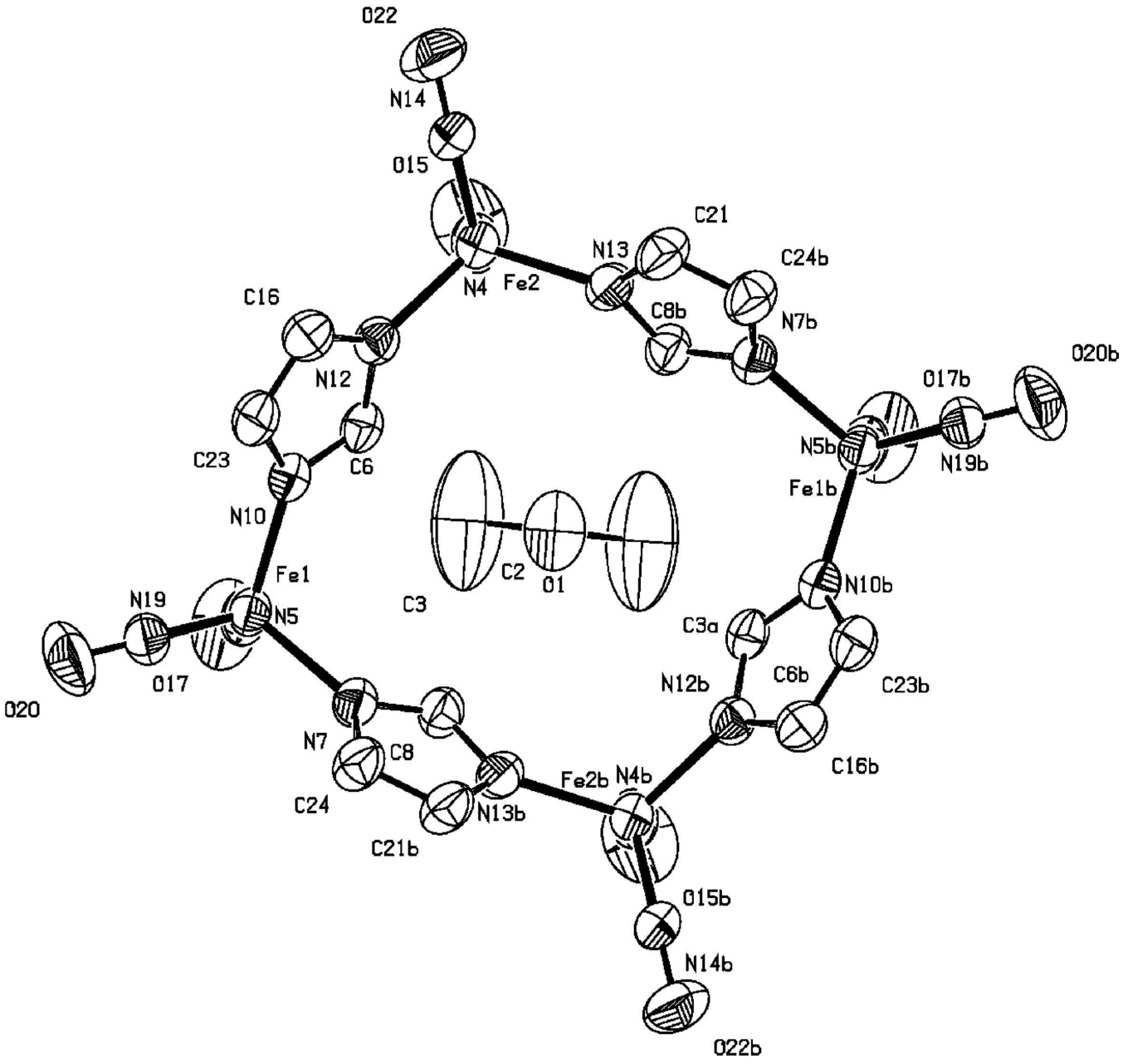

Figure 9.

X-ray crystal structure of **43** with anisotropic thermal displacement ellipsoids drawn at 50% [174].

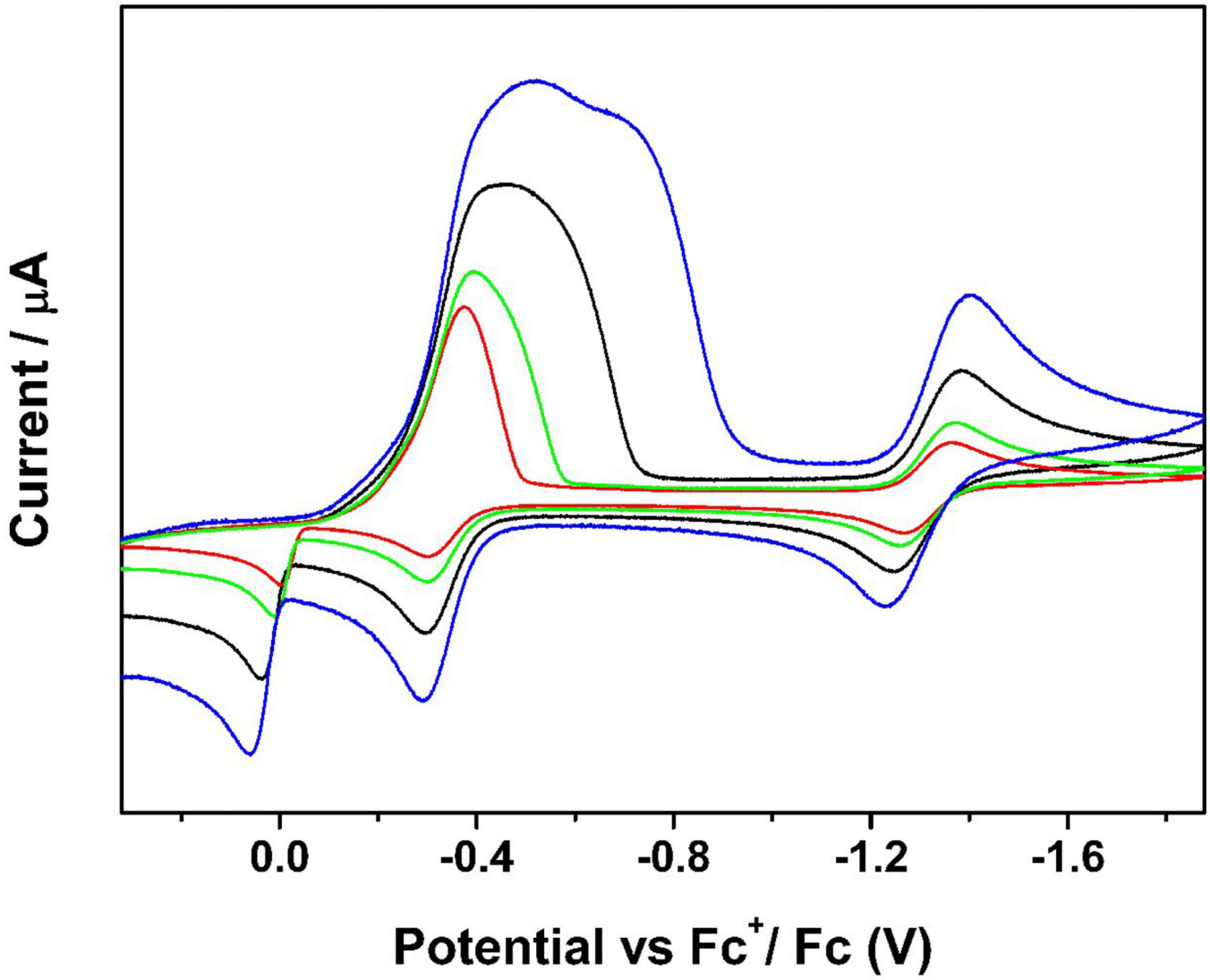

Figure 10.

Cyclic voltammograms of a 1mM solution of $[(n\text{-Bu})_4N]_2[Fe_6S_6(NO)_6]$ in 0.1 M (NBu4) (PF6) / CH3CN at scan rate of 0.10 (red), 0.20 (green), 0.50 (black) and 1.00 (blue) V/S. Reprinted with permission from [161]. Copyright 2010 American Chemical Society.

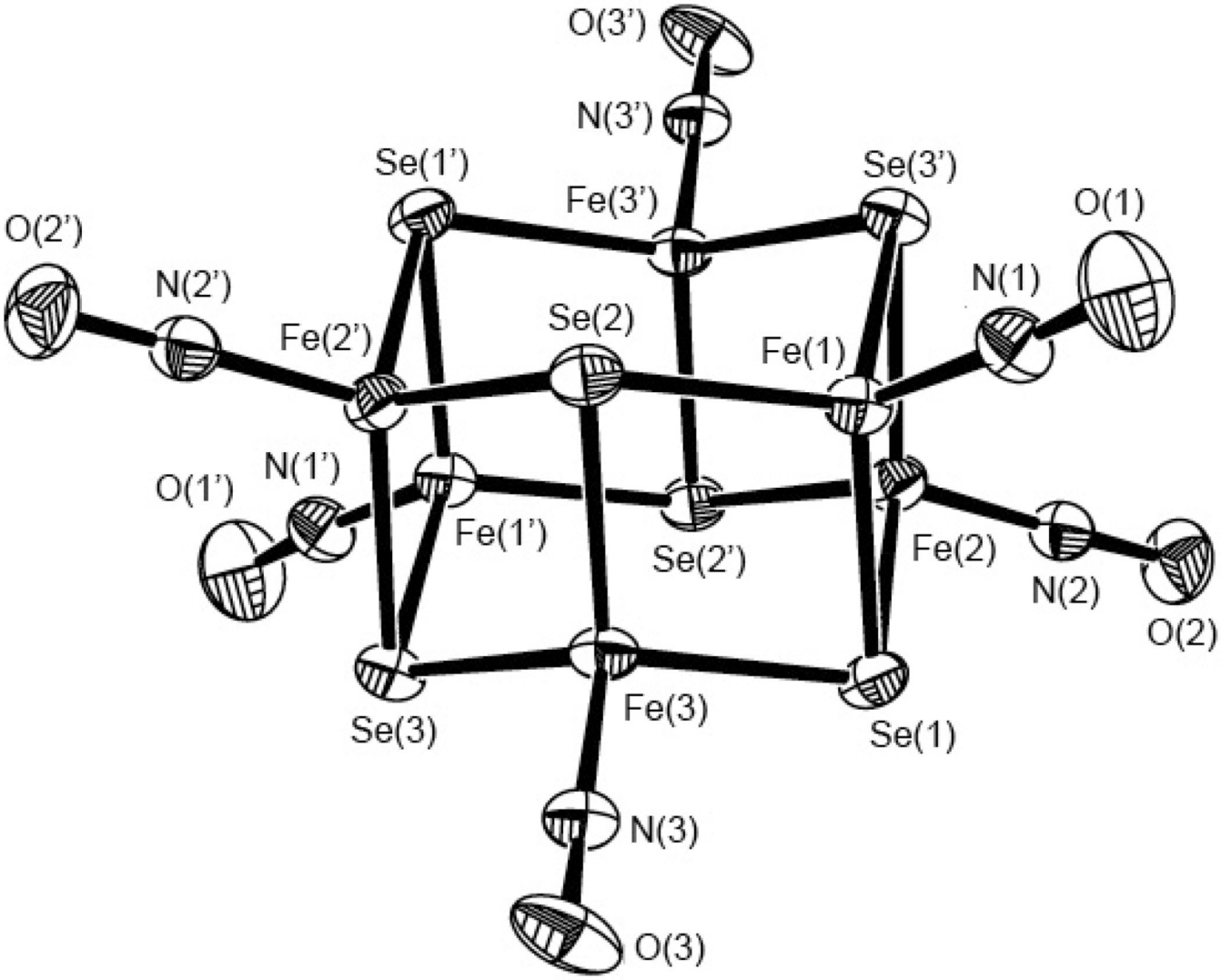

Figure 11.

The X-ray crystal structure of $[Fe_6Se_6(NO)_6]^{2-}$ with thermal ellipsoids drawn at 50% probability. Reprinted with permission from [161]. Copyright 2010 American Chemical Society.

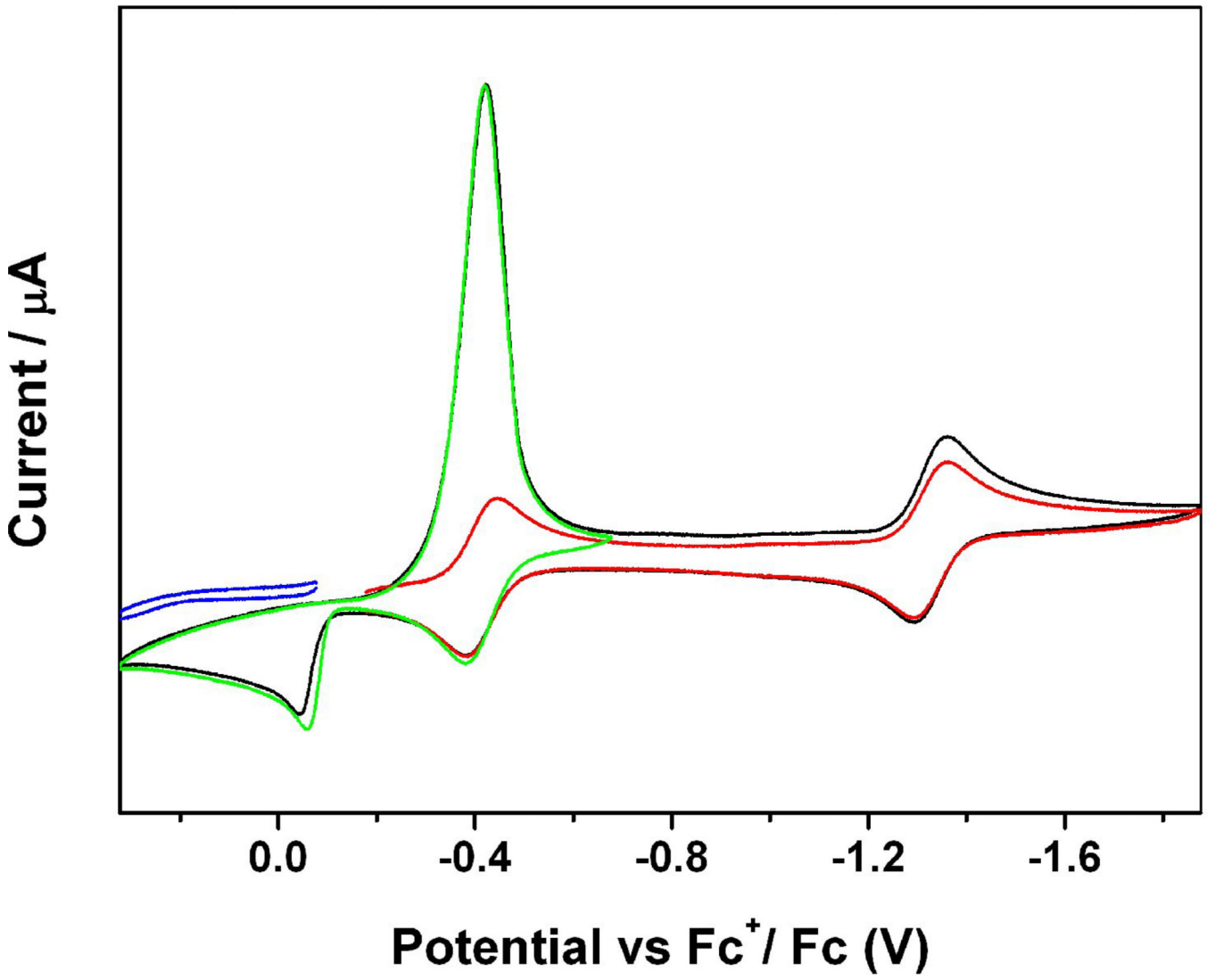

Figure 12.

Cyclic voltammograms of a 1mM solution of $[(n\text{-}Bu)_4N]_2[Fe_6Se_6(NO)_6]$ in 0.1 M $(NBu_4)(PF_6)$ / CH_3CN at scan rate of 100 mV/S. Reprinted with permission from [161]. Copyright 2010 American Chemical Society.

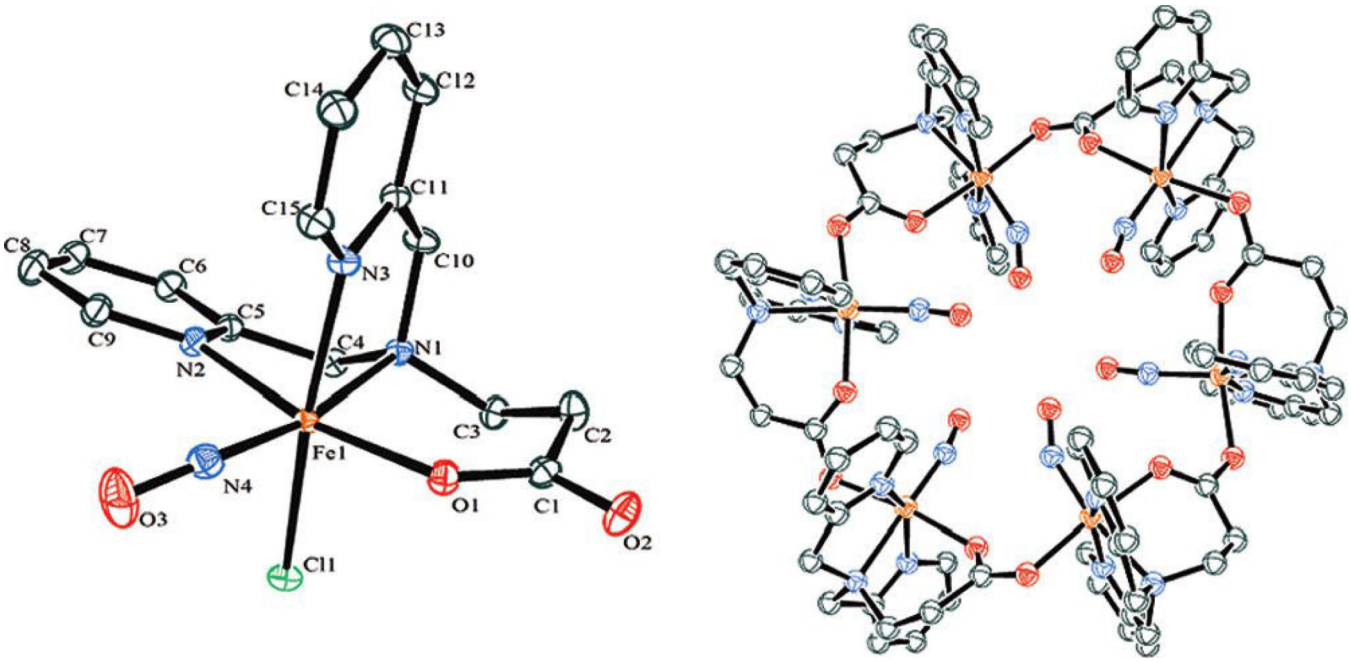

Figure 13.

Crystal structures of [Fe(BMPA-Pr)(NO)]Cl and a metallacrown hexamer complex, $[[Fe(BMPA\text{-}Pr)(NO)]_6[ClO_4]$. All of the solvent molecules and H atoms have been omitted for clarity. Reprinted with permission from [181]. Copyright 2011 American Chemical Society.

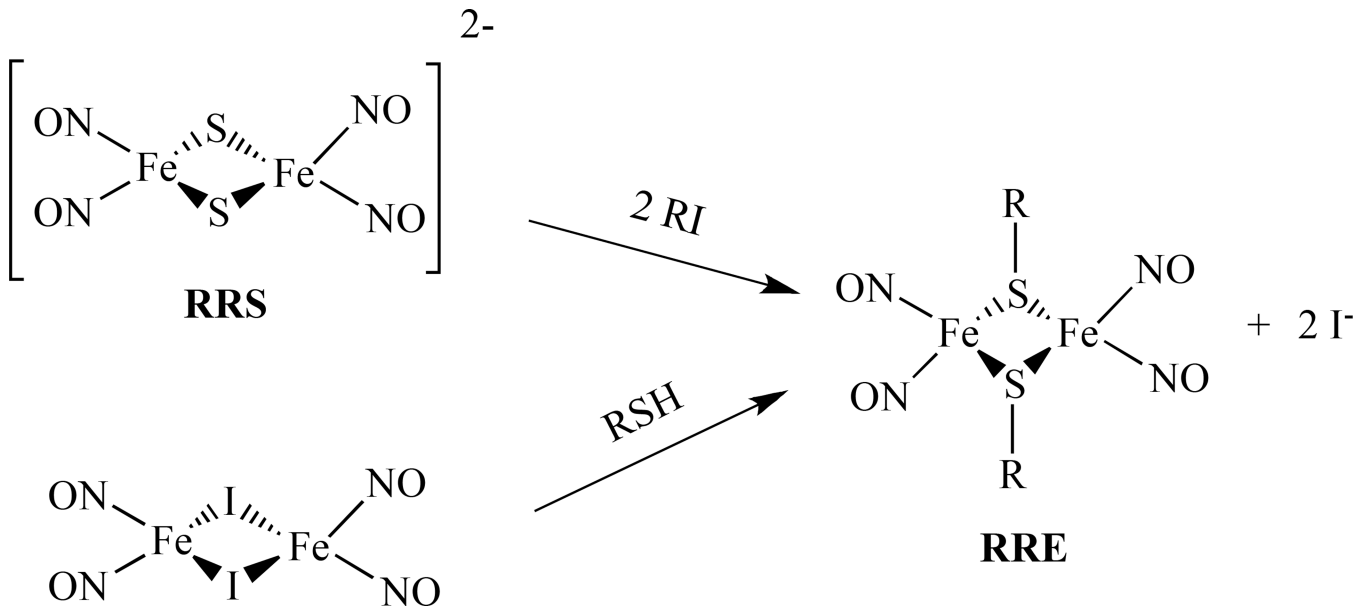

Scheme 1.
Generalized synthetic pathway for the conversion of RRS to RRE.

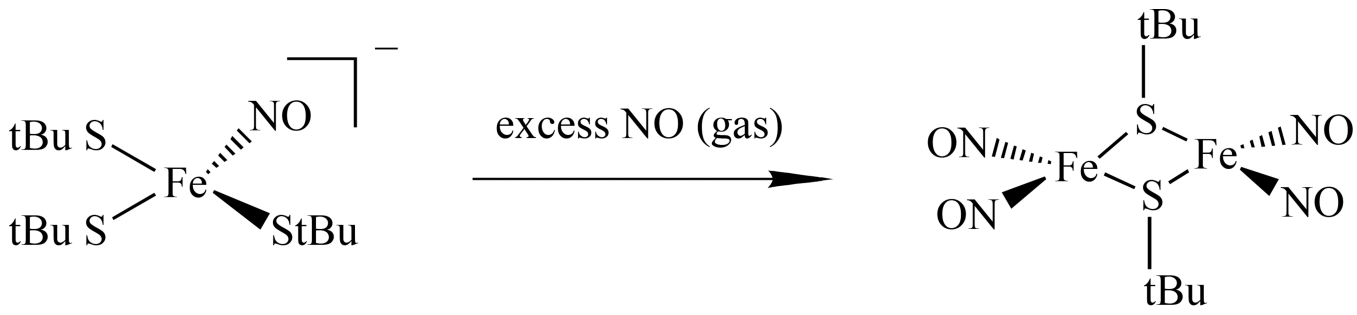

1

Scheme 2.
Synthetic scheme for the RRE from $(Et_4N)[Fe(StBu)_3(NO)]$ and NO [58].

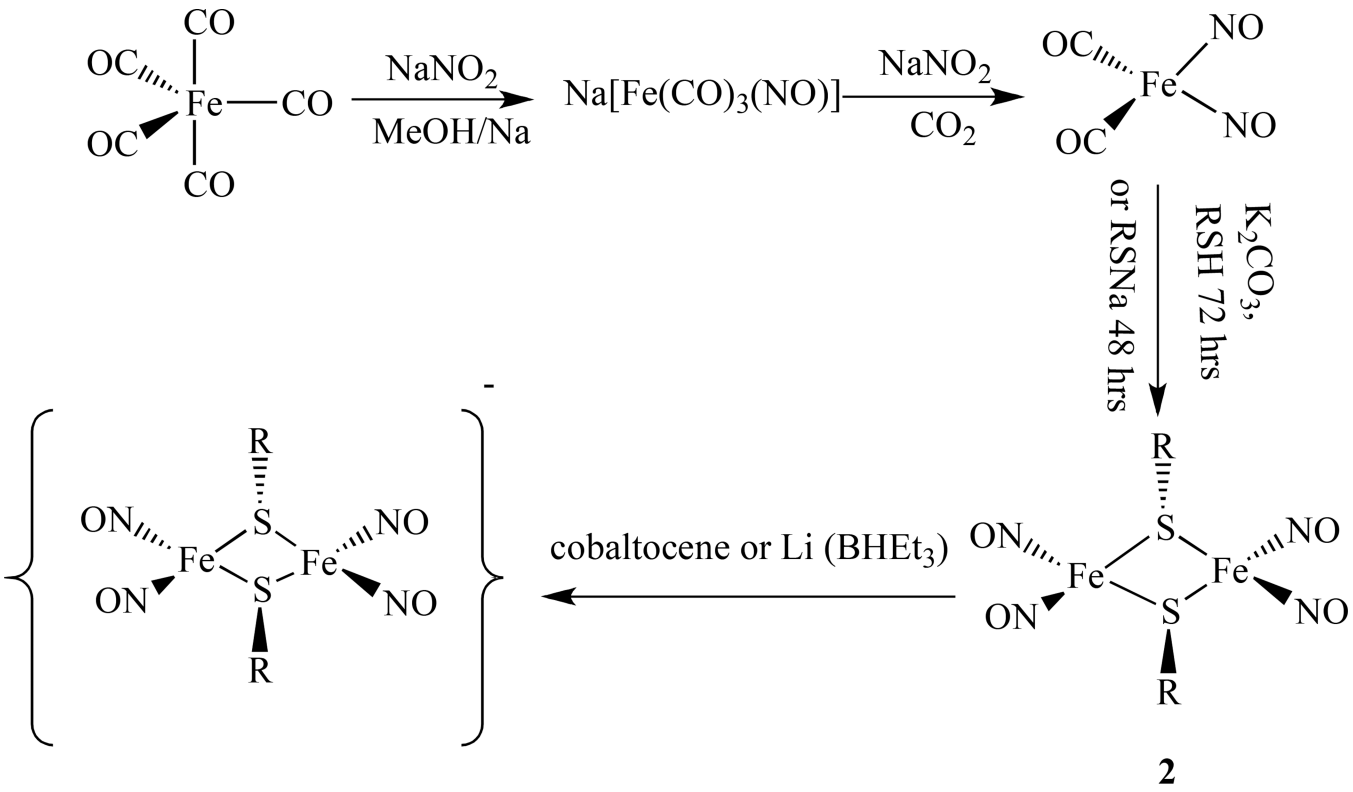

R = n-Pr, **2a**, t-Bu, **2b** or **1**, 6-methyl-2-pyridyl, **2c**, and 4,6-dimethyl, **2d**

Scheme 3.
Synthetic scheme for the formation of RRE from $Fe(CO)_5$ and $NaNO_2$ [59].

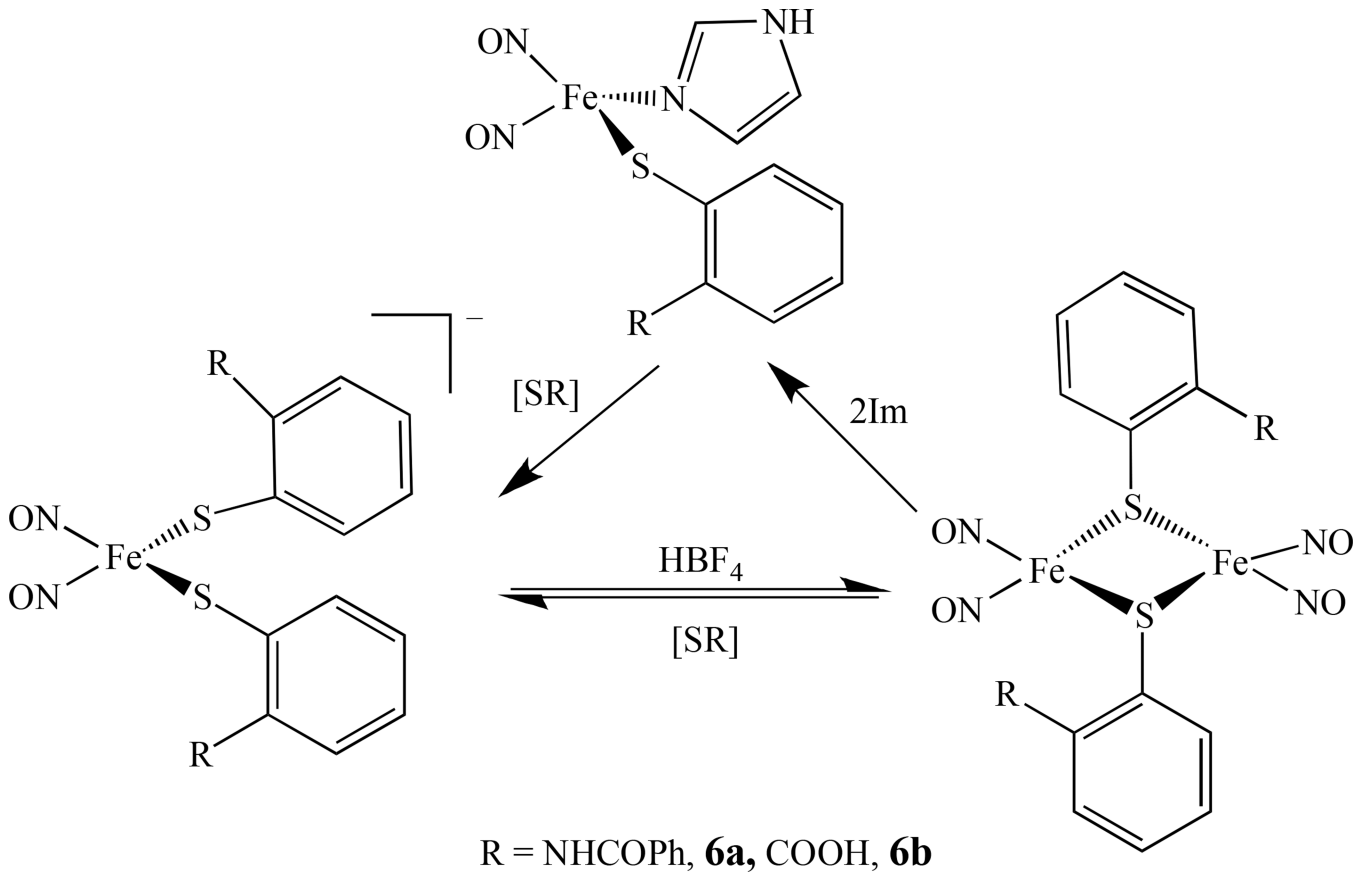

Scheme 4.
Conversion of DNIC to RRE [79].

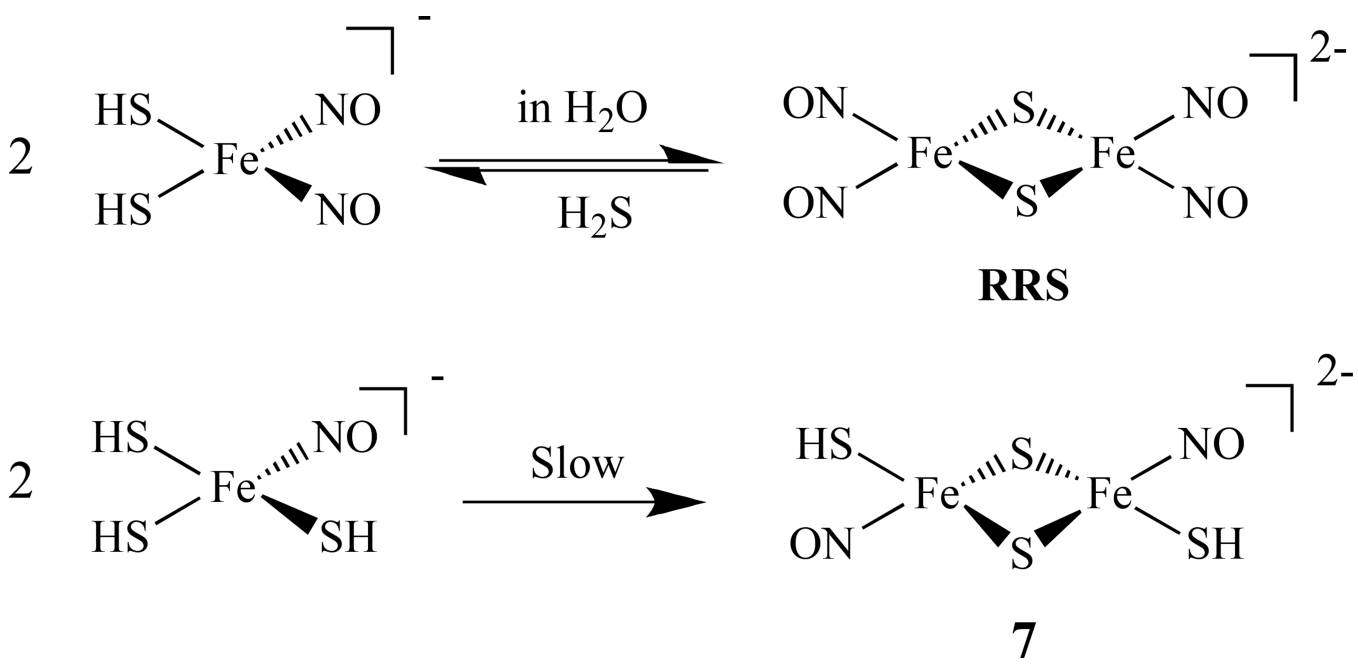

Scheme 5.
Conversion of DNICs to RRS and **7** [80].

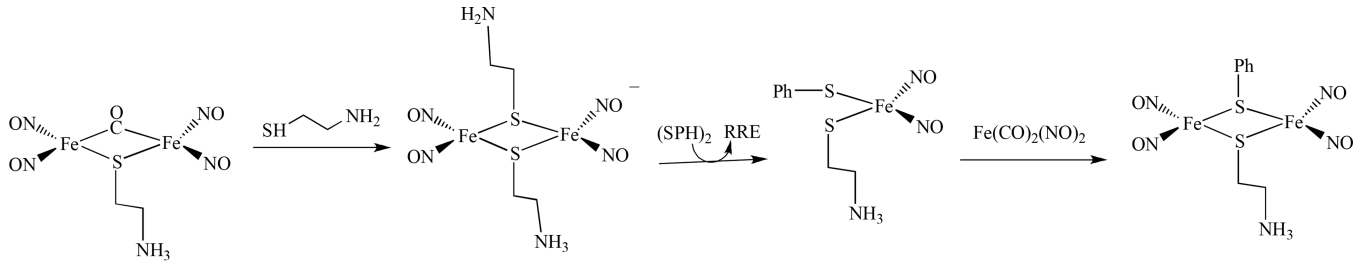

8 **9**

Scheme 6.

The reaction pathway between RRE and a mixed-thiolate-containing reduced RRE via a DNIC [81].

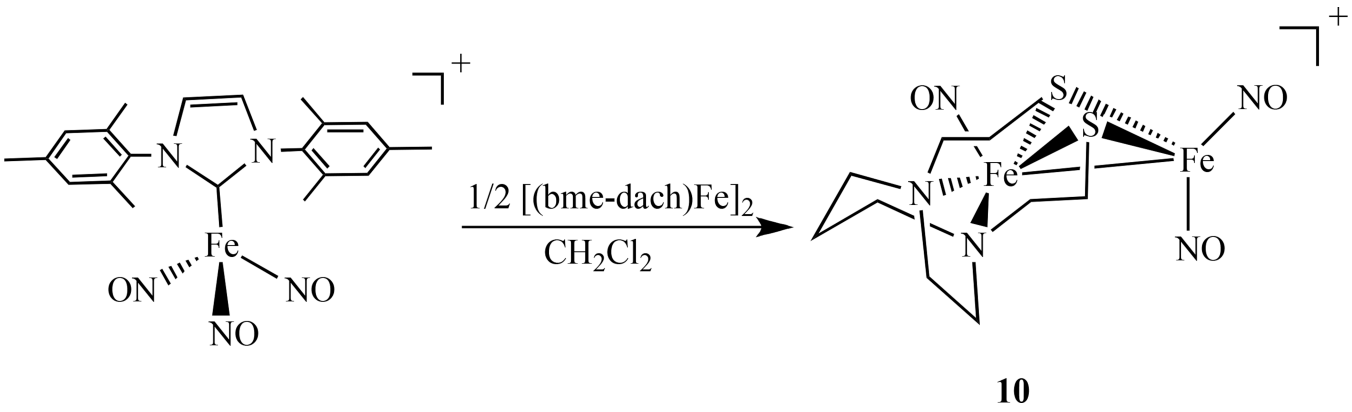

10

Scheme 7.

Synthetic scheme for a sulfur linked dinuclear complex with $\{Fe(NO)_2\}$ and $\{Fe(NO)\}$ centers [84].

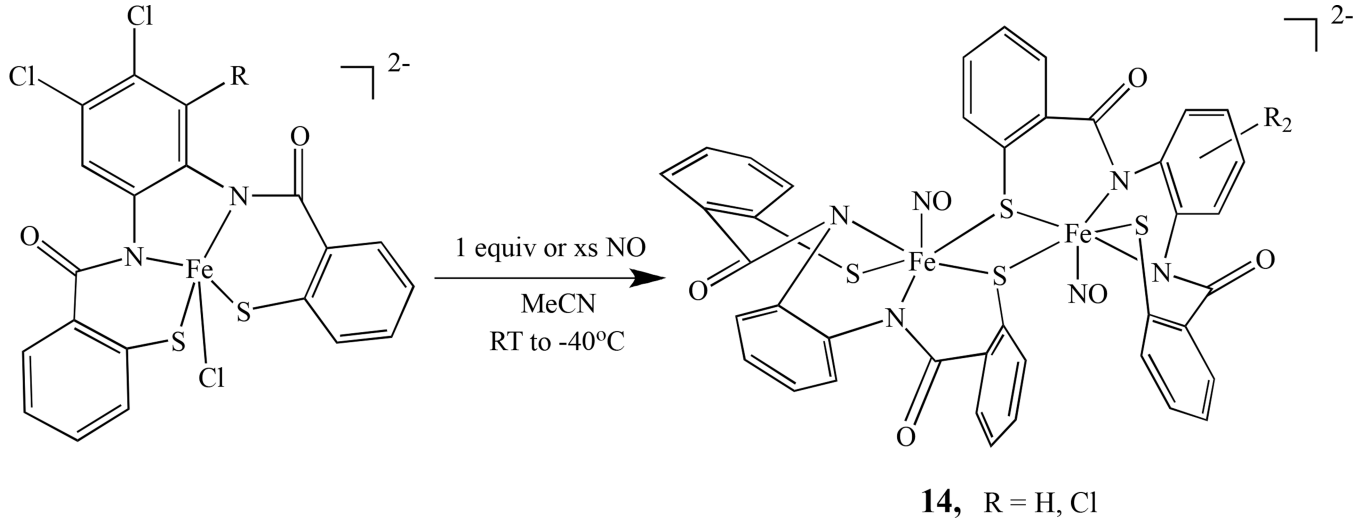

14, R = H, Cl

Scheme 8.

Synthetic scheme for the formation of a sulfur linked dinuclear complex with {Fe(NO)} and {Fe(NO)} centers [91].

2-

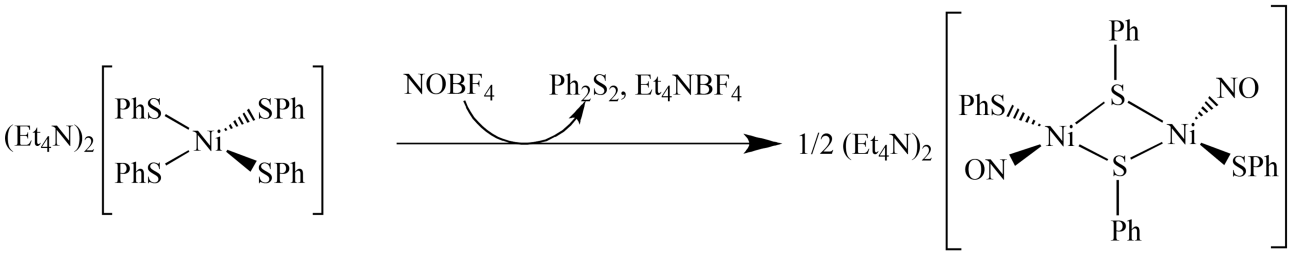

16

Scheme 9.
Preparation of dinuclear nickel mononitrosyl compound linked by a thiol ligand [94].

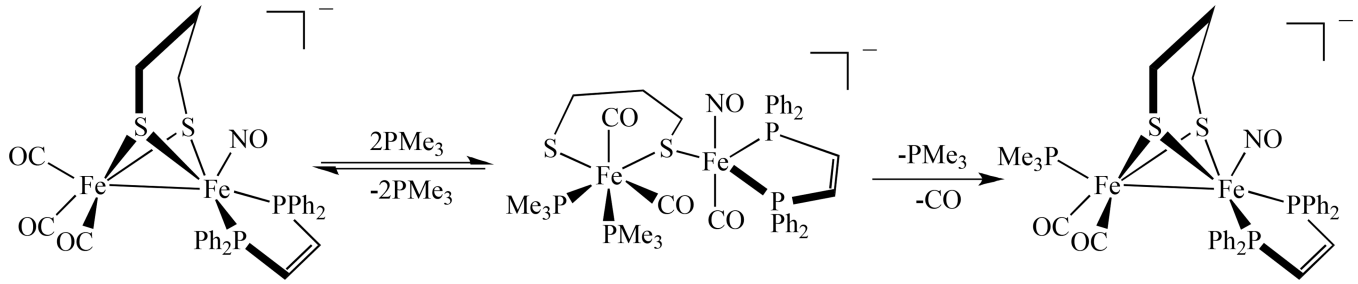

Scheme 10.
Synthesis of diiron dithiolato carbonyl compounds with a single terminal NO [96].

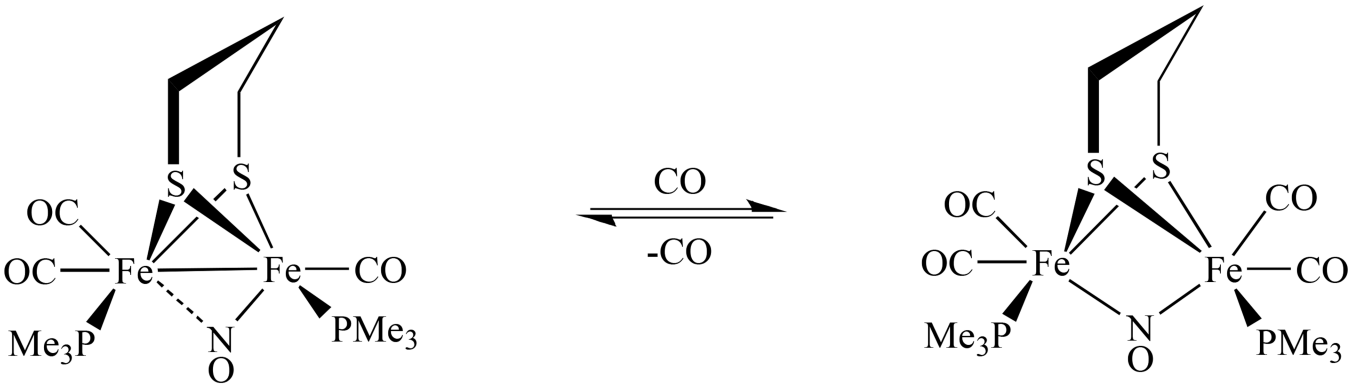

17

Scheme 11.
Conversion of single bridged NO/CO between two iron centers [97].

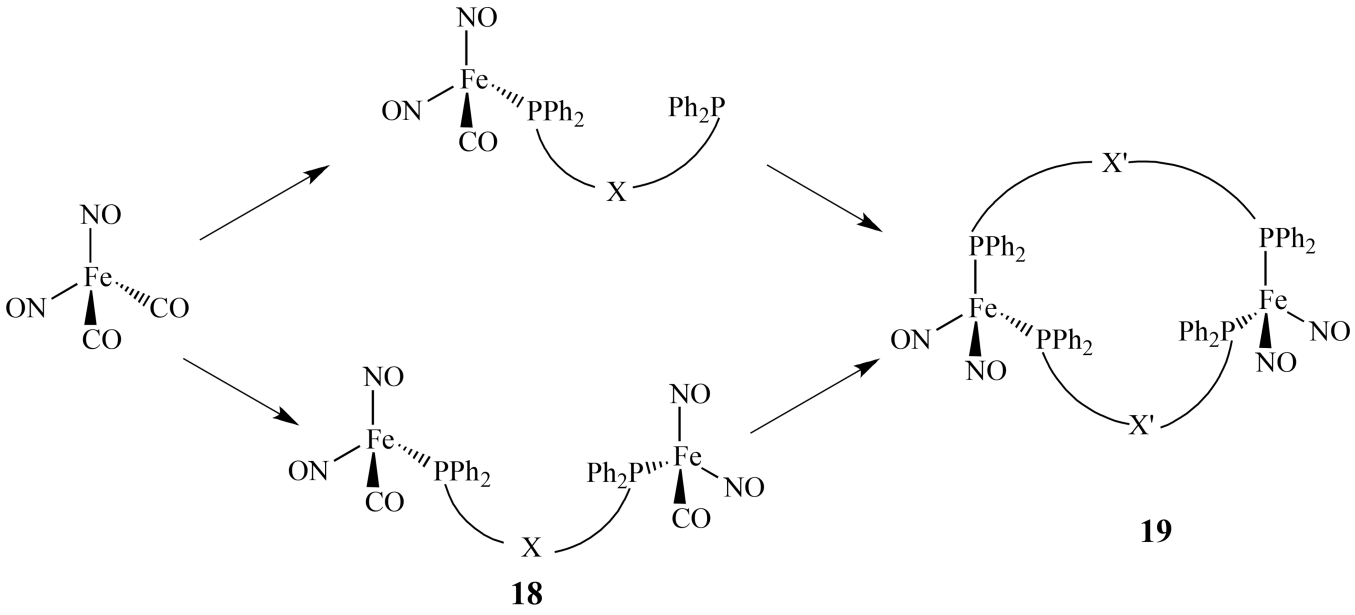

X = CH_2, **18a,** C≡C, **18b,** $(CH_2)_4$, **18c,** *p*-C_5H_4, **18d**

X' = CH_2, **19a,** C≡C, **19b**

Scheme 12.

Synthetic scheme for dinulear iron dinitrosyl linked by bisphosphines [103].

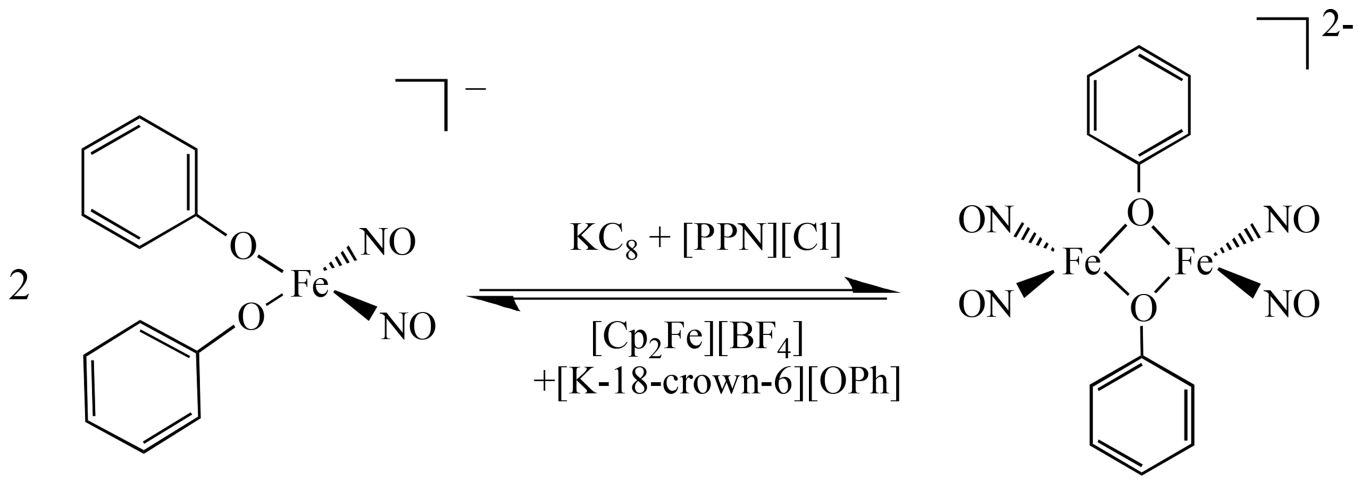

21

Scheme 13.
Synthesis of dinuclear iron dinitrosyl linked by oxygen atoms [107].

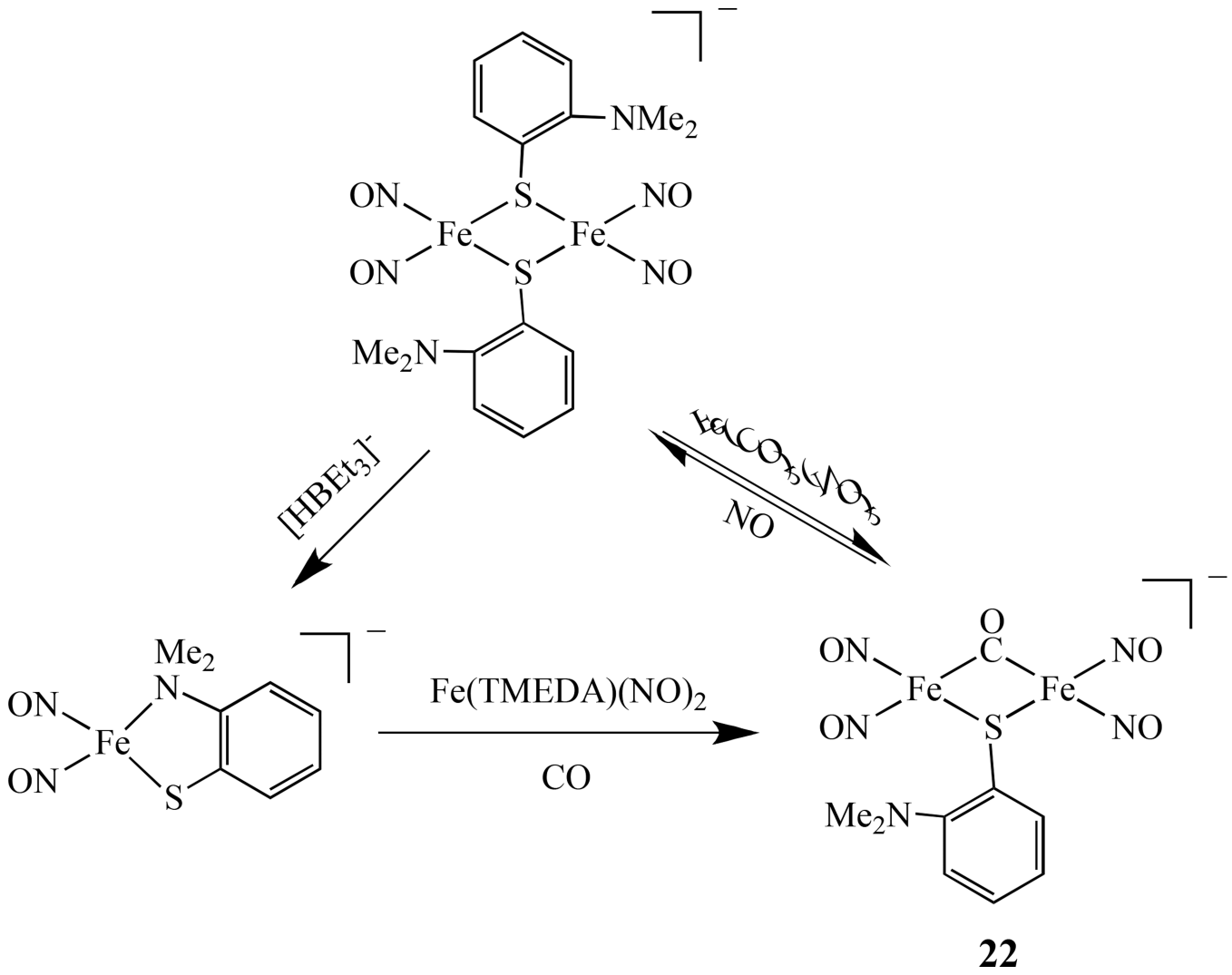

Scheme 14.
Synthesis of dinuclear iron dinitrosyl with mixed thiolate-CO-bridged ligands [108].

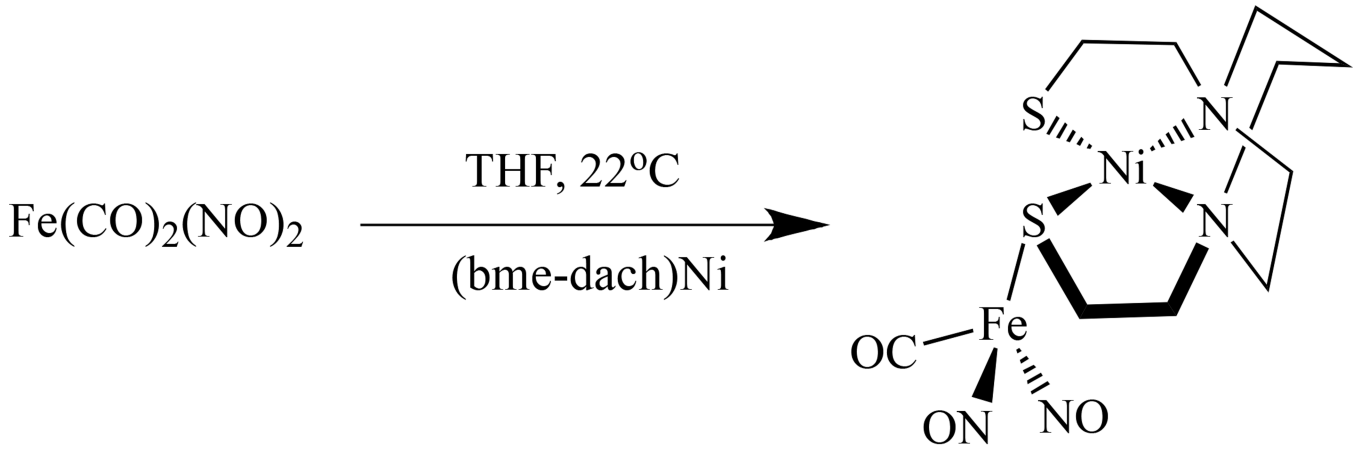

28

Scheme 15.
Reaction scheme showing formation of $[Ni(N_2S_2)]Fe(NO)_2(CO)$ [134–135].

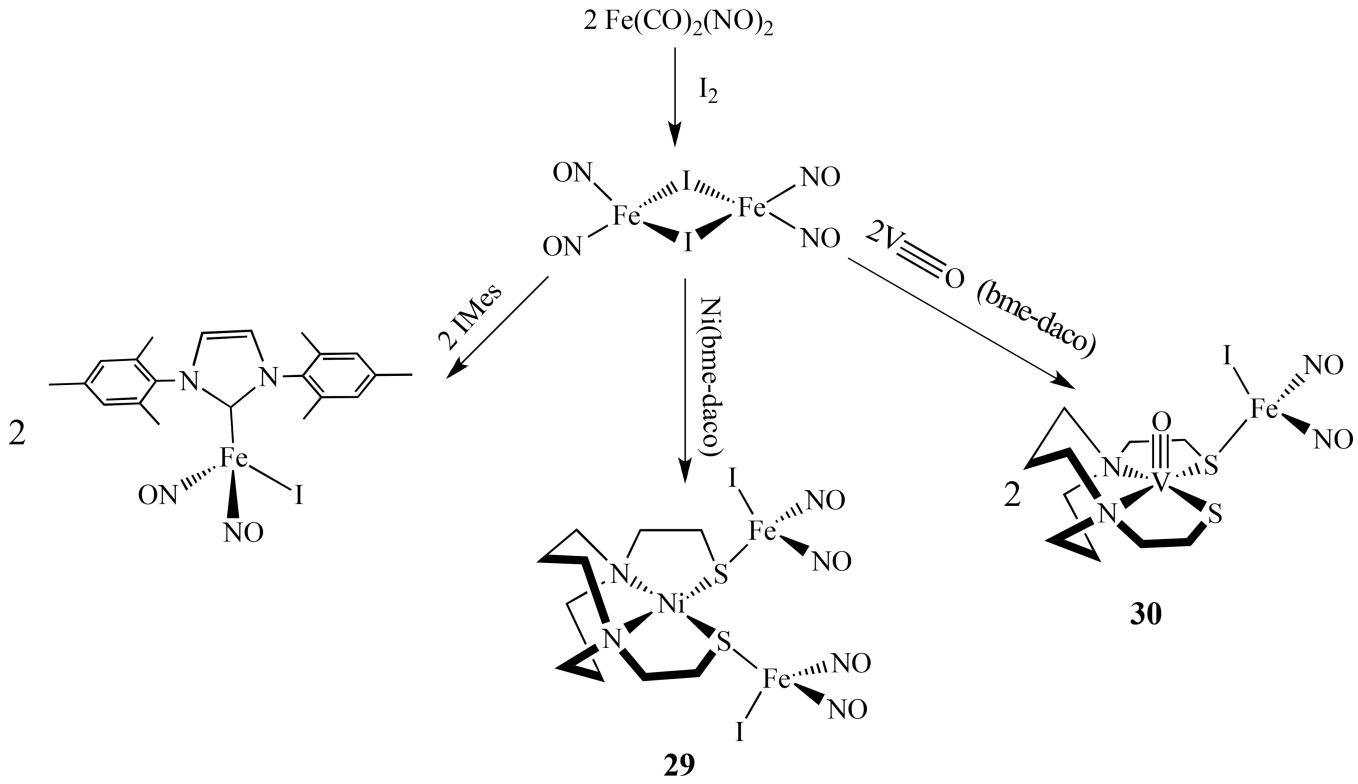

Scheme 16.
Synthesis of {Ni(bme-daco)·[Fe(NO)$_2$I]$_2$]} and [V≡O(bme-daco)·Fe(NO)$_2$I] [136].

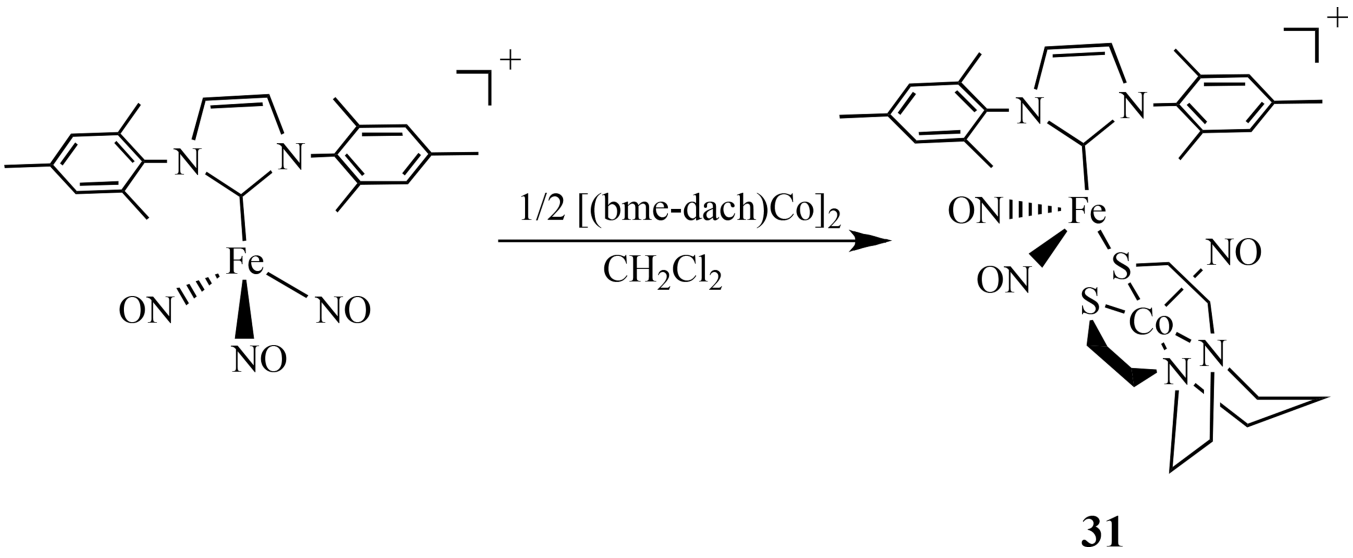

Scheme 17.
Synthesis of a {Co(NO)}–{Fe(NO)$_2$} bimetallic complex [137].

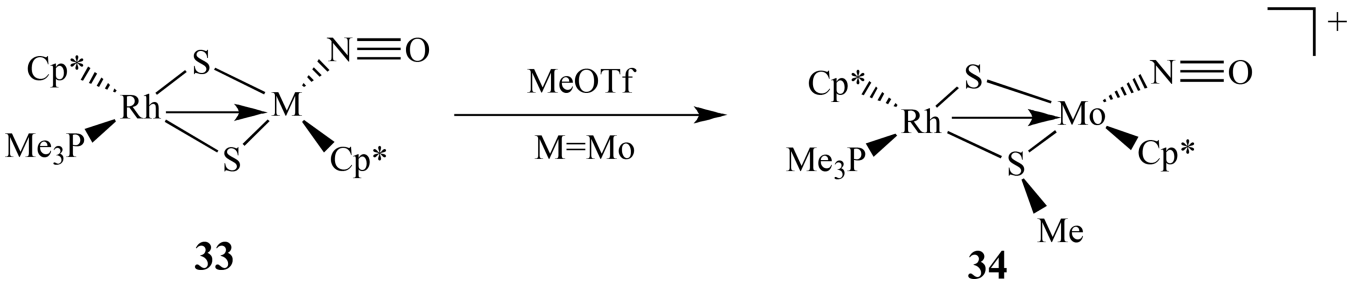

33 **34**

Scheme 18.
Examples of a heteronuclear organometallic metal nitrosyl complexes [141].

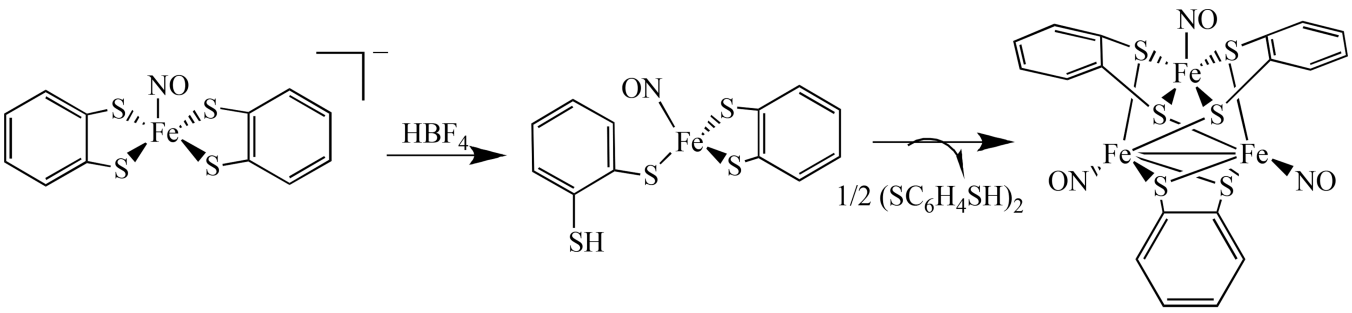

36

Scheme 19.

Synthesis of a trinuclear iron-thiolate-nitrosyl compound $[(ON)Fe(\mu\text{-}S,S\text{-}C_6H_4)]_3$**36** [145].

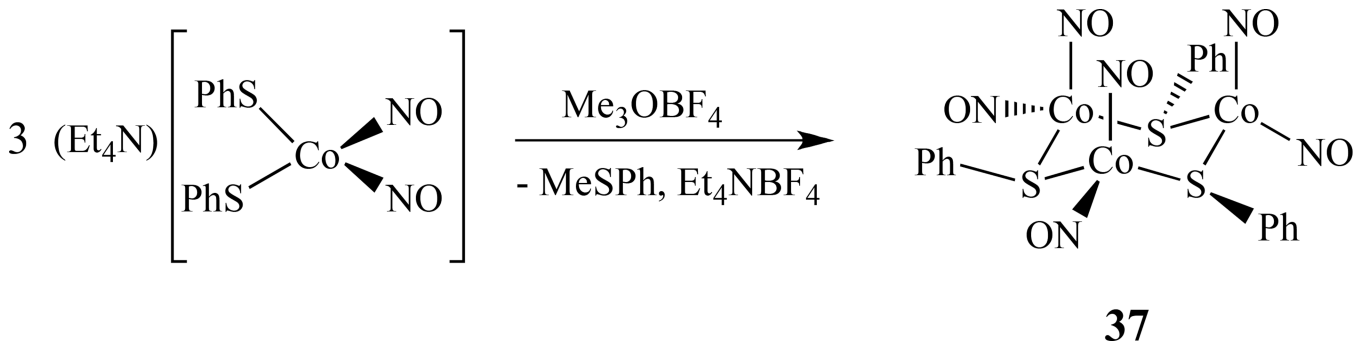

37

Scheme 20.
Synthesis of trimetallic cobalt nitrosyl complex $[Co(NO)_2(SPh)]_3$ [146].

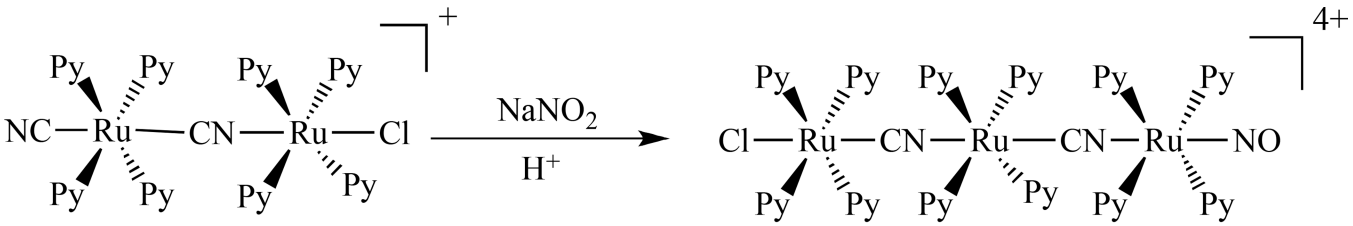

39

Scheme 21.

Synthesis of a homotrinuclear compound *trans*-[ClRu(py)$_4$(NC)Ru(py)$_4$(CN)Ru(py)$_4$(NO)](PF$_6$)$_4$ [151].

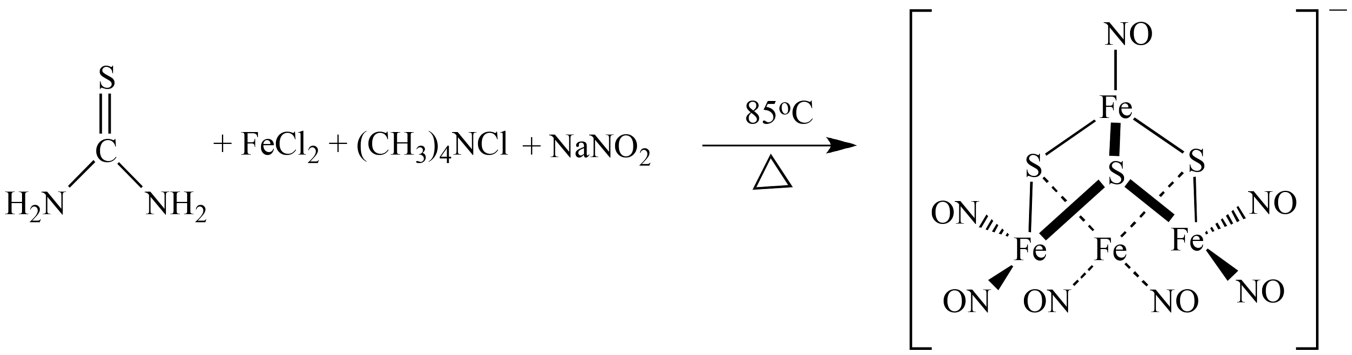

Scheme 22.
Solvent-thermal synthesis of a tetranuclear cluster $(Me_4N)[Fe_4S_3(NO)_7]$ [161].

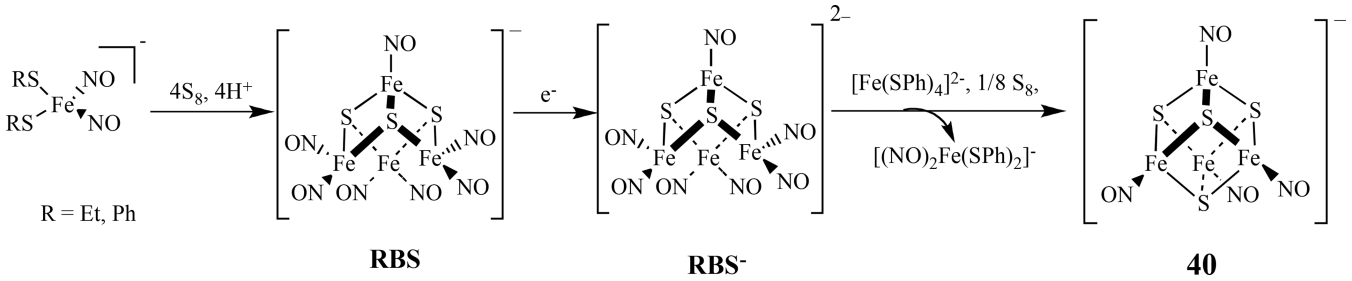

RBS **RBS^{-}** **40**

Scheme 23.

Conversion between DNIC, RBS, reduced RBS $[Fe_4S_3(NO)_7]^{2-}$, and $[Fe_4S_4(NO)_4]^{2-}$ [169].

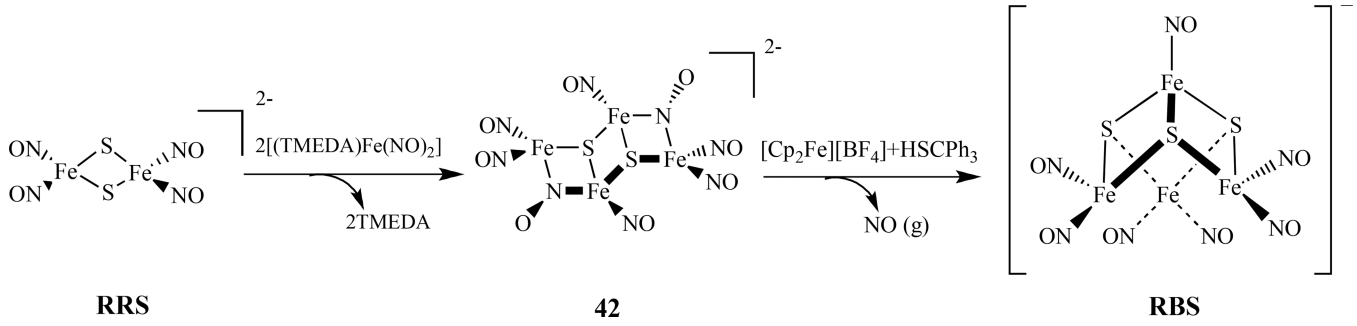

RRS **42** **RBS**

Scheme 24.

Synthesis of $[Fe_4(\mu_3\text{-}S)_2(\mu_2\text{-}NO)_2(NO)_6]^{2-}$ **42**, from RRS and a proposed conversion of **42** to RBS [171].

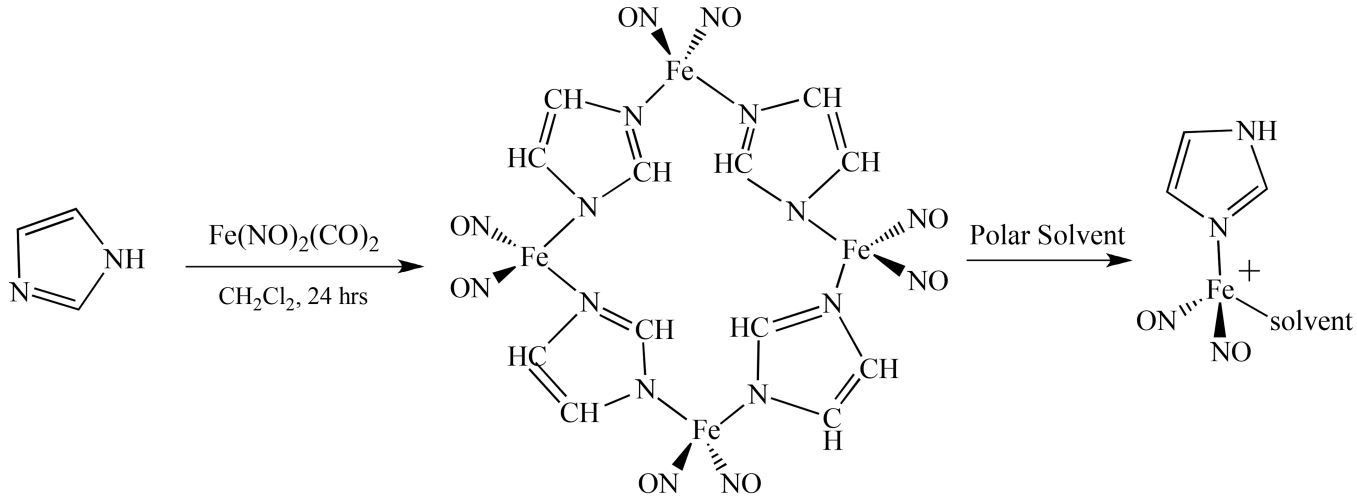

43

Scheme 25.

Synthesis of a tetranuclear nitrosyl complex linked by nitrogen atoms, $Fe_4(NO)_8(Im\text{-}H)_4$ **43**, and it's conversion to solvated species [174].

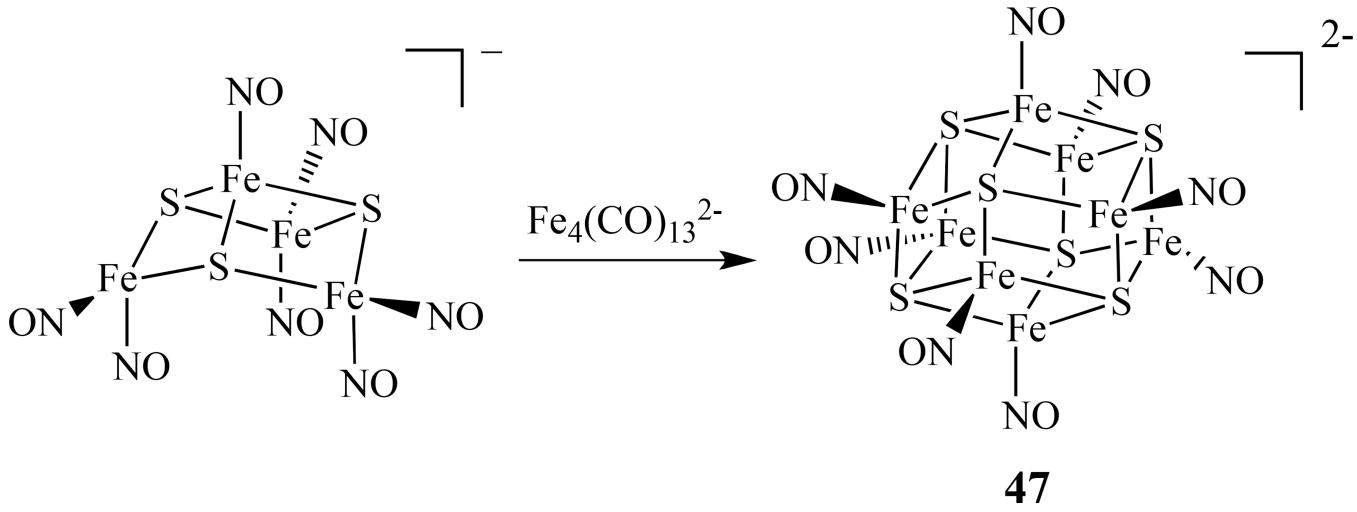

47

Scheme 26.

Synthesis of octanuclear iron-sulfur nitrosyl cluster of $[Fe_8S_6(NO)_8]^{2-}$ **47** [182].

Table 1

List of IR, UV-vis, EPR and Electrochemical Parameters of Selected Multinuclear Metal Nitrosyl Complexes

Complexes	IR (ν_{NO}, cm^{-1})	UV-Vis (nm)	$E_{1/2}$° (V)	EPR g value	ref
$[Fe_2(\mu\text{-}Sn\text{-}Pr)_2(NO)_4]$, **2a**	1809, 1774, 1747 (THF) 1782, 1729 (KBr)	239(sh), 312, 363	−1.16, −1.84		59
$[Fe_2(\mu\text{-}St\text{-}Bu)_2(NO)_4]$, **2b**	1805, 1770, 1743 (THF) 1776, 1725 (KBr)	241, 313, 358	−1.20, −1.81		59
$Fe_2(\mu\text{-}SMePr)_2(NO)_4]$, **2c**	1818, 1786, 1755 (THF) 1796, 1728 (KBr)	389	− 0.99		59
$Fe_2(\mu\text{-}SMe_2Pr)_2(NO)_4]$, **2d**	1823, 1793, 1759 (THF) 1791, 1748 (KBr)	237(sh), 363	− 0.91		59
$[Fe_2(\mu\text{-}Sn\text{-}Pr)_2(NO)_4]^-$, **2a**$^-$	1673, 1655 (THF)			1.9988	59
$[Fe_2(\mu\text{-}St\text{-}Bu)_2(NO)_4]^-$, **2b**$^-$	1670, 1650 (THF)			1.9988	59
$[Fe_2(\mu\text{-}SMePr)_2(NO)_4]^-$, **2c**$^-$	1690, 1670 (THF)			2.0036	59
$[Fe_2(\mu\text{-}SMe_2Pr)_2(NO)_4]^-$, **2d**$^-$	1693, 1674 (THF)			2.0040	59
$[Fe(NO)(SH)(\mu\text{-}S)]_2^{2-}$, **7**	1683, 1668 (CH_3CN) 1671, 1651 (KBr)	329, 407, 585			80
$[(\mu\text{-}S(CH_2)_2NH_2)Fe(NO)_2]_2^-$, **8**	1658, 1678 (THF)	320, 358, 452, 650, 962			81
$[(\mu\text{-}SC_6H_5)(\mu\text{-}S(CH_2)_2NH_3)Fe_2(NO)_4]^-$, **9**$^-$	1665, 1685 (THF)			1.999	81
[(NO)Fe(bme-dach)Fe$(NO)_2$][BF_4], **10**	1795, 1763, 1740 (THF)				84
$[(NO)_2Fe(\mu\text{-}SEt)(\mu\text{-}S)Fe(NO)_2]^-$, **13**	1710, 1687 (THF)	259, 326, 376,	−1.61		89
$(NO)_2FePPh_2\text{-}CH_2\text{-}PPh_2Fe(NO)_2$, **18a**	1760, 1719, 1702 (KBr)				103
$(NO)_2FePPh_2\text{-}C{\equiv}C\text{-}PPh_2Fe(NO)_2$, **18b**	1767, 1716 (KBr)				103
$(NO)_2FePPh_2\text{-}(CH_2)_4\text{-}PPh_2Fe(NO)_2$, **18c**	1755, 1701 (KBr)				103
$(NO)_2FePPh_2p\text{-}C5H_4\text{-}PPh_2Fe(NO)_2$, **18d**	1760, 1707 (KBr)				103
$[(NO)_2Fe]_2(PPh_2\text{-}CH_2\text{-}PPh_2)_2$, **19a**	1733, 1721, 1687, 1668 (KBr)				103
$[(NO)_2Fe]_2(PPh_2\text{-}C{\equiv}C\text{-}PPh_2)_2$, **19b**	1723, 1679 (KBr)				103
$[Fe_2(C_{14}H_{12}N_3S)_2(NO)_4]$, **20**	1789, 1732 (CH_2Cl_2) 1781, 1715 (KBr)	229, 287, 376(sh), 437(sh)			105

Complexes	IR (ν_{NO}, cm^{-1})	UV-Vis (nm)	$E_{1/2}$° (V)	EPR g value	ref
$[Fe(NO)_2(\mu\text{-}OPh)]_2^{2-}$, **21**	1651, 1602 (CH_3CN) 1651, 1600 (KBr)	272, 310, 381, 854			107
$[Fe(NO)_2(\mu\text{-}SC_6H_4\text{-}o\text{-}N(CH_3)_2)(\mu\text{-}CO)Fe(NO)_2]^-$, **22**	1705, 1691 (THF)	314, 381, 606, 975			108
$[Co_2(NO)_4$(TC-6,6)], **23**	1799, 1722 (KBr)	382, 454, 619(sh)			109
$[(ON)Fe(\mu\text{-}S,S\text{-}C_6H_4)]_3$, **36**	1760 (THF) 1751 (KBr)				145
$[Co(NO)_2(SPh)]_3$, **37**	1844, 1819, 1780, 1764 (THF) 1840, 1817, 1779, 1744 (KBr)	325, 421, 656			146
$[Fe_4S_4(NO)_4]^-$, **40**	1725 (CH_2Cl_2)			2.014, 2.026, 2.049	169
$(PPN)_2[Fe_4S_4(NO)_6]$, **41**	1700, 1668 (KBr)				170
$[Fe_4(\mu_3\text{-}S)_2(\mu_2\text{-}NO)_2(NO)_6]^{2-}$, **42**	1742, 1701, 1668 (CH_3CN) 1739, 1702, 1685, 1668, 1510 (KBr)	273, 343, 478			171
$Fe_4(S_3')_2(NO)_8$	1779, 1755 (THF)				172
$Fe_4(NO)_8(Im\text{-}H)_4$, **43**	1796, 1726 (THF)			2.023(solid) 2.031(THF)	174
$(Me_4N)[Fe_4S_3(NO)_7]$, **RBS**	1799, 1744, 1710 (CH_3CN) 1798, 1728, 1712 (KBr)	265, 357, 434, 584	−1.09, −1.71, -2.21		161
$[(n\text{-}Bu)_4N]_2[Fe_6S_6(NO)_6]$, **44**	1694 (CH_3CN), 1683 (KBr)	259, 297	−0.04(irr), -0.14, −1.33		161
$[(n\text{-}Bu)_4N]_2[Fe_6Se_6(NO)_6]$, **45**	1698 (CH_3CN), 1678 (KBr)	288	0.07 (irr), -0.33, −1.32		161
$[Fe(BMPA\text{-}Pr)(NO)]_6[ClO_4]$, **46**	1777 (KBr)	255, 350, 354, 430			181